HEAT TRANSFER TO LIQUID METALS, WITH OBSERVATIONS ON THE EFFECT OF SUPERIMPOSED FREE CONVECTION IN TURBULENT FLOW

(Warmteoordrag aan vloeibare metale, met opmerkings oor die invloed van ooreenliggende natuurlike konveksie in turbulente stroming.)

by

HEINRICH OTTO BUHR

Submitted
in fulfilment of the requirements
for the degree of
Doctor of Philosophy
of
The University of Cape Town.

April, 1967.

"Heat transfer to liquid metals, with observations on the effect of superimposed free convection in turbulent flow" by H.O. Buhr.

SUMMARY AND STATEMENT OF MAJOR CONTRIBUTION

Evaluation of the different theories of heat transfer to liquid metals requires values of the ratio of eddy diffusivities of heat and momentum, which may be obtained from temperature and velocity profiles measured in the flowing liquid metal. Temperature profiles have been reported by a number of workers, but these results are in poor agreement and this investigation was undertaken to measure further profiles and thus obtain reliable eddy diffusivities.

Chapter 1 introduces the background to liquid metal heat transfer theory, and Chapter 2 contains a discussion of the experimental apparatus that was constructed for the purposes of this investigation. A description of this equipment has been published (Ref.64*) and the material is included here with the permission of the candidate's supervisor. Chapter 3 discusses the unsuccessful attempts to measure velocity profiles, and then goes on to consider appropriate values of the eddy diffusivity of momentum, based on the universal velocity profile. The data of Nikuradse* are recommended after a careful study of all the available data and the author believes that this is a conclusion which will be useful to other workers in the field, who usually make an essentially random choice of eddy diffusivities.

Twenty-three temperature profiles are reported in Chapter 4, and represent a contribution to the body of available data. These profiles also show inconsistencies when compared on the classical basis of the same Reynolds number, but the author suggests that the discrepancies observed are due to a superimposed free convection effect, and proposes a criterion as well as a method of correlation (Fig. 25) whereby such an effect is

* References are given in the text.

ACKNOWLEDGEMENTS

The author wishes to express his sincere appreciation to Professor A.D. Carr for his constant encouragement and generous assistance during the course of this work.

He also wishes to thank Drs. W.L. Grant and R.E. Robinson of the S.A. Atomic Energy Board for their interest and assistance with the loan of the mercury.

The author is grateful for the financial assistance of the S.A. Atomic Energy Board and the University of Cape Town Staff Research Fund.

TABLE OF CONTENTS

ABSTRACT ii

ACKNOWLEDGEMENTS iii

TABLE OF FIGURES vii

CHAPTER 1 INTRODUCTION 1

1.1 THE ANALOGY BETWEEN HEAT AND MOMENTUM TRANSFER 1

1.2 HEAT TRANSFER TO LIQUID METALS 2

1.3 THE RATIO OF EDDY DIFFUSIVITIES 6

1.4 SCOPE OF EXPERIMENTAL WORK 8

CHAPTER 2 EXPERIMENTAL EQUIPMENT 10

2.1 THE TEST LOOP 10

2.2 TEMPERATURE AND VELOCITY PROBES 14

2.3 HEATING SECTION 15

2.4 COOLING SECTION 19

2.5 TEMPERATURE MEASUREMENT 19

2.51 Thermocouples 19

2.52 Temperature readings 20

2.6 PUMPING AND FLOW MEASUREMENT 21

2.7 DIFFERENTIAL PRESSURE MEASUREMENT . . . 23

2.8 TESTING AND FILLING 24

CHAPTER 3 VELOCITY PROFILES AND THE EDDY DIFFUSIVITY OF MOMENTUM 28

3.1 EXPERIMENTAL WORK 28

3.11 Profiles in mercury 28

3.12 Profiles in air 31

3.13 Further work in mercury 33

3.2 THE UNIVERSAL VELOCITY PROFILE 35

3.21 The turbulent boundary layer . . 36

3.3 THE EDDY DIFFUSIVITY OF MOMENTUM, ϵ_M . 40

3.31 The recommended form of ϵ_M/Ru^* vs. y/R 42

CHAPTER 4 TEMPERATURE PROFILES 50
4.1 TEST PROCEDURE 50
4.2 RESULTS 54
4.3 DISCUSSION OF RESULTS 59
CHAPTER 5 CORRELATION OF DATA 65
5.1 THE EFFECT OF FREE CONVECTION 65
5.2 CHOICE OF A CORRELATING PARAMETER 66
5.21 Rayleigh number 66
5.22 Prandtl number 68
5.23 D/L Ratio 68
5.24 Reynolds Number 69
5.3 VALUES OF Z 69
5.4 FORM OF CORRELATION 70
5.5 THE CORRELATION OF FIG. 25 70
5.6 UNDISTORTED TEMPERATURE PROFILES 73
CHAPTER 6 CONCLUSIONS AND RECOMMENDATIONS 76
6.1 THE EDDY DIFFUSIVITY RATIO, ϵ_H/ϵ_M 76
6.2 HEAT TRANSFER COEFFICIENTS 77
6.3 SUMMARY OF RESULTS 81
6.4 RECOMMENDATIONS 82
NOMENCLATURE 85
LIST OF REFERENCES 88
APPENDICES 95
APPENDIX A VELOCITY PROFILES A-1
APPENDIX B TEMPERATURE PROFILE MEASUREMENTS . . . B-1
B.1 RESULTS B-1
B.2 CALCULATION PROCEDURE B-5
APPENDIX C VALUES OF THE PARAMETERS Y AND Z . . . C-1
C.1 THE YANTOVSKII CRITERION, Y C-1
C.2 THE NATURAL CONVECTION CRITERION, Z . . . C-4

APPENDIX D RATIO OF EDDY DIFFUSIVITIES D-1

D.1 CALCULATED RESULTS D-1

D.2 CALCULATION PROCEDURE D-2

APPENDIX E CALCULATION OF ϵ_M/Ru^* E-1

E.1 VALUES OF ϵ_M/Ru^* E-1

E.2 CALCULATION METHOD E-5

APPENDIX F EQUIPMENT DETAILS F-1

F.1 HEATING COILS F-1

F.2 THERMOCOUPLES F-4

F.3 ORIFICE METER F-6

APPENDIX G HEAT TRANSFER COEFFICIENTS G-1

G.1 NUSSELT NUMBERS G-1

G.2 NUSSELT NUMBER FROM DIMENSIONLESS TEMPERATURE PROFILE G-2

G.3 EFFECT OF VELOCITY PROFILE ON NUSSELT NUMBER G-3

APPENDIX H PHYSICAL PROPERTIES H-1

H.1 PHYSICAL PROPERTIES OF MERCURY H-1

H.2 PHYSICAL PROPERTIES FOR THE NaK EUTECTIC MIXTURE H-4

TABLE OF FIGURES

FIGURE		PAGE
1	Heat transfer data for liquid metals	4
2	Ratio of eddy diffusivities for mercury at $Re=10^5$, from Carr and Balzhiser (38) . .	9
3	The test loop	11
4	Upper part of test loop	12
5	Lower part of experimental equipment	13
6	Probing station nozzles and static tap . . .	16
7	Details of temperature probe	16
8	Details of velocity probe	17
9	Reference emf circuit	22
10	Gas pressuring manometer system	25
11	Null-type differential manometer	26
12	Velocity profiles in mercury	30
13	Influence of probe position on pressure reading at static tap	32
14	Velocity profiles in air	34
15	Comparison of single velocity traverses with equn. 3.9.	39
16	Values of ϵ_M/Ru^* from various sources . . .	41
17	Comparison of velocity defect relations with actual experimental data near the tube centre	46
18	Slopes of velocity profiles from various workers	47
19	Recommended values of ϵ_M/Ru^*, after Nikuradse (9)	49
20	Typical temperature recording, Run 10. . .	56
21	Typical temperature profile	58

(continued)

FIGURE		PAGE
22	Temperature profiles for Re ≈ 10^4	61
23	Temperature profiles in the NaK eutectic for Re ≈ 4×10^4	62
24	Temperature profiles for Re ≈ 4×10^4	63
25	Correlation of dimensionless temperature profiles	71
26	Undistorted temperature profiles from Fig. 25.	75
27	Ratio of eddy diffusivities	78
28	Plot of Nusselt numbers obtained in this investigation	79
A.1	Velocity profile in mercury, Run V.7.	A-2
B.1	Temperature profile, Run 10.	B-10
E.1	Slope of Laufer's (45) velocity profile at Re=428,000	E-6
F.1	Heating circuits	F-2
F.2	Thermocouple switching panel	F-5
F.3	Portion of thermocouple calibration chart	F-7
G.1	Distorted velocity profiles	G-4
H.1(a)	Physical properties of mercury	H-2
H.1(b)	Prandtl number for mercury	H-3
H.2	Kinematic viscosity and Prandtl number for the NaK eutectic	H-6

CHAPTER 1
INTRODUCTION

1.1 THE ANALOGY BETWEEN HEAT AND MOMENTUM TRANSFER

The rates at which heat and momentum are transported across the radius for a fluid flowing in a circular tube are given by the following well-known forms of the energy and momentum equations:

$$q / \rho c_p = -(\alpha + \epsilon_H)\, dT/dy \qquad (1.1)$$

$$\tau / \rho = (\nu + \epsilon_M)\, du/dy \qquad (1.2)$$

The quantities α and ν represent molecular transport of heat and momentum respectively, and are the only significant factors in laminar flow, while the "eddy diffusivities" of heat and momentum, ϵ_H and ϵ_M represent the additional transport occurring by eddy motion for the case of turbulent flow.

In 1874 Osborne Reynolds (1) recognised that heat is transported away from a hot surface primarily by turbulent eddies, and since these eddies are also mainly responsible for the pressure loss due to friction, the concept of an analogy between heat and momentum transfer has arisen. In its simplest form, the analogy states that the molecular diffusivities of heat and momentum are negligible, or equal, the eddy diffusivities of heat and momentum are equal, and turbulence extends right up to the wall. These assumptions lead to the relation

$$St = f/2 \qquad (1.3)$$

which has become known as the Reynolds analogy. ($St = h/cG$ and f is the friction factor).

The concept of similarity between heat and momentum transfer was extended by Prandtl (2) and Taylor (3) who postulated the existence of a laminar layer next to the wall, and by von Karman (4) who introduced an intermediate or buffer region between the laminar and turbulent layers, following on the suggestion of Eagle and Ferguson (5). The equation given by von Karman is

$$St = \frac{f/2}{1 + 5\sqrt{f/2}\{Pr - 1 + \ln[1 + (5/6)(Pr - 1)]\}} \qquad (1.4)$$

and is based on the velocity distribution

$$0 < y^+ < 5, \qquad u^+ = y^+ \tag{1.5a}$$

$$5 < y^+ < 30, \qquad u^+ = -3.05 + 5 \ln y^+ \tag{1.5b}$$

$$y^+ > 30, \qquad u^+ = 5.5 + 2.5 \ln y^+ \tag{1.5c}$$

The von Karman equation was further extended by Boelter, Martinelli and Jonassen (6) to include the effect of variation of fluid properties with temperature.

All the analyses referred to above contained the assumption of complete identity of the mechanisms of heat and momentum transfer in the turbulent core, which in effect meant equality of the eddy diffusivities of heat and momentum and negligible molecular transport. In 1947 Martinelli (7), however, in a refinement of the work of Boelter et al. (6), recognised

(a) that the eddy diffusivities may not always be equal, and carried the ratio

$$\epsilon = \epsilon_H / \epsilon_M$$

through his analysis, although he subsequently equated ϵ to 1·0 to get numerical results,

(b) that the molecular diffusivity of heat will not be negligible in the turbulent core in some cases, such as fluids with very high thermal conductivities, for example liquid metals.

Martinelli accordingly defined a factor F which is the ratio of the thermal resistance due to the total (molecular plus eddy) diffusion to the resistance due to eddy diffusion alone, in the turbulent core. The resulting relation is

$$St = \frac{\epsilon \sqrt{f/2}\ (T_w - T_c)/(T_w - T_{av})}{5\ [\ \epsilon Pr + \ln(1 + 5\epsilon Pr) + 0.5 F \ln \frac{Re}{60} \sqrt{f/2}\ ]} \tag{1.6}$$

1.2 HEAT TRANSFER TO LIQUID METALS.

Applications for liquid metals as heat transfer media in nuclear reactors have arisen in recent years, due to their thermal stability, high boiling points, and low neutron capture cross-section.

The Martinelli equation, (1.6) above, was the first heat transfer theory to take account of the special properties of liquid metals, and in 1951 Lyon (8) also produced an analysis for heat transfer to liquid metals, for the case of constant heat flux through the tube wall. Lyon evaluated his integral equation for the Nusselt number in the Prandtl number range 0 to 0·1, using the velocity data of Nikuradse (9), and found that his results, as well as those of Martinelli, could be reasonably described by the simple approximate equation

$$Nu = 7 + 0.025(\epsilon\, Pe)^{0.8} \qquad (1.7)$$

This relation, with $\epsilon=1$, has become known as the Martinelli-Lyon equation and has been widely accepted for the prediction of heat transfer coefficients in liquid metals.

An alysis for the case of constant wall temperature by Seban and Shimazaki (10) resulted in a similar equation with the constant equal to 5 instead of 7.

Styrikovich and Semenovker (11) were the first to present experimental data for forced convection heat transfer to liquid metals and further data have followed from many other investigators (12-17). In 1956 Lubarsky and Kaufman (18) reviewed all the experimental results available at that time, and presented them on a consistent basis. They distinguished between data based on overall measurements, for which a higher Nu is usually obtained, and data based on a fully developed temperature profile, as well as between cases of uniform wall temperature and uniform heat input. The shaded area in Fig. 1 represent the bulk of the data correlated by Lubarsky and Kaufman, on a plot of Nusselt vs. Peclet numbers, for the case of fully developed heat transfer at uniform heat flux. Further measurements have been presented by Brown et al. (19) and a number of Russian investigators (20-26). The data of Subbotin et al (22) are also shown in Fig. 1. These latter data are typical of Nusselt numbers obtained for the alkali metals, which in general agree with the Martinelli-Lyon

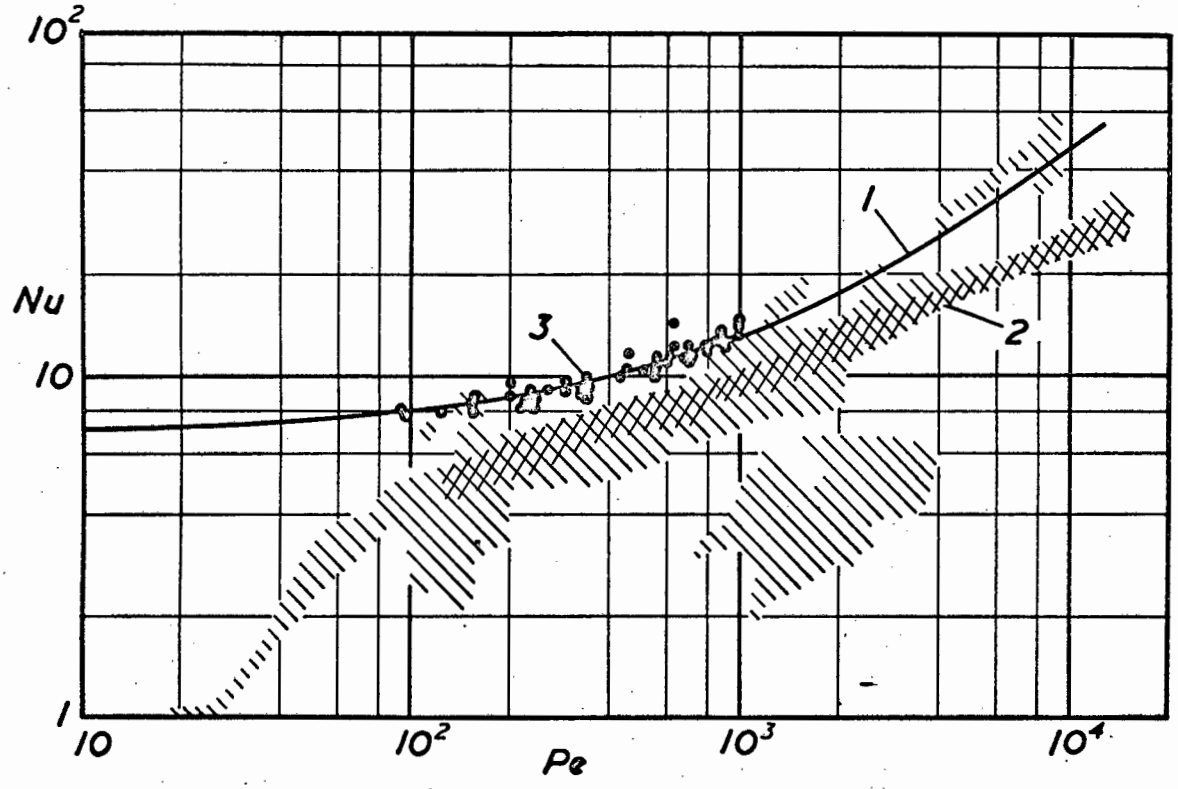

FIG. 1 HEAT TRANSFER DATA FOR LIQUID METALS.

1. Martinelli-Lyon equation $Nu = 7 + 0.025(Pe)^{0.8}$
2. Bulk of experimental data for fully developed flow at uniform heat flux, after Lubarsky and Kaufman (18).
3. Alkali-metal data of Subbotin et al. (22).

equation given by the solid curve in Fig. 1. In contrast to the alkali metals, data for the heavy metals (mercury, lead-bismuth), which form the bulk of the cases investigated by Lubarsky and Kaufman, are seen to fall about 30% below this curve. Better agreement is obtained at higher Peclet numbers, while wide discrepancies are observed between predicted and experimental Nusselt numbers at low Pe. The latter range is represented mainly by the data of Johnson et al. (15)

Attempts to reconcile the Martinelli-Lyon theory with the experimental results have centred mainly on the two concepts of

(a) a thermal contact resistance between the wall and the fluid, which could result in calculated heat transfer coefficients which are unrealistically low, and

(b) the possibility that the ratio of eddy diffusivities might be less than unity, which would lower the Martinelli-Lyon curve (see equn. 1.7).

The agreement obtained between alkali metal data, determined in carefully cleaned test sections, and the Martinelli-Lyon equation, has been taken to indicate the existence of a thermal contact resistance with the heavy metals, due to oxide or gas films, or non-wetting of the surface of the test section by the liquid metal. While the effect of a contact resistance should be absent in heat transfer coefficients calculated from temperature profile measurements, such measurements do not, in general, support the Martinelli-Lyon theory. Furthermore, MacDonald and Quittenton (27), in a critical analysis of the available data, concluded that, while non-wetting of the tube wall may result in an appreciable electrical resistance, the thermal resistance is negligible. However, until an explanation of the discrepancies is found, the possibility of a thermal contact resistance can obviously not be discounted.

A number of theories have been put forward to evaluate the ratio of the eddy diffusivities of heat and momentum. These theories are

discussed in the next section. It has also been suggested, both by Jakob (28) and by Lyon (29), that low values of the Nusselt number may be caused by a free connection effect, particularly at low Peclet numbers. This aspect has not so far received any attention.

1.3 THE RATIO OF EDDY DIFFUSIVITIES

A number of theoretical analyses have been made to predict the value of the ratio of eddy diffusivities in liquid metals. Jenkins (30) in 1951 considered the heat loss from an eddy, or "lump" of fluid, during its flight from one layer of fluid to another at a lower temperature, and by means of assumptions regarding the size of the eddy and the nature of the momentum eddy diffusivity, derived an expression for the ratio of eddy diffusivities, ϵ_H/ϵ_M. The same line of reasoning has been followed by other investigators, who considered the heat loss from an eddy, and made various assumptions about the transfer of momentum. Correlations for ϵ_H/ϵ_M have, for example, been presented by Deissler (31), Lykoudis and Touloukian (32), Azer and Chao (33), Dwyer (34) and Sesonske et al. (35-37). These theories all predict values of ϵ less than unity, so that, when values of ϵ (radial average) are substituted into equn. 1.7, better agreement with experimental data is obtained.

In order to test predicted values of ϵ, a number of experimental investigations have been made. The eddy diffusivities ϵ_H and ϵ_M may be determined from the energy and momentum equations 1.1 and 1.2, by evaluating the slopes of experimental temperature and velocity profiles. Such profiles were first measured by Isakoff (17) in 1952 and by Brown et al (19) in 1957, with mercury as the test fluid. Since 1961 an appreciable number of temperature profiles have been reported, in both mercury and liquid metals. A list of investigators is given in Table 1.1. In a recent paper Carr and Balzhiser (38) have reviewed temperature profile data currently available and have presented values of the eddy diffusivity ratio on a common basis. Fig. 2, which is taken from Ref. (38) shows values of ϵ at Re $\approx 10^5$

TABLE 1.1

LIQUID METAL TEMPERATURE PROFILE MEASUREMENTS

Investigator	Year	Liquid Metal	Flow Direction	Number of profiles reported	Re x 10^{-3}
Isakoff (17)	1952	Hg	↑	12	37.6 - 373
Brown et al.(19)	1957	Hg	↑ †	5	244 - 731
Kirillov et al.(20)	1959	NaK(78%K)	↑	6	4.5 - 36.4
Subbotin et al.(21)	1961	Hg	↑	2	26.9 & 228
Subbotin et al.(22)	1961	Hg	↑	2	24.2 & 204
		NaK(78%K)	↑	2	16.2 & 24.7
Buyco (36)	1961	Hg	→	5	55.5 - 111
Kokorev and Ryaposov (23)	1962	Hg	→	*	110 - 160
Subbotin et al.(25)	1963	Hg	↑	28	22.1 - 427
Borishanskii et al.(26)	1963	Na	↑	1	50.7
Schrock (37)	1964	NaK(56%K)	→	23**	2.1 - 76.8

† The tests of Brown et al.(19) were conducted on mercury that was being cooled. In the cases of the other investigators, the liquid metal was heated.

* These investigators do not report individual profiles. An "averaged" profile is given for three values of Re.

** These profiles include vertical, horizontal and 45° traverses.

together with the theoretical values of Deissler (31), Azer and Chao (33) and Dwyer (34), and provides a good example of typical experimental results and their relationship to the various theories. It is clear that the experimental data available so far are not consistent or accurate enough to provide a check on eddy diffusivity theories, but it does appear that ϵ often exceeds unity, in contrast to the theoretical predictions which all call for ϵ to be less than 1.0.

1.4 SCOPE OF EXPERIMENTAL WORK.

In a recent review on liquid metal heat transfer, Dwyer (39) expresses the belief that future progress in establishing the Nusselt-Peclet relationship, particularly at low Peclet numbers, will depend more on reliable experimental results than on theoretical analysis. The present investigation was undertaken in an attempt to elucidate some of the discrepancies in liquid-metal heat transfer theory pointed out in the previous section, and specifically to determine reliable values of ϵ_H/ϵ_M. To this end it was proposed to measure temperature and velocity profiles in mercury, with particular attention to the low-Pe range.

At the time that this project was initiated, the detailed report of Isakoff (17) formed a convenient starting point and the experimental equipment was thus desiged following Isakoff's principles, with changes incorporated where the experience of that investigator had indicated them to be necessary.

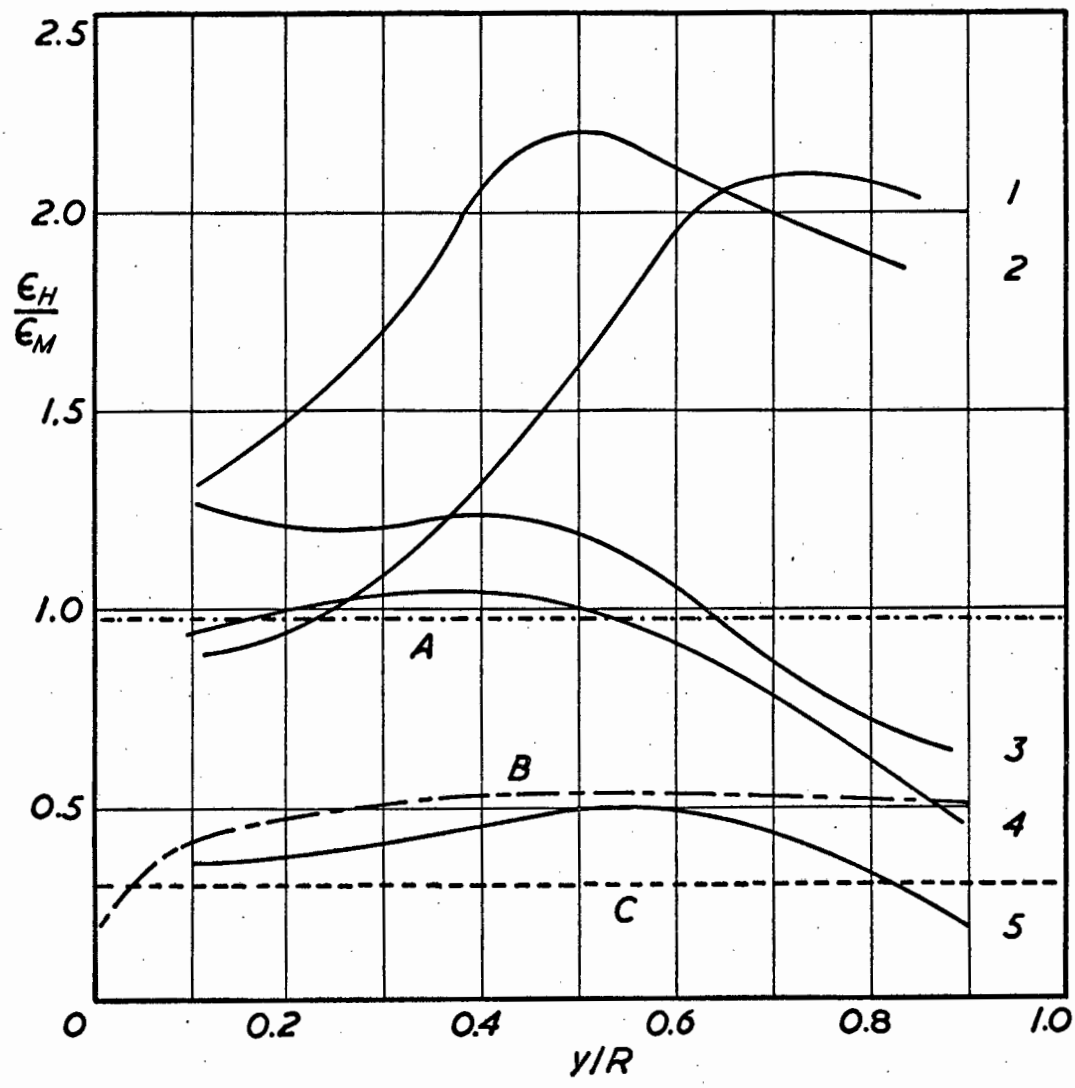

FIG. 2 RATIO OF EDDY DIFFUSIVITIES FOR MERCURY AT Re = 10^5, FROM CARR AND BALZHISER (38).

1. Subbotin et al. (21), revalued 2. Kokorev and Ryaposov (23)
3. Buyco (36) 4. Isakoff (17) 5. Brown et al. (19)

A. Dwyer (34) theoretical B. Azer and Chao (33) theoretical
C. Deissler (31) theoretical

CHAPTER 2

EXPERIMENTAL EQUIPMENT

2.1 THE TEST LOOP

The test loop is shown schematically in Fig. 3. Mercury flowed vertically upwards through an electrically heated test section 16.3 ft. long, and vertically downwards through a second test section, which was water-jacketed over a length of 14.7 ft. The test sections were constructed of 1.624 in. I.D. seamless stainless steel tubing, 0.138 in. thick, and each incorporated a probing station which consisted of a temperature and a velocity probe, installed at right angles to each other. These probing stations were situated at 105 and 98 diameters from the start of the heated and cooled test sections, respectively.

A centrifugal pump and orifice meter were situated at the top of the loop to minimise static pressure on the pump gland and meter connections. The pump was operated at low speeds and was bolted to a platform 20 ft. above the laboratory floor. Because of the large weight of mercury, special consideration had to be given to supports for the loop. These supports consisted of a coil spring on a hydraulic jack, enclosed in a steel pipe, underneath each vertical leg. The hydraulic jack supported the weight of the apparatus while the coil spring allowed for thermal expansion during operation.

Fig. 4. is a photograph of the top part of the loop and shows the pump drive system, as well as the orifice meter and overhead expansion chamber. Fig. 5 shows the lower portion of the experimental apparatus, and includes the two vertical test sections, the variable transformer for the heating coils and the general instrumentation and recording equipment. The assembled probing station in the water-jacketed section can be seen in the photograph, as well as the two supports for the loop. The horizontal section connecting the

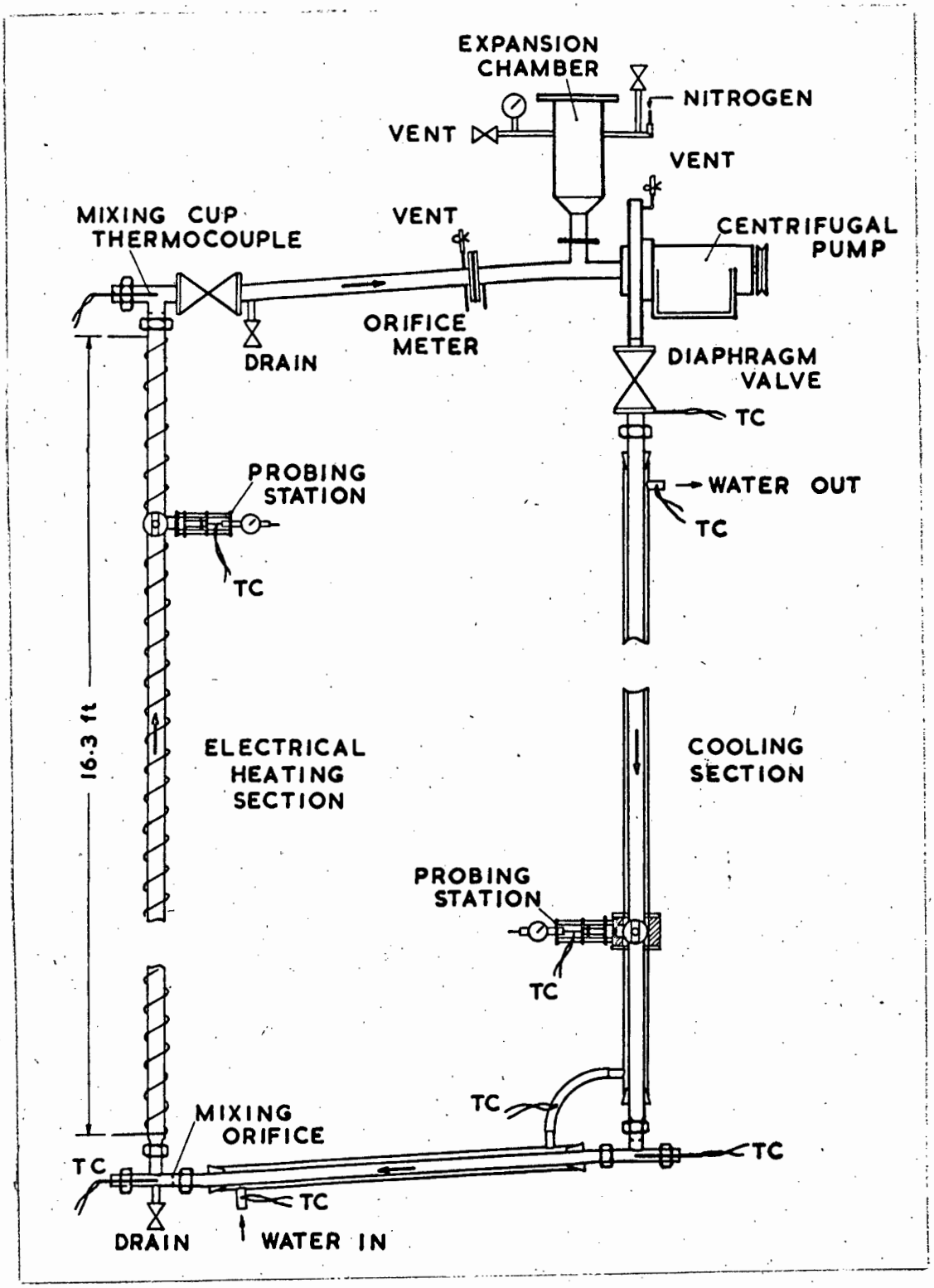

FIG. 3 THE TEST LOOP.

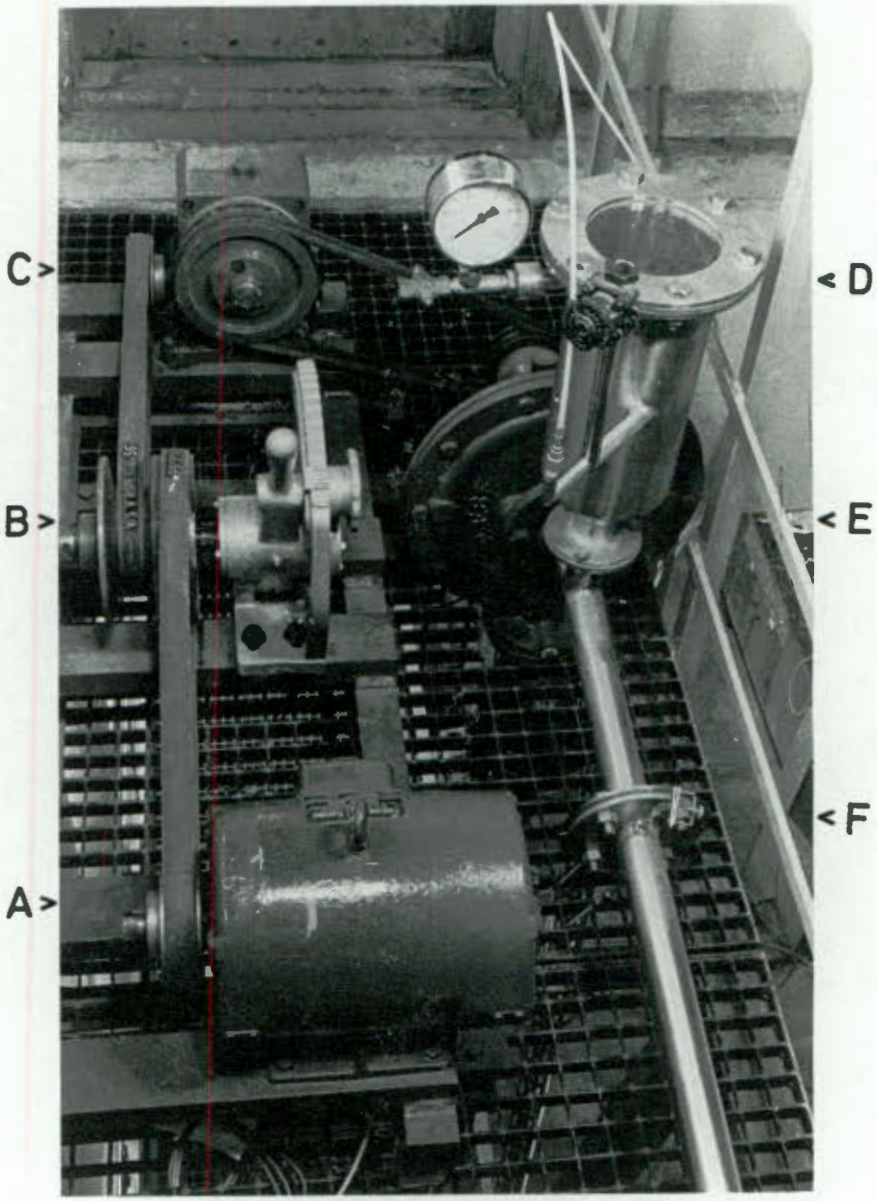

FIG. 4 UPPER PART OF TEST LOOP.

A. Motor B. Variable speed drive C. Reduction gearbox D. Expansion chamber with perspex observation port, mercury filling valve and nitrogen supply E. Centrifugal pump, discharge port facing downwards F. Upper crosslink of loop (insulation removed) showing orifice meter.

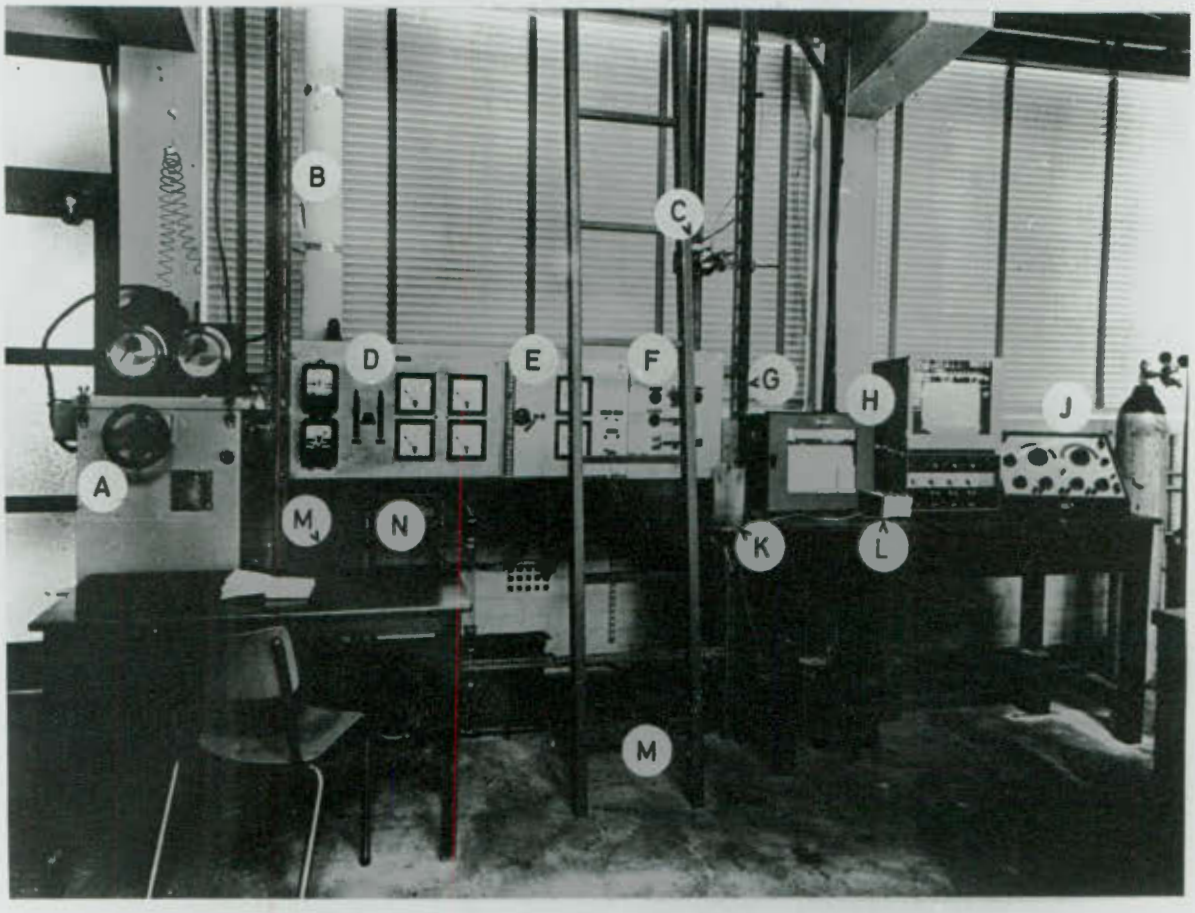

FIG. 5 LOWER PART OF EXPERIMENTAL EQUIPMENT.

A. Variable transformer B. Heated vertical test section C. Cooled vertical test section with cooling jacket, and probing station showing velocity and temperature probes D. Meter panel for upper and lower heating circuits, including variable resistors in lower circuit E. Panel for auxiliary heater F. Thermocouple switching panel G. Thermocouple leads H. Multipoint temperature recorder and millivolt recorder J. Potentiometer K. Double-walled container for ice reference point L. Millivolt reference source M. Supports N. Cooling water supply

heating and cooling test sections is obscured by the control panel.

2.2 TEMPERATURE AND VELOCITY PROBES

Each of the two probing stations consisted of two nozzles welded onto the tube at right angles to each other; one nozzle carried the temperature probe and the other the total-head probe for measuring the velocity profile. A static tap was situated at 135° away from each nozzle, as shown in Fig. 6. The tap consisted of a single 1/16 in. D. hole, carefully deburred, in a plane a short distance upstream from the centreline of the nozzles.

An assembled temperature probe is shown in Fig. 7. The thermocouple was made from 36-guage lacquered iron and constantan wires by discharging a 30-μf condenser across the ends. With some experimentation, a junction could be obtained which was reasonably strong, but no larger in size than the combined diameters of the wires. This thermocouple was then threaded through a 22-guage (0.028 in OD) hypodermic needle which was held by a fibre sleeve and cemented into a 1/8 in. strut with an epoxy resin. The needle was bent down for 7/16 in. to nearly a right angle with the strut and the thermocouple wire itself was bent slightly forward so that, on advancing the probe to the wall, the thermocouple would contact the wall first. The wall position could therefore be accurately determined by electrical contact. The tip of the needle was also sealed with epoxy resin.

The probe carriage was held onto the nozzle by six bolts and traversing of the probe was achieved by a knurled wheel which acted on a threaded spindle locked to the strut. The position of the probe was indicated by a dial guage reading to 0.0002 in. The probe entered the test section through a slit filed in the tube wall. The slit was made just large enough to allow the probe to pass through, so as to minimise disturbance to the flow. Mercury

leakage was prevented by the two neoprene washers shown.

The total-pressure velocity probe was constructed in the same way as the temperature probe. The hypodermic needle, which carried a thermocouple in the temperature probe, was left open in this case, and the end was flattened into a semi-rectangular shape. The hypodermic wall thickness in the region of the probe tip was carefully reduced by using a miniature grinding tool under a microscope, and the tip was then polished with fine emery paper. Outside dimensions of the tip were approximately 0.030 in x 0.017 in, the smallest dimension being in the radial direction. Details are shown in Fig. 8. While the end of the hypodermic needle extended slightly outwards towards the wall, the tip was flattened off normal to the flow direction.

A thin wire was attached to the hypodermic needle of the velocity probe and the wall position was determined by electrical contact and simultaneous visual observation, as also in the case of the temperature probe.

2.3 HEATING SECTION

Two modes of heat input, constant heat flux and constant wall temperature, have been treated theoretically (7,10). Constant heat flux has been most widely used in experimental investigations and this method of heating was employed here, so as to obtain comparable results. A nichrome heating ribbon, $\frac{1}{2}$ in. wide, was evenly wound round the test section, with adjacent windings spaced as closely as possible. The windings were then held in place by pipe clamps, applied over woven asbestos tape, at frequent intervals.

The heating ribbon was separated from the pipe by a layer of woven glass fibre tape. It was found that two layers of 0.007 in. asbestos paper held to the pipe with sodium silicate,

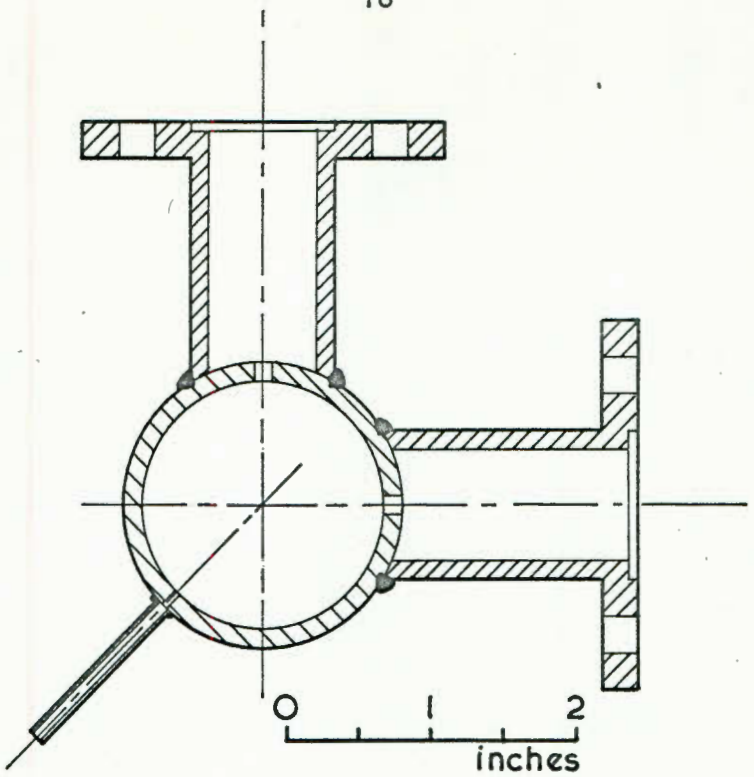

FIG. 6 PROBING STATION NOZZLES AND STATIC TAP.

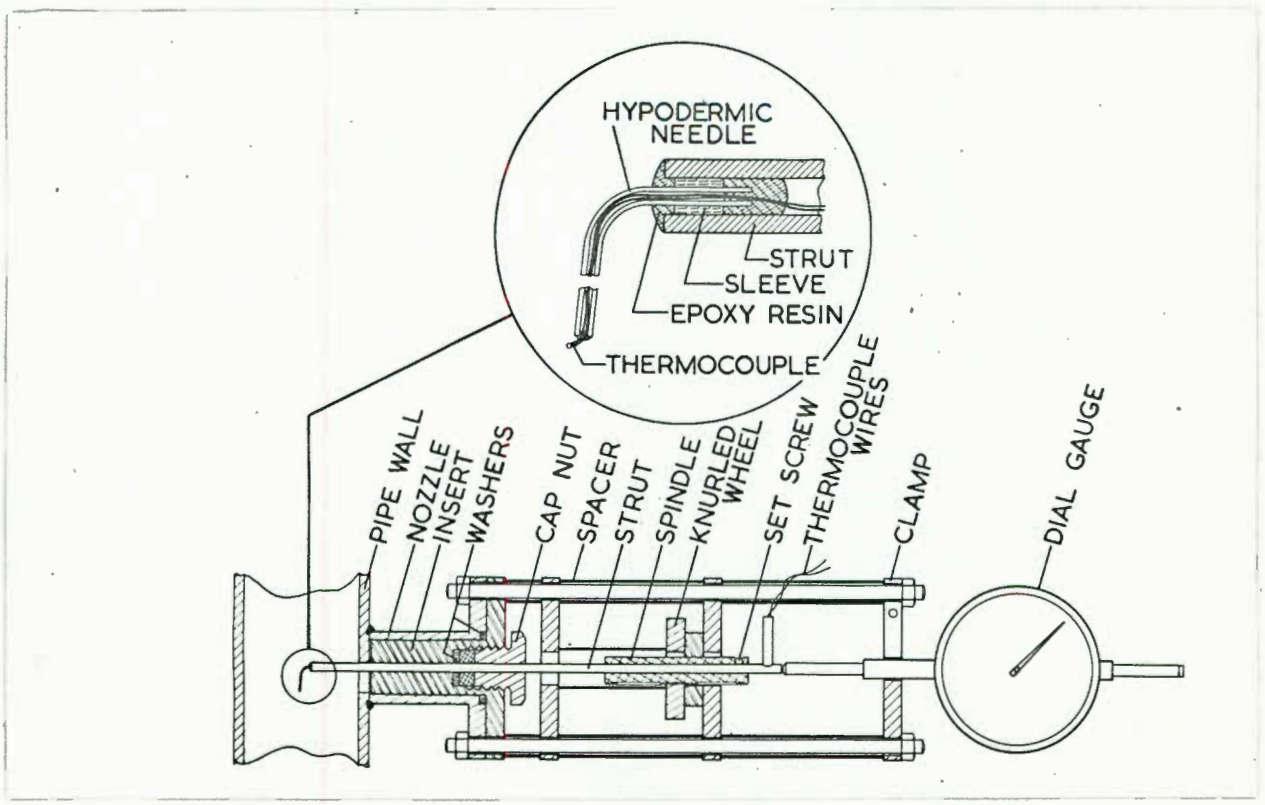

FIG. 7 DETAILS OF TEMPERATURE PROBE.

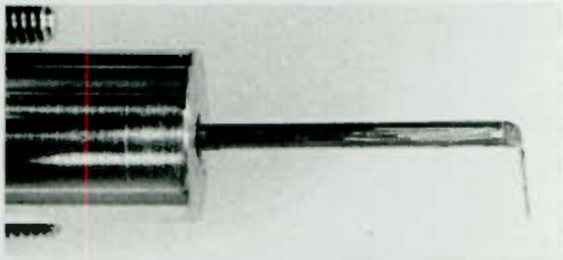

(a) The velocity probe, and part of insert, removed from apparatus.

(b) Detail of probe tip.

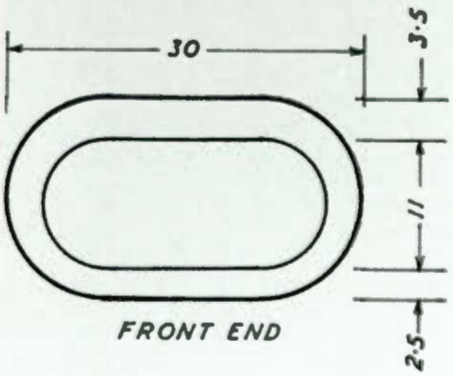

(c) Approximate dimensions of tip, inches x 1000.

FIG. 8 DETAILS OF VELOCITY PROBE.

as recommended by Isakoff (17), did not give sufficient electrical insulation and short-circuiting between the heating coil and the pipe occurred. It is suspected that this may have been due to the moisture content of the asbestos paper and sodium silicate. The glassfibre insulation gave a heating ribbon-to-tube resistance of about 10^5 ohms and will withstand temperatures up to 700° F.

A connection on the heating coil halfway along the test section allowed the heating current to be applied in two parallel sections from a variable transformer capable of supplying a maximum of 100 amps at 160 volts. The resistance of each half circuit was approximately 3.3 ohms which allowed operation at a maximum current of 50 amps through each section. Details of the resistances and areas covered by the heating coil are given in appendix F.1. In order to allow balancing of the rates of heat input through the upper and lower coils an additional variable resistance was inserted into the lower circuit. Each circuit contained an ammeter, voltmeter and an induction-type kilowatt-hour meter, connected as shown in appendix F.1. Heat input was determined by timing a number of revolutions of the disc of the KWH meter.

The main heating coil had to be broken in order to pass over the probing station, and was reconnected with a length of thick copper braid. The area left uncovered was then filled in with an auxiliary winding which consisted of 24-gauge nichrome wire threaded through woven asbestos tape. The area covered by this auxiliary heater was only about one-half of the area left uncovered, the rest being taken up by the probe nozzles. It seems reasonable to assume, however, that the small extent of this area, and the relatively thick pipe wall, would smooth out any irregularities in the heat flux introduced at this point.

The heating section was insulated with asbestos rope and sections of preformed glassfibre pipe insulation. Thermocouples

inserted on the inner and outer surfaces of the latter insulation, just inside the cloth covering, allowed the rate of heat loss to be estimated.

2.4 COOLING SECTION

A jacket of 2.5 in. I.D. PVC pipe was fitted over the cooling test section, as well as over the bottom cross-link. The jacket was held onto the pipe by annular rubber stoppers at either end, and was connected across the probing station by flanging the PVC pipe on either side and fitting a split gasket of thick rubber, shaped to fit over the probe nozzles. Three studs, halfway along the test section, centralised the stainless steel pipe in the jacket. Cooling water was routed through the jacket counter-currently to the mercury flow. By regulating the water flow to be thermally equivalent to the flow of mercury, constant heat flux conditions could thus be obtained. The same procedure was used by Brown et al. (19). Copper-constantan thermocouples in the water jacket allowed the temperature gradient to be determined.

2.5 TEMPERATURE MEASUREMENT

2.51 Thermocouples

Mixing cup temperatures at the inlet and outlet of both the heated and cooled test sections were obtained from iron-constantan thermocouples located at the bends of the test loop. The couples were placed in lengths of 1/8 in. stainless steel tubing welded through caps on the corner tees and sealed with epoxy resin. Mixing was obtained by means of orifice plates, with the orifice just slightly smaller than the pipe ID, welded into the pipes just ahead of the bends. In the case of the inlet to the cooling section, mixing was ensured by the pump, and the thermocouple consisted of an iron wire fixed to a

constantan wire strung across the flow path, the wires passing out through the valve gasket.

Each test section was ringed with a total of ten thermocouples in the vicinity of the probe, cemented into holes drilled 1/16 in. into the pipe wall. Since the exact distance of these thermocouples into the wall could not be determined, readings from these couples could be approximate only, as discussed in appendix B. Further thermocouples indicated the temperatures of the heating coil and auxiliary heater, as well as the insulation and water temperatures already mentioned.

All thermocouples were connected to leads of the same material and taken to a switching panel on the ground floor level. Further details are given in appendix F.2.

2.52 Temperature readings

Certain thermocouples were connected to a Honeywell multipoint recorder, as an indication of the approach to equilibrium, and as a check on operation. Thermocouple readings in general could be measured on a Pye precision potentiometer, reading to 1μV , with reference to either the test section inlet, or to ice. The ice point reference was obtained from a thermocouple placed in a double-walled perspex container filled with crushed ice.

Initial readings for the temperature profile in the heated test section were taken on the potentiometer, using the inlet thermocouple as a reference point. Unsymmetrical profiles were obtained. This discrepancy was corrected by using ice as a reference and it is

presumed that contact between the two couples through the mercury was a cause of the observed asymmetry. Tests on the cooled test section also showed an asymmetry, which could not be corrected by using an external reference point. Extensive tests led to the conclusion that a short-circuit existed within the probe assembly itself. This defect could not be conveniently corrected and temperature profile measurements on the cooling side were consequently abandoned.

Difficulty was experienced in determining an accurate average reading from the fluctuations in temperature observed on the potentiometer, and the probe thermocouple emf was accordingly recorded on a Kipp millivolt recorder. This enabled the average temperature to be accurately estimated. A further improvement was effected by opposing the thermocouple emf with a known standard, nearly equal to itself, thereby enabling the use of a more sensitive recorder scale factor. The reference used in the first instance was boiling carbon disulphide, which was subsequently replaced by the system shown in Fig. 9. A typical temperature profile recording is shown in Fig. 20, in Chapter 4.

2.6 PUMPING AND FLOW MEASUREMENT

Difficulty in pumping mercury has been reported (17) when using rotary gear pumps. In a preliminary test, it was found that an ordinary centrifugal pump gave excellent results when run at low speeds. A 12 in. centrifugal pump was accordingly used in the test loop, and was belt driven by a 3-h.p. motor through a sliding-pulley variable speed

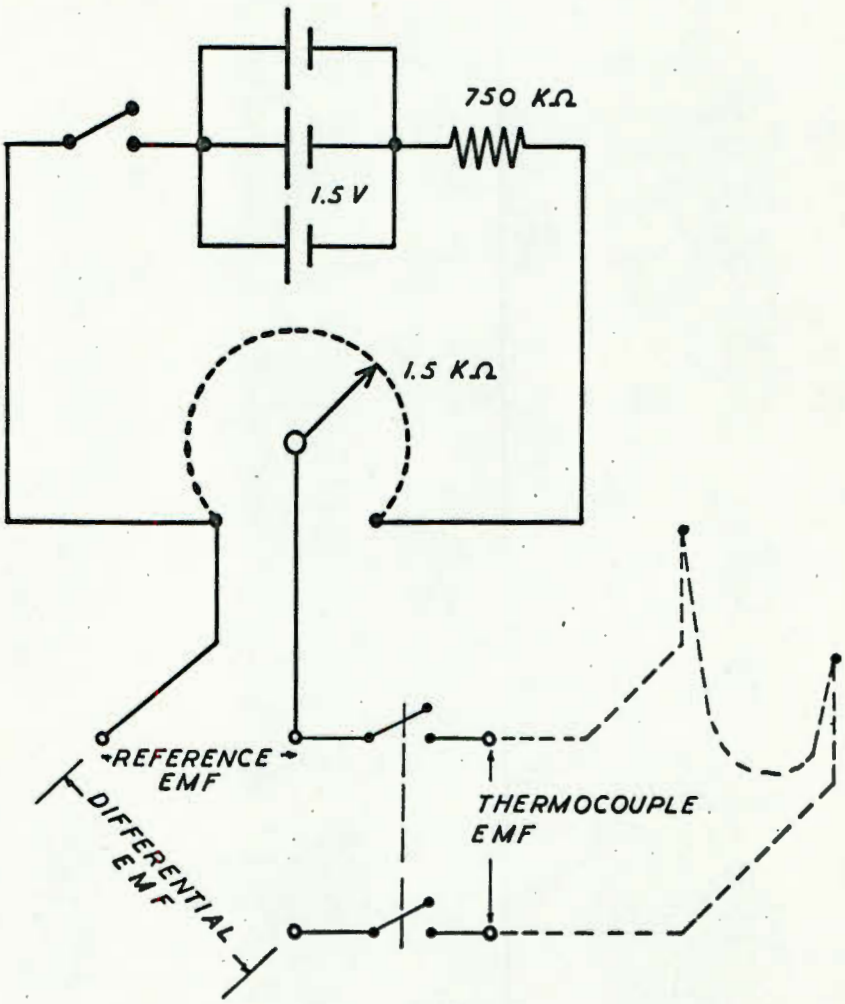

FIG. 9 REFERENCE EMF CIRCUIT.

drive and a 10-to-1 reduction gearbox. This arrangement gave a speed range of 70 to 300 r.p.m. The graphited packing in the pump gland was replaced with Teflon rings to avoid contamination of the mercury and to reduce friction. Little or no mercury leakage occurred.

Flow control was achieved by varying the pump speed and using a diaphragm-type outlet valve. The flow rate was measured with an orifice meter, equipped with an inverted mercury-air manometer. The flow meter had been previously calibrated with water (see appendix F.3) and was mainly used initially to set the flow rate for test runs. Accurate flow rates could be obtained by heat balances over the test section.

2.7 DIFFERENTIAL PRESSURE MEASUREMENT

Measurements of differential pressure were required for the two velocity probes and for the static pressure taps which were installed in the heated test section. The latter taps were the static tap at the probe and another, 149 in. upstream, for measurement of the friction pressure loss. Pressure taps were connected to a switching system on the upper platform through 1/8 in. nylon tubing.

Determination of the velocity profile required the measurement of relatively low differential pressures. This presents considerable problems, and a variety of manometers, inclined manometers and pressure transducers were employed. Initially the apparatus was equipped with a gas pressurising system as used by Isakoff (17), which was subsequently replaced by a form of inclined "Prandtl gauge" and variations thereof.

The gas pressurising system is illustrated in Fig. 10, and consists of two pressure pots, each equipped with inlet

and outlet solenoid valves, which permit a slow leak of nitrogen into or out of the pots. Nitrogen was supplied from a high-pressure cylinder and needle valves allowed the inlet and outlet rates of leakage to be adjusted. Each of the two relevant mercury legs were connected to a contact cell which was in turn connected to the pressure pot, and the nitrogen pressure in this vessel was intended to counter-balance the mercury pressure. Contact between the mercury level and a tungsten electrode actuated the solenoid valves to control the nitrogen pressure. Suitable capacitors over the contact point prevented excessive sparking and "chatter". The gas pressure was then measured on an inclined water manometer. This system effected an approximately 100-to-1 amplification compared with a vertical mercury manometer.

Another type of mercury manometer used is shown in Fig. 11, and utilises the well known principle of one large and one small leg, where the movement is essentially confined to the small inclined calibrated leg shown in the figure. The large glass vessel shown was supported on the stand of a travelling telescope and could thus be moved so as to obtain a convenient zero position, and readings taken on the inclined manometer, or alternatively the system could be operated on the null principle, whereby the large vessel is moved to return the level in the inclined leg to the null position and the pressure difference is read on the vernier scale of the travelling telescope. The space above the mercury was filled with de-aerated water.

2.8 TESTING AND FILLING

In order to allow the ready escape of gas on filling the apparatus, the crosslinks connecting the two vertical

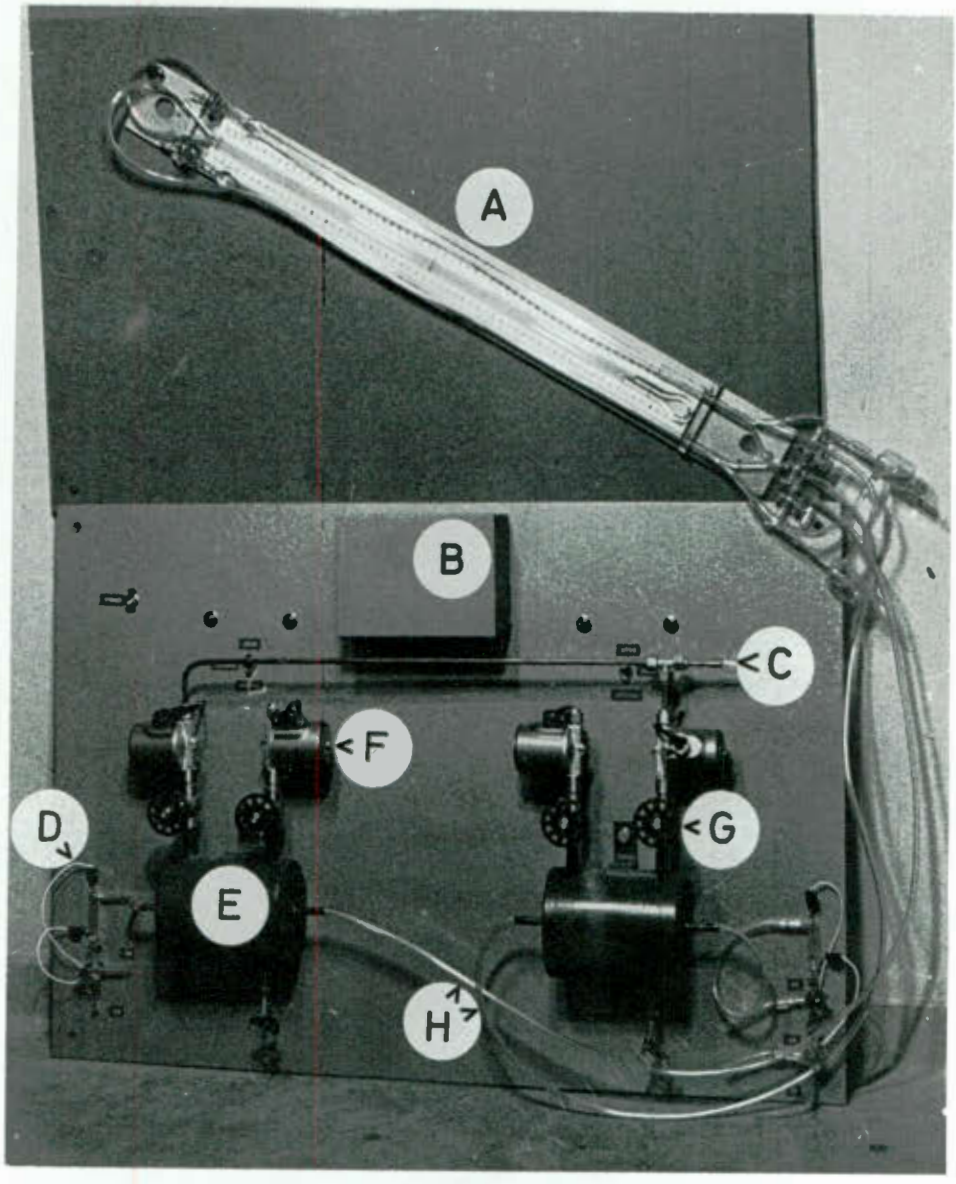

FIG. 10 GAS PRESSURING MANOMETER SYSTEM.
(Disconnected from apparatus).

A. Adjustable inclined manometer B. Relay switching box. (Electric wiring runs behind panel C. Nitrogen inlet (Supply disconnected) D. Contact cell (mercury pressure leads disconnected) E. Pressure pot F. Solenoid valve (on outlet) G. Needle valve (on inlet) H. Leads to manometer.

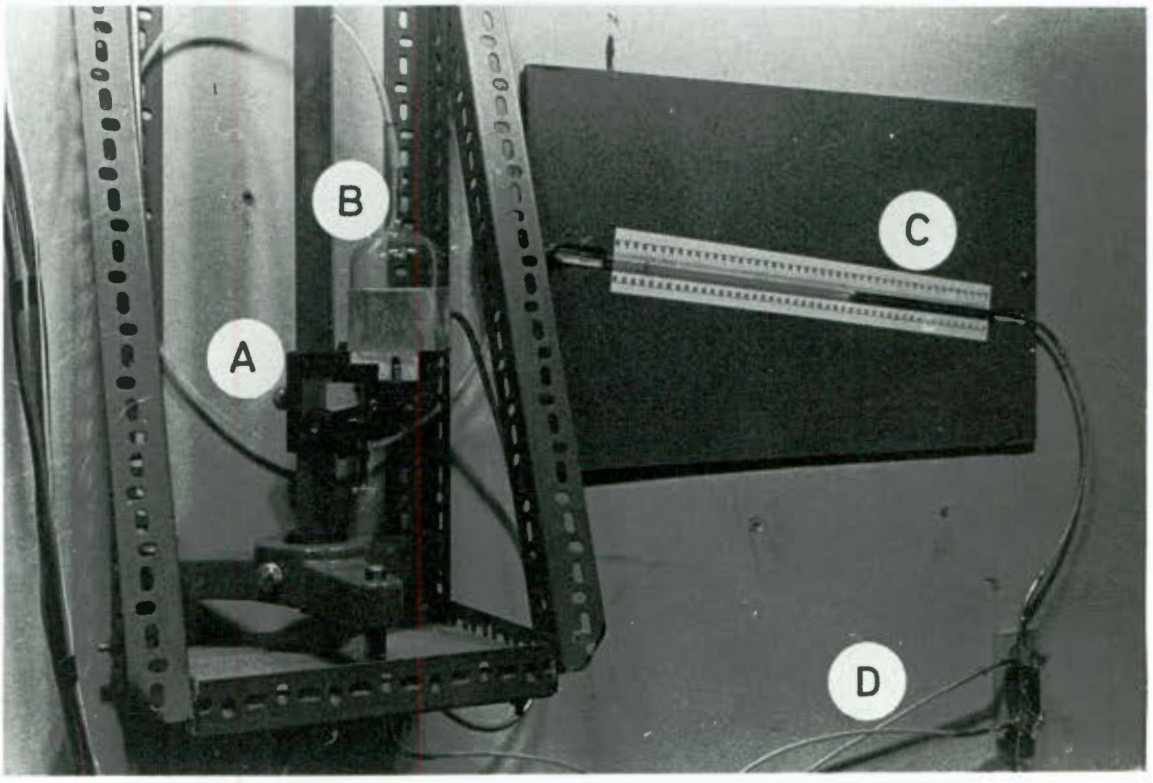

FIG. 11 NULL-TYPE DIFFERENTIAL MANOMETER.

A. Reservoir carriage with vernier slide B. 3-in. D. reservoir (mercury level obscured) C. Inclined tube D. Pressure leads from equipment.

test sections were given an upward slope. Air vents were installed just upstream of the orifice meter and on the highest point of the pump to allow residual gas to be bled off.

An expansion chamber, to allow for expansion of mercury during heating, was provided at the top of the loop. This vessel was off-set from the main flow path so as to obviate the gas entrainment problems encountered by other workers (17,27), and incorporated the mercury filling valve, a nitrogen supply and a bleed valve.

Before charging, the loop was pressurised to 20 psi and all leaks, as indicated by a soap bubble test, were eliminated. Connections in this loop were either flanged or union-type fittings with cork gaskets on the faces. After testing, the loop was filled with carbon tetrachloride which was then pumped around the system to remove any oily contamination. The loop was then drained, dried out with nitrogen, and filled with mercury until the level, observed through the perspex top of the expansion chamber, was well into that vessel. Filling the apparatus required 680 lb. of mercury.

A drain point was provided at the lowest point of the loop. The drain valve was connected by means of a hose to a steel box which served as an emergency dump tank.

CHAPTER 3

VELOCITY PROFILES AND THE EDDY DIFFUSIVITY OF MOMENTUM

3.1 EXPERIMENTAL WORK

In order to measure velocity profiles, the centrifugal pump was switched on and the variable speed drive advanced until the desired flow rate, indicated on the orifice meter, was reached. Cooling water was run through the jacket in order to prevent temperature changes in the mercury. The total-pressure probe was then advanced to the desired radial position and the differential pressure between the probe and the static tap measured.

About 40 experimental runs were carried out, under isothermal conditions, both with mercury and with air as the test fluid, and using a number of pressure measuring devices. In general, the results can not be considered to be reliable, due to certain deficiencies in the experimental equipment which became apparent during the course of the experimental work. The extent of the experimental attempts to measure velocity profiles is briefly outlined below. In a further section the available literature is reviewed and values of the eddy diffusivity of momentum are recommended.

3.11 Profiles in mercury

Initial tests showed that an inverted mercury manometer was not sensitive enough to measure the differential pressures obtained. A gas pressurising system as used by Isakoff (17) and described in Chapter 2 was therefore built. By this means the

mercury pressure was transduced into a gas pressure which could be measured on an inclined water manometer. On an 8:1 inclination, this produced an increase in sensitivity of about 110. Fluctuations in the readings were observed, but by careful adjustment of the inlet and outlet needle valves on the pressure pots, fluctuation of the mercury level in the contact cells were reduced to a minimum and insertion of lengths of capillary tubing in the manometer leads removed any residual fluctuations on the manometer.

Results for a number of runs are compared on a u^+ vs. y^+ basis with the universal relationship of von Karman (4), equn. 1.5, in Fig. 12. Typical calculations are shown in appendix A. Good agreement is obtained over the central portion of the tube, but in the vicinity of the wall, results fall above the von Karman curve. It was considered, however, that the readings near the wall might be in error, since the pulsing of the mercury in the contact cells would create conditions of alternate suction and blowing at the probe tip, and this would interfere with the pressure reading, particularly at low velocities.

Since it was thus concluded that the gas pressurising method would not give accurate results, a null-type Prandtl gauge, as described in Chapter 2, was constructed. It was possible to read this instrument more accurately than a manometer, although the advantage of a lighter manometer fluid was lost. (An attempt was made to construct a type of inverted Chattock manometer, which measures the movement of an air bubble in water along a capillary tube, caused by the displacement of water

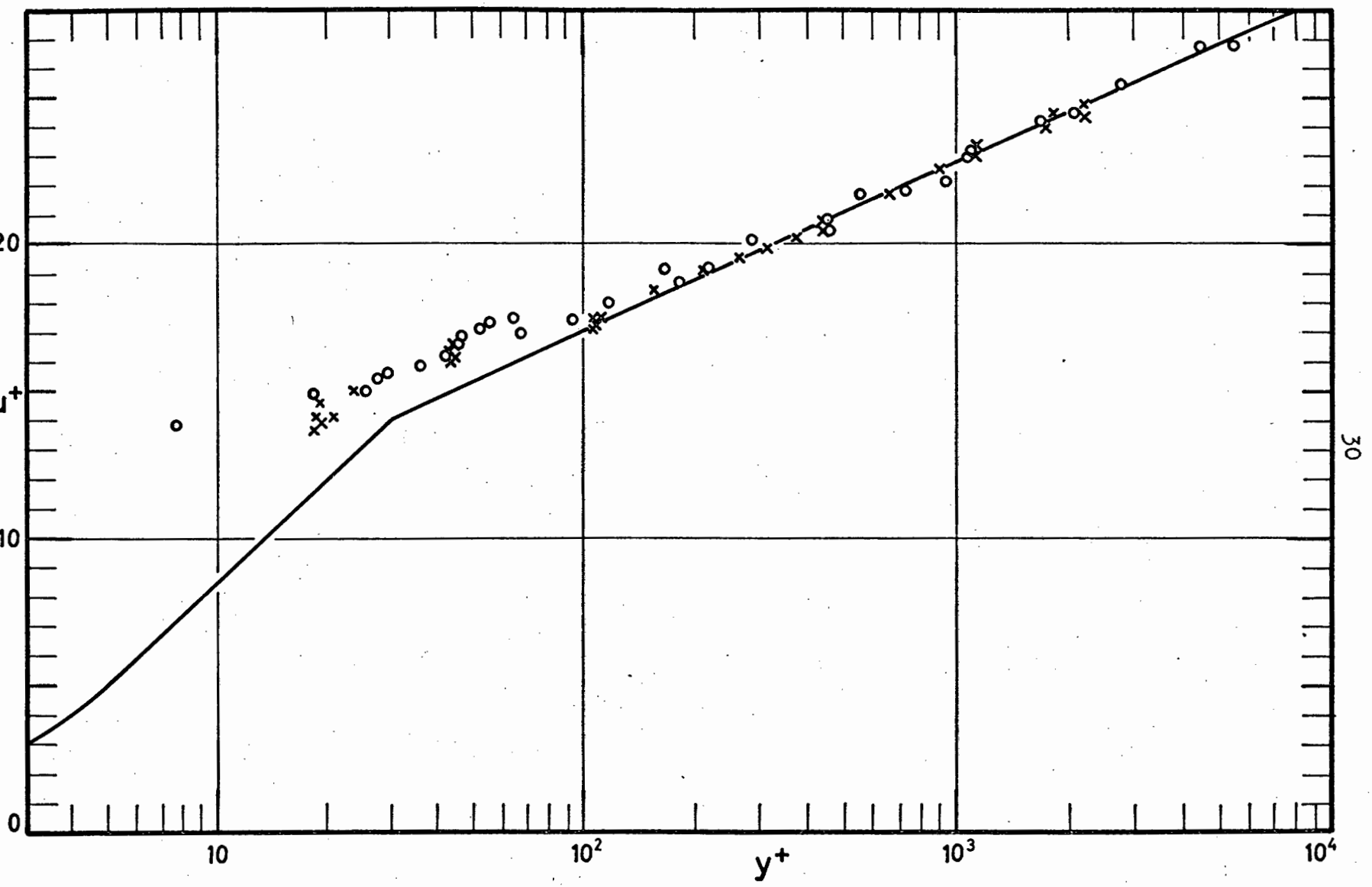

FIG. 12 VELOCITY PROFILES IN MERCURY.

—— Equn. 1.5 o Runs using gas pressuring system x Runs using null gauge

by mercury in a wider vessel. This apparatus proved very awkward in operation and the method was discarded). Results of runs with the Prandtl gauge are also shown in Fig. 12. Data points near the wall are closer to, but definitely above, the von Karman curve.

3.12 Profiles in air

Since it is known that air follows the universal velocity profile, the apparatus was drained of mercury in order to measure the velocity profile in air, and thus to obtain a check on the correct functioning of the probe and static tap system. At the same time the probe was removed and inspected for defects but found to be in good condition. A vertical hexane manometer was connected and a number of velocity profiles measured by blowing air through the test section.

No appreciable improvement was obtained in the velocity profile plotted on a dimensionless basis. However, a degree of asymmetry in the differential pressure measurements taken on either side of the tube centre, was noticed. The static pressure reading was then observed while traversing the total-pressure probe over the tube cross-section. A definite increase in the pressure at the static tap was recorded as the probe approached the wall, as shown in Fig. 13. As a check, the observed difference in the static pressure reading was subtracted from the differential pressure readings taken in the normal way under the same conditions, and good agreement with the von Karman relations was found. It thus appears that the presence of the total-pressure probe interfered with the reading of the static tap.

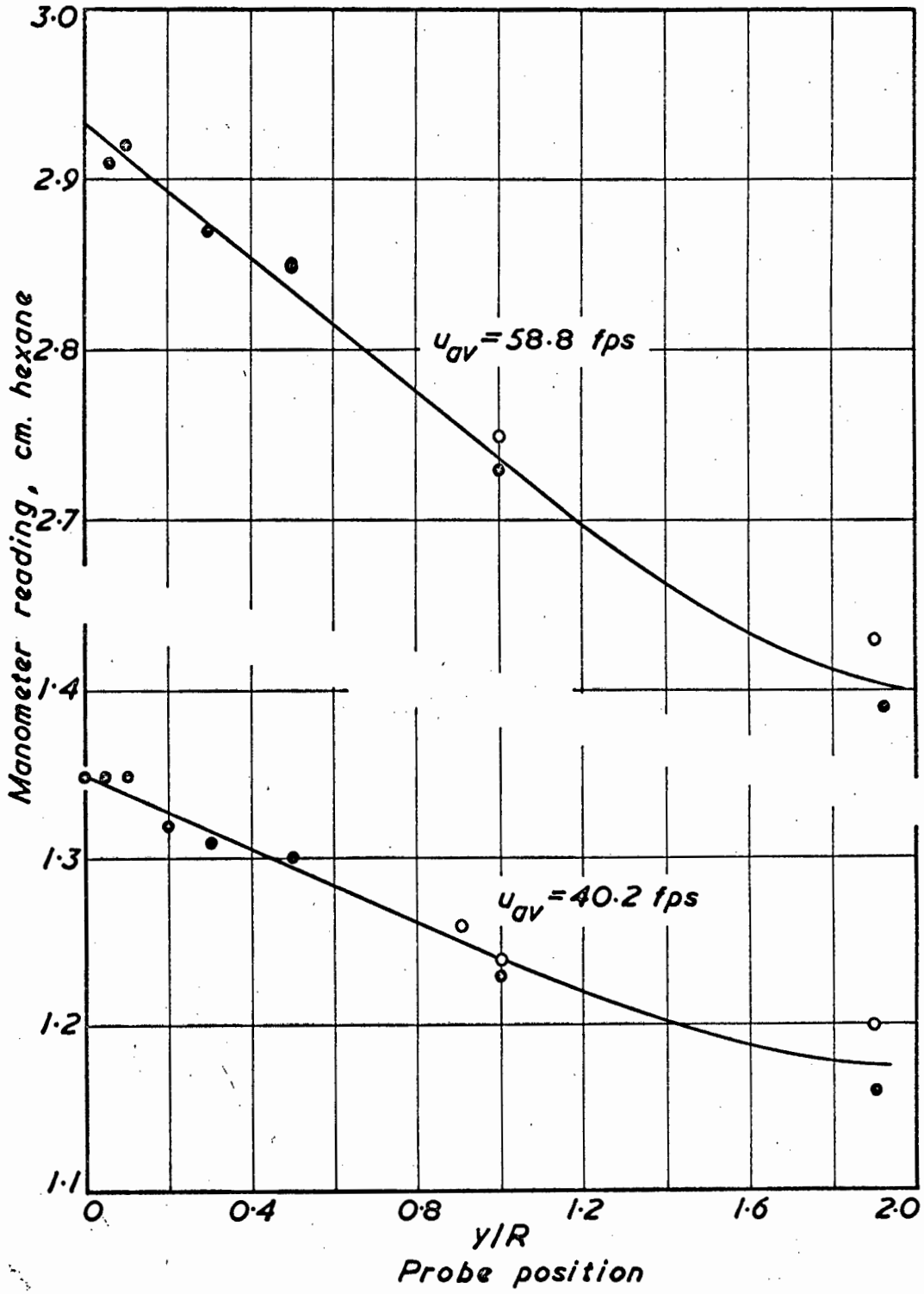

FIG. 13 INFLUENCE OF PROBE POSITION ON PRESSURE READING AT STATIC TAP.

Test fluid: Air. ● Probe travelling towards wall ○ towards centre

It must therefore be concluded that, in general, the use of a single static hole for differential-pressure measurement can lead to erroneous results, and the use of a piezometer ring is strongly recommended.

In order to eliminate the effect of interference on the static tap, a number of runs were carried out by taking total-pressure readings only. The static reading was taken at the beginning and end of a run, with the probe retracted as far as possible. This procedure is admittedly open to error, but was used to determine whether or not the test loop would give profiles in agreement with the universal velocity distribution. Results are shown in Fig. 14. Fair agreement is obtained and it may be concluded that the test section is hydrodynamically sound.

3.13 Further work in mercury

The test loop was cleaned and refilled with mercury, and a new pressure measuring device constructed, for measuring probe and static tap pressures separately. This consisted of a 3-in D glass vessel, connected at the bottom to the pressure tap and at the top to an inclined capillary tube. Mercury filled half of the vessel and the rest of the space was occupied by water, which extended into the capillary. A very small movement of the mercury level thus caused a large water level change so that the apparatus essentially acted as a transducer from a mercury pressure to a water pressure. With a 10:1 inclination on the capillary tube, a sensitivity of well over 100 was obtained. The apparatus was calibrated and the zero could be set by adjusting the 3-in. vessel. Runs were carried

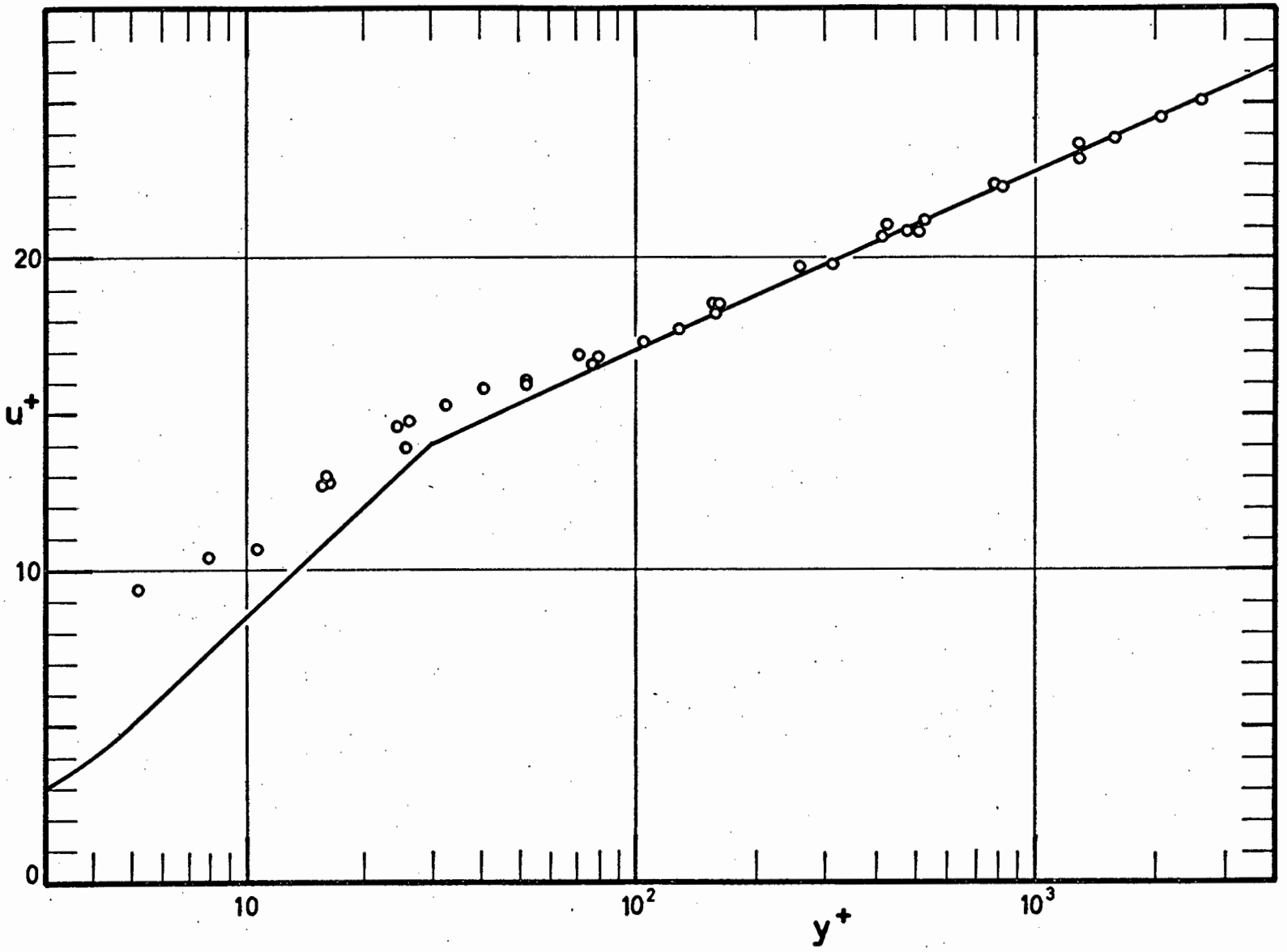

FIG. 14. VELOCITY PROFILES IN AIR.

— Equn. 1.5 o Experimental data obtained from total-pressure readings.

out by reading the pressure at the total-pressure probe only, with static pressure readings at the beginning and end of a run, as before. When the resulting velocity profiles were integrated for average velocity, and compared with the reading of the orifice meter, no consistent agreement could be obtained, and it was thus concluded that the above method of measurement could at best give approximate results.

In the light of the foregoing conclusions, further attempts to determine the velocity profile in mercury, in the present apparatus, were abandoned at this stage, and the second phase of the work, measurement of temperature profiles, started. It is still necessary, however, to obtain values of ϵ_M for mercury, if the ratio of eddy diffusivities is to be calculated. From the approximate velocity results of Fig. 12 it seems reasonable to assume that mercury behaves in the same way as other Newtonian fluids and will follow the universal velocity distribution. In other respects a similarity in the behaviour of mercury and other fluids has been demonstrated. Grigull and Tratz (40), for example, have shown that the friction pressure drop in mercury follows the Hagen-Poiseuille and the Blasius equations.

The universal velocity distribution and the eddy diffusivity of momentum for the common fluids, notably water and air, are examined in the following sections, and it will be assumed that these relations apply to mercury as well.

3.2 THE UNIVERSAL VELOCITY PROFILE

The division of the boundary layer next to a solid

surface into laminar, buffer and fully turbulent layers, following the concepts of Prandtl (41) and von Karman (4,42), is well known. The velocity distribution in the first two layers may be described by

$$0 < y^+ < 5, \qquad u^+ = y^+ \quad \text{(laminar layer)} \tag{1.5a}$$

$$5 < y^+ < 30, \quad u^+ = -3.05 + 5 \ln y^+ \quad \text{(buffer layer)} \tag{1.5b}$$

These simple equations are only approximate and more complex relations have been proposed (43, 44) to give a smoother transition between the three layers and to account for the presence of turbulent fluctuations in the "laminar" layer. In the study of velocity profiles, however, these layers usually form only a small part of the total profile and the approximate relations given above will be satisfactory.

3.21 The turbulent boundary layer

For the turbulent boundary layer, ν is usually negligible in comparison with ϵ_M and equn. 1.2 may be written as

$$(\tau_w/\rho)\ \psi(y/R) = \epsilon_M\ (du/dy) \tag{3.1}$$

where $\psi(y/R)$ represents the variation of the shear stress across the width of the boundary layer. For flow in circular pipes $\psi(y/R)$may be shown to be linear with radius on the assumption of constant radial static pressure. This has been experimentally confirmed by Laufer (45) and equn. 3.1 thus becomes

$$u^{*2}\ (1 - y/R) = \epsilon_M\ (du/dy) \tag{3.2}$$

where u^* is defined as $\sqrt{\tau_w/\rho}$ and is known as the friction velocity.

Prandtl (41) proposed, as a simplification, that, in the region close to the wall, the shear stress may be taken as constant at the wall value and the size of the eddies are dependent only on the distance from the wall, i.e.

$$l = K y \tag{3.3}$$

where l is the Prandtl "mixing length" or eddy size. It is easily shown that the eddy diffusivity of momentum is the product of l and the friction velocity, so that

$$\epsilon_M = K y u^* \tag{3.4}$$

Substituting the Prandtl proposals into equn. 3.2 gives

$$u^{*2} = K y u^* (du/dy) \tag{3.5}$$

which, on integration, becomes

$$u/u^* = (1/K) \ln y + C . \tag{3.6}$$

In order to render the right-hand side of this equation dimensionless, Prandtl introduced the length parameter ν/u^*. This was used in preference to the radius R in accordance with the postulate that the distance from the wall is the only significant dimension in the conditions considered here. Thus by letting

$$C = A - (1/K) \ln (\nu/u^*) \tag{3.7}$$

equn. 3.6 becomes

$$u^+ = A + B \ln y^+ \tag{3.8}$$

where $u^+ = u/u^*$, $y^+ = yu^*/\nu$ and $B = 1/K$.

On applying this relationship to the velocity distribution data obtained in pipes, it was found to represent the data quite well right up to the pipe centre, and not only in the region close to the wall. Values for the constants A and B have been proposed by various workers,

the best known equation being that given by Nikuradse (9),

$$u^+ = 5.5 + 2.5 \ln y^+ \qquad (3.9)$$

This simple relation gives a good fit to the bulk of the experimental data, but some discrepancies emerge when single traverses are plotted, as shown in Fig. 15. Ross (46) pointed out that the logarithmic line is a good fit only for y/R up to 0.15 and that this line has a slope of 2.43. Beyond y/R = 0.15 it therefore appears that u^+ depends also on the radius and that a correlation of the dimensionless velocity against y/R would be more appropriate than a correlation against y^+.

An approach which recognises that the u^+ vs. y^+ form of correlation is not applicable to the central portion of the tube is known as the "defect profile", where the velocity defect, $(u_c^+ - u^+)$ is plotted against the radial position y/R. Such a plot appears to be universal (47) and Hinze (48) has suggested a relation, partly based on the logarithmic profile, but incorporating a correction dependent on radial position,

$$u_c^+ - u^+ = -2.44 \ln (y/R) + 0.8 + h(y/R) \qquad (3.10)$$

where h(y/R) is the radial correction evaluated from Laufer's (44) data.

The eddy diffusivity of momentum depends on the slope of the velocity profile and is thus very sensitive to the shape of the profile. While the velocity relationships discussed above give a good representation of the velocity profile itself, they are not necessarily accurate enough for the evaluation of ϵ_M, and it is thus advisable to investigate actual values of ϵ_M obtained by experiment.

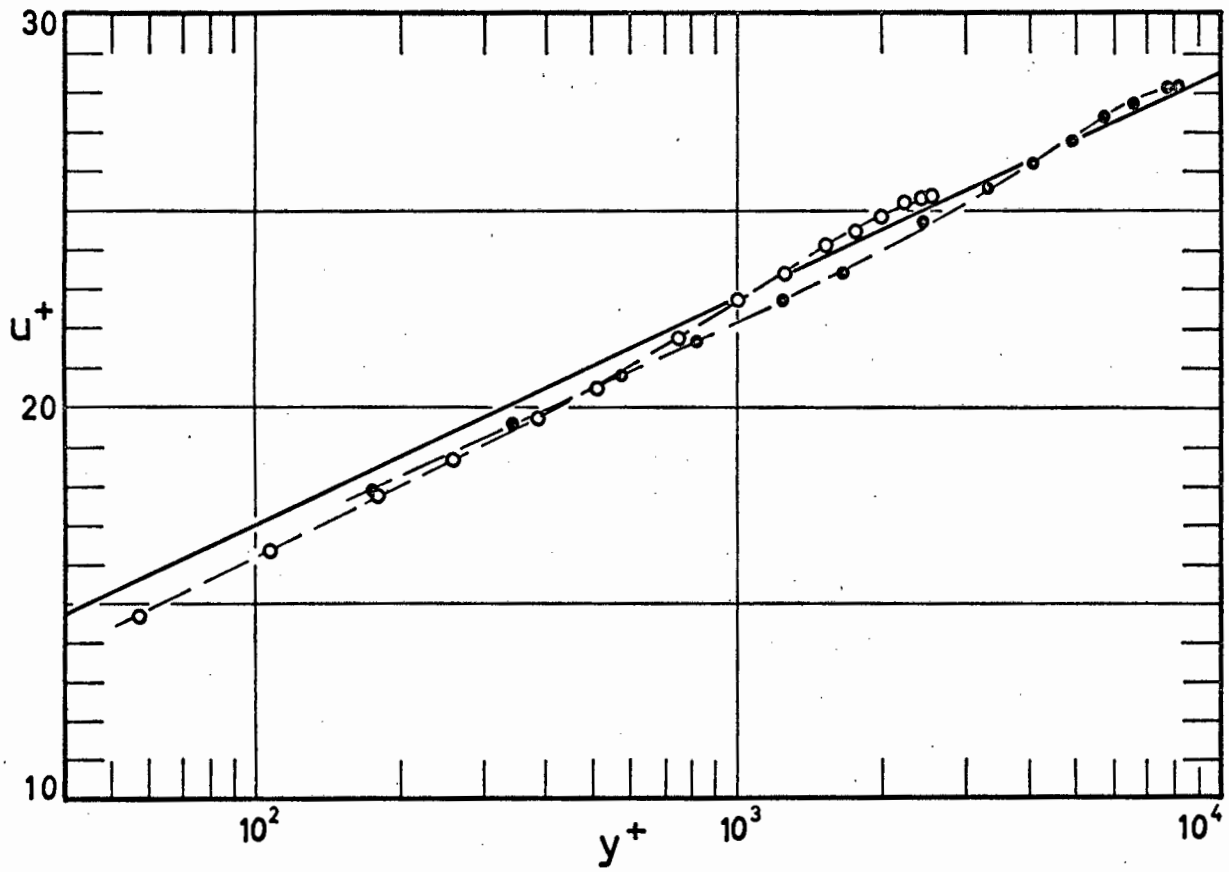

FIG. 15 COMPARISON OF SINGLE VELOCITY TRAVERSES WITH EQUN. 3.9

—— Equn. 3.9, $u^+ = 5.5 + 2.5 \ln y^+$

– –o– Nikuradse (9), Re = 105 × 10³

– –●– -do- Re = 396 × 10³

3.3 THE EDDY DIFFUSIVITY OF MOMENTUM, ϵ_M.

A comprehensive series of velocity profile measurements in water was carried out by Nikuradse (9), who calculated values of ϵ_M and presented the data in the form ϵ_M/Ru^*, plotted vs radial position. This appeared to be a universal curve for Reynolds numbers above 10^5, with values increasing slightly at lower Re. Values of this dimensionless group may be calculated from a velocity profile by the relation

$$\epsilon_M/Ru^* = \frac{(1 - y/R)}{du^+/d(y/R)} \qquad (3.11)$$

which is obtained by rearranging equn. 3.2.

Values of ϵ_M/Ru^* calculated from equn. 3.11 are shown in Fig. 16 for the data of Laufer (45), Stanton (49), Sleicher (50) and Rein (51) in air, Sesonske et al. (35) in mercury, Beckwith and Fahien (52) in water, and Page et al. (53) for air in channels. Slopes of the velocity profiles were determined as derivatives of a least-squares second-order polynomial passed through five points in the immediate vicinity of the point under consideration. By plotting the straight lines resulting from the differentiation, a very good impression of direction changes in the slope curve could be obtained. The procedure is illustrated and typical calculations for ϵ_M/Ru^* are shown in appendix E.

From the data plotted in Fig. 16, the concept of a universal curve for ϵ_M/Ru^* appears to be a reasonable one. Bearing in mind that a very small difference in the velocity profile can cause an appreciable change in ϵ_M, the agreement obtained for the flow of air, water and mercury in pipes over a wide range of Reynolds numbers is good. The spread of the data can probably be attributed to experimental error and

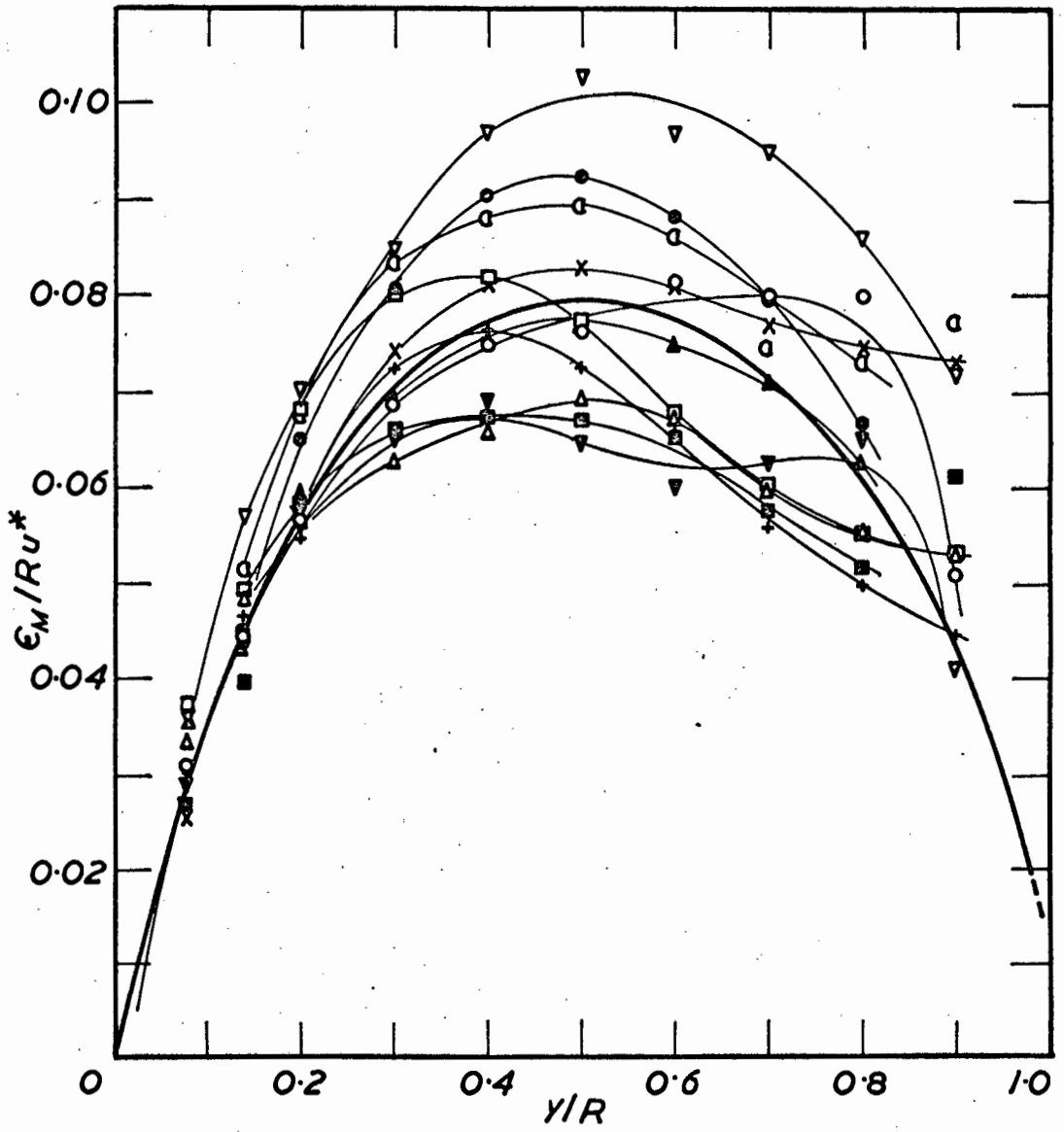

FIG. 16 VALUES OF ϵ_M/Ru^* FROM VARIOUS SOURCES

—o— Laufer (45), Re=428,000 ×Air
—▼— Laufer (45), Re=40,300 Air
—+— Rein (51), Re=36,700 Air
—■— Sleicher (50), Re=40,000 Air
—▲— Stanton (49), Re=40,900 Air
—x— Page et al. (53), Re=53,200 Air, in channels.
—▽— Beckwith and Fahien(52), Re=18770 Water
—o— Sesonske et al. (35), Re=99,000 Hg
—▲— Sesonske et al. (35), Re=62,000 Hg
—□— This work, Re=89,200 Hg
—o— This work, Re=89,700 Hg
—— Nikuradse (9), Re > 10^5 Water

differences in experimental technique. The eddy diffusivity data for channels are in good agreement with those for pipes.

Some well known profile measurements have not been included here. The data of Reichardt (54) and Deissler (55) are often quoted, but the former has indicated that his experimental values for u^* were incorrect and his data have therefore been omitted; Deissler's experimental equipment had a single static pressure hole rather than a piezometer ring, and during measurements, the probe closely approached this static hole. This procedure, as discussed in Section 3.12 can lead to erroneous results.

While the measurements of Nikuradse indicated a slight increase in ϵ_M/Ru^* for $Re < 10^5$ such a trend is not detectable in the data of the other investigators, and for the purposes of this work, the existence of a universal relationship of ϵ_M/Ru^* vs y/R will be assumed. It now remains to determine the correct form of this relationship.

3.31 The recommended form of ϵ_M/Ru^* vs y/R.

Miller (56) has shown that Nikuradse apparently adjusted his values of y^+ by a figure of 7, and Ross (46) has indicated that the low-Re profiles are not accurate, but apart from these criticisms, which do not affect the profiles away from the wall and at the higher Reynolds numbers, the data of Nikuradse have gained wide acceptance. In the same way the more recent data of Laufer (45) who reported profiles at Reynolds numbers of 40,300 and 428,000* measured in a 10-in.

---

* The values of 50,000 and 500,000 given by Laufer are based on pipe-centre velocities.

pipe, are generally considered to be accurate. This applies particularly to the data for Re = 428,000, which are more frequently quoted, as, for example, by Hinze (48).

It is therefore likely that the average curve of Nikuradse ($Re > 10^5$) and the curve of Laufer for Re = 428,000 represent the most accurate values of ϵ_M/Ru^*. These two curves are in good agreement up to $y/R = 0.50$. They also agree with the relation

$$\epsilon_M/Ru^* = \frac{y/R}{2.43}(1 - y/R) \qquad (3.12)$$

up to $y/R = 0.10$. This equation is obtained by differentiation of the relation of Ross (46) for the region close to the wall. The fact that a reasonable fit here exists only to $y/R = 0.10$ instead of 0.15 as found by Ross, illustrates again the sensitivity of ϵ_M as a measure of the shape of the velocity profile. The above relation is not shown in Fig. 16, to preserve the clarity of the diagram, but values are easily calculated.

Beyond $y/R = 0.50$ the wider disagreement between the curves reflects the difficulties experienced in determining accurate slopes in an area where the velocity profile is relatively flat. It must thus be accepted that relatively large errors are possible in this region, but an attempt will be made to estimate the probably correct shape of ϵ_M/Ru^*.

A number of workers favour an approximately constant eddy diffusivity in the central portion of the tube. Hinze (57) presents a curve of ϵ_M/Ru^*, based on Laufer's data at Re = 428,000, which rises to a maximum at $y/R \approx 0.35$ and then falls to a slightly lower, constant value. (This description does not quite agree with the curve of Laufer given in Fig. 16. The data presented here are believed to be correct).

Wasan et al. (58) suggest a value of

$$\epsilon_M/\nu = 0.082\ (Re/2)\ \sqrt{f/2} \qquad (3.13)$$

for the central core. This is equivalent to a constant value of $\epsilon_M/Ru^* = 0.082$, which is only slightly higher than the maximum of Nikuradse's curve and the average value for Laufer's curve above $y/R = 0.35$. It has been suggested by Clauser (59) that, in the outer portion of the boundary layer eddy size should depend only on the boundary layer thickness. For flow in pipes, this would be equivalent to

$$\epsilon_M = K\ R\ u^*, \quad \text{or} \quad \epsilon_M/Ru^* = K \qquad (3.14)$$

When such an assumption of a constant ϵ_M/Ru^* is substituted into equn. 3.11, integration gives the velocity profile

$$u_c^+ - u^+ = \frac{1}{2K}\ (1 - y/R)^2. \qquad (3.15)$$

Some support for this relation is found; Stanton (49) suggests an equation of the form

$$u_c - u = A\ (1 - y/R)^2 \qquad (3.16)$$

to represent his data, where the constant A is stated to be proportional to u_c. Pai (60) derived the semi-empirical velocity distribution equation

$$u/u_c = 1 - 0.204\ (r/R)^2 - 0.796\ (r/R)^{32} \qquad (3.17)$$

and if the last term on the right is neglected near the tube centre, where r/R is small, this relation may be written as

$$u_c - u = 0.204\ u_c\ (1 - y/R)^2 \qquad (3.18)$$

This is of the same form as equn. 3.15 and therefore, in the same way as Stanton's relation, implies that ϵ_M/Ru^* is constant.

While a constant value of ϵ_M/Ru^* in the central portion of the tube is an attractive concept, the corresponding velocity distribution, equn. 3.15, does not agree with the experimental data near the tube centre. This is clearly shown in Fig. 17, where equn. 3.15, with $K = 0.08$ and 0.06 is compared with the

experimental data of various investigators. From the figure it appears that this equation does not have the right shape to fit the data. A much lower value of K will be required to give a good fit at $y/R = 0.90$ than is required at $y/R = 0.70$.

A better representation of the data is obtained by the equation of von Karman as given by Nikuradse (61)

$$u_c^+ - u^+ = -\frac{1}{K}\left[\ln\left(1 - \sqrt{r/R}\right) + \sqrt{r/R}\right] \qquad (3.19)$$

which is also shown in Fig. 17, with the value of $K = 0.30$ recommended by Ross (46). This velocity distribution equation corresponds to an eddy diffusivity of momentum which is not constant, but decreases as the tube centre is approached, and is in good agreement with Nikuradse's curve.

It is obvious from the above considerations that the shape of the ϵ_M/Ru^* curve near the pipe centre is critically affected by the precise form of the velocity distribution. The appreciable differences in values of ϵ_M/Ru^* exist largely because the velocity profile is very flat in the central portion of the pipe and slopes are therefore very difficult to determine accurately. Nikuradse was aware of this problem (62) and made a special effort to take measurements close to the pipe centre. The resulting curves of slope of the velocity profile, shown in Fig. 18, have an unexpected shape in comparison with the straight line connecting $y/R = 0.50$ and the centre. This straight line corresponds to a constant value of ϵ_M/Ru^*. Closer investigation of the slopes of other workers, calculated by the curve fitting procedure already mentioned, and given in Fig. 18, also show a tendency for the curve to flatten off near the centre, rather than to approach a zero slope gradually, as might be expected. Lynn (63) has suggested that Nikuradse's data should be flattened off to give a more obviously flat profile near the centre, but this

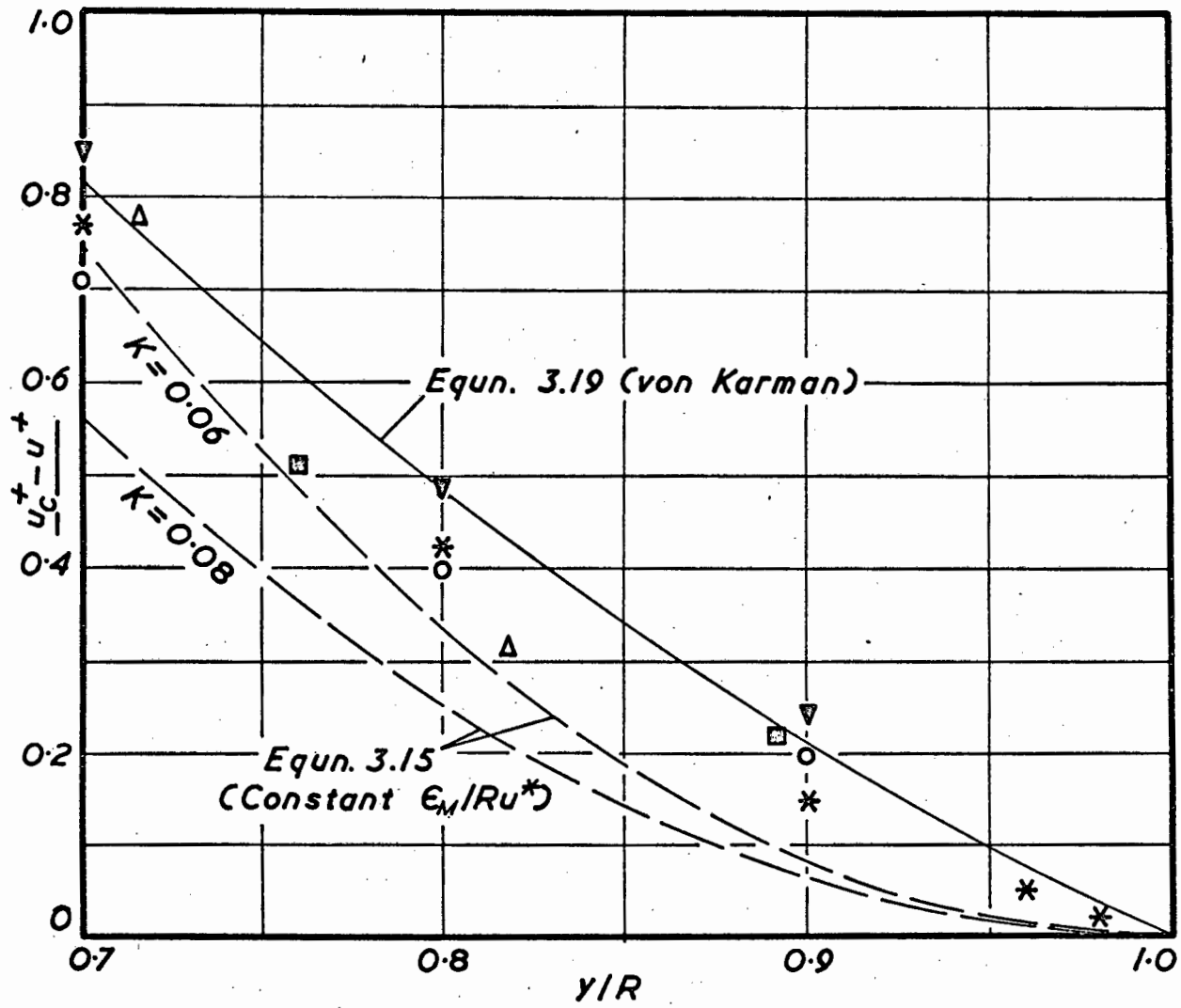

FIG. 17 COMPARISON OF VELOCITY DEFECT RELATIONS WITH ACTUAL EXPERIMENTAL DATA NEAR THE TUBE CENTRE.

○ Laufer (45), Re = 428,000 ▼ Laufer (45), 40,300 ✱ Nikuradse (9), $> 10^6$ (average) ■ Sleicher (50), 40,000 ▲ Stanton (49), 40,900.

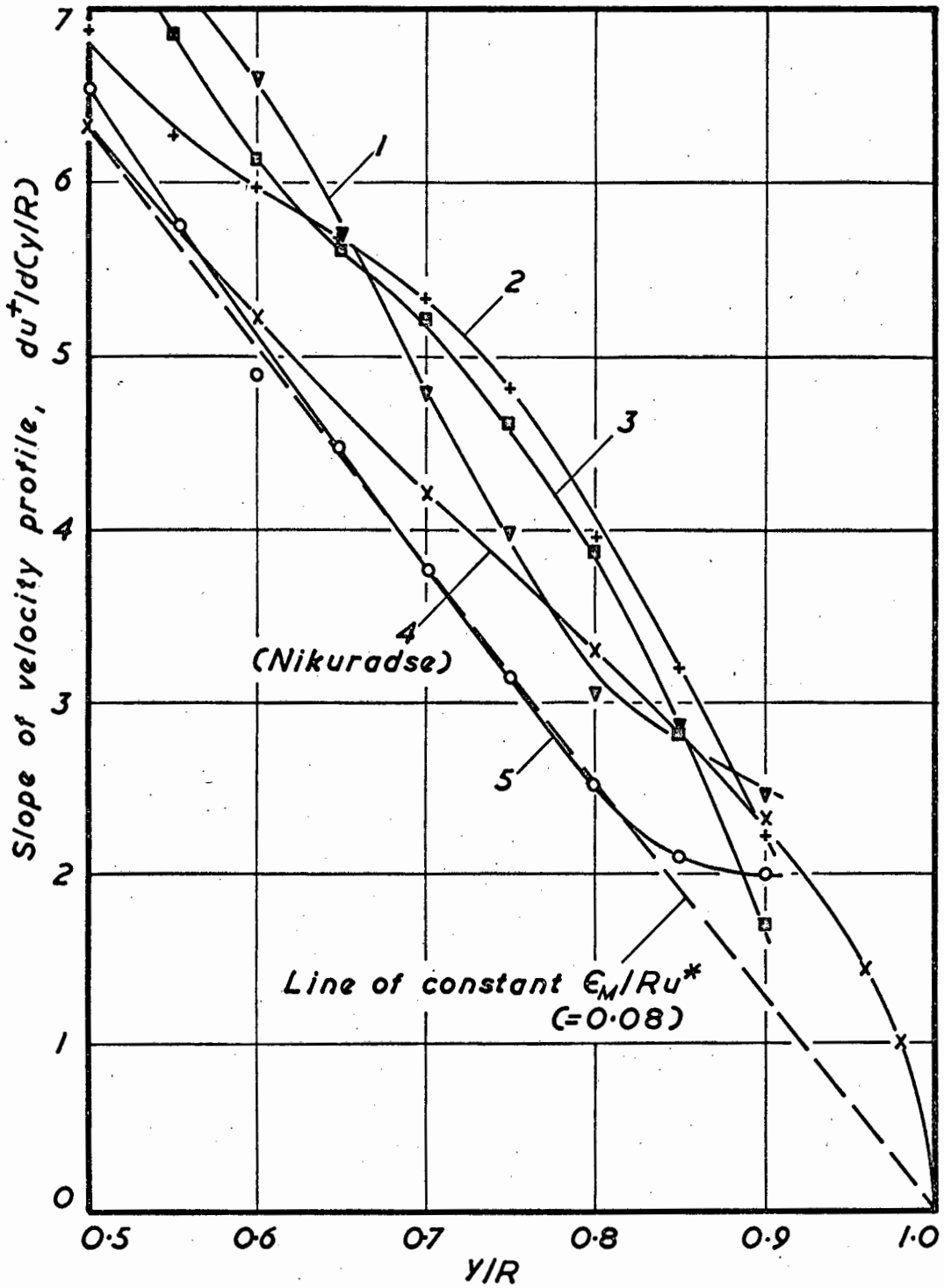

FIG. 18 SLOPES OF VELOCITY PROFILES FROM VARIOUS WORKERS.

1. Laufer (45), Re = 40,300 2. Rein (51), 36,700
3. Sleicher (50), 40,000 4. Nikuradse (9), > 10^5 (average) 5. Laufer (45), 428,000.

seems to be a rather arbitrary procedure. Other arguments for dismissing the indicated trend as not significant are usually based on velocity measurements which, in the vicinity of the centre, are at intervals no closer than 10% of the radius together.

It is not possible to discard the conclusions of Nikuradse on any basis such as the above. The slope curve shown in Fig. 18 was established after careful investigation, involving measurements within 2% and 4% of the tube centre, and the existence of a deviation from a simple straight-line approach to a centre zero must be accepted in the absence of accurate data to the contrary. This curve of $du^+/d(y/R)$ gives values of ϵ_M/Ru^* which decrease from a maximum of 0.0798 at $y/R=0.50$ to a value of approximately 0.0135 at the centre, as shown in Fig. 17 and repeated in Fig. 19.

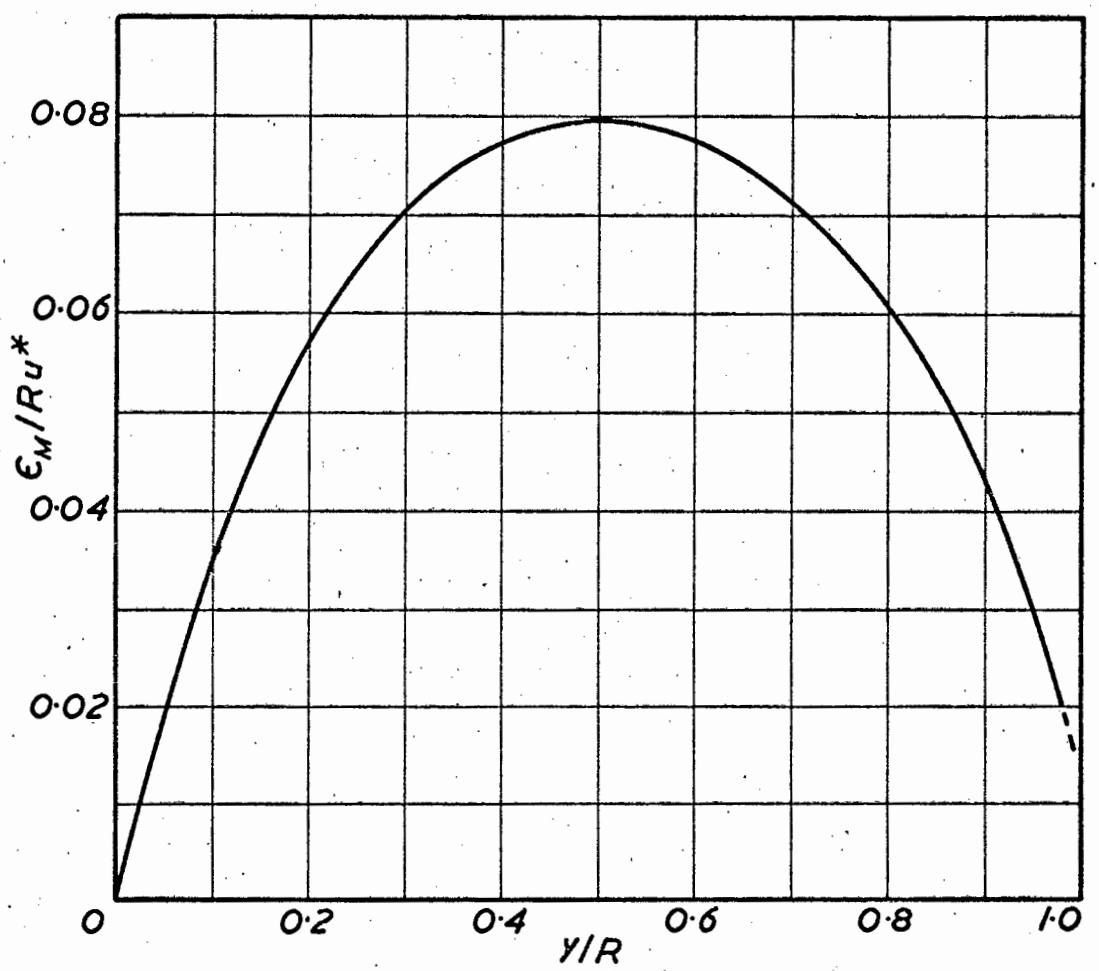

FIG. 19 RECOMMENDED VALUE OF ϵ_M/Ru^*, AFTER NIKURADSE (9).

CHAPTER 4

TEMPERATURE PROFILES

4.1. TEST PROCEDURE

In order to commence a test run, the centrifugal pump motor was switched on and the variable speed drive advanced to the desired flow rate. Alternatively, for low flow rates, the outlet valve opening was reduced. The electrical heating system and the cooling water system were then brought into operation, and during the warm-up period, the transformer voltage and the cooling water rate were adjusted to obtain the desired test section inlet and outlet temperatures.

The ratio between the heat inputs to the upper and lower heating coils was adjusted during initial tests, by means of the variable resistor in the lower circuit. For constant heat flux, the ratio required was equal to the ratio of the areas covered by the respective windings, i.e. (4.062/3.948) = 1.029. The actual ratio obtained for each run is shown in Table B.1 (appendix B) and has an average slightly higher than the desired value, but it is unlikely that this influenced the measured temperature profiles. It was decided to use an auxiliary heater input such as to give a constant heat flux over the area opposite the probe entry, rather than to attempt to compensate for the area covered by the nozzles, by an increased heat input. This procedure was adopted since it was felt that, as profiles would be measured by advancing the probe from the centre to the wall away from the inlet nozzle, a local "hot spot" would be more likely to cause spurious readings than the loss of some heat at the nozzles.

The auxiliary heater input was adjusted simultaneously with the main transformer voltage to obtain a heat input ratio of approx 0.29% (see calculation in appendix F.12) and the ratio actually obtained is shown in Table B.1.

No difficulty was experienced in removing heat from the mercury by means of the cooling section. It was found, however, that extremely low cooling water flow rates had to be used in order to obtain test section inlet temperatures appreciably above the water inlet temperature (counterflow was employed). In the later runs, at a higher outlet temperature, and where low flow rates and relatively high inlet temperatures were used, it was necessary to disconnect the vertical cooling jacket and pass cooling water only through the short horizontal section. Air was passed through the vertical section to keep the PVC jacket at an acceptable temperature. The cooling arrangement could have been improved by allowing several outlet positions on the cooling jacket, thus reducing the available heat transfer area and allowing the use of larger cooling water flow rates. This method was used in the apparatus constructed by Carr (64).

Mercury, cooling water and pipe wall temperatures at several positions, as well as the winding temperatures, were recorded on a 12-point recorder. This system indicated the approach to equilibrium, as well as providing safety and steadiness checks during operation. Steady conditions were generally reached within $\frac{1}{2}$ hr.; very low flow rates took appreciably longer.

The millivolt recorder, potentiometer and voltage reference system were switched on and allowed to warm up. A reference voltage was chosen to balance the probe thermocouple reading at a convenient recorder zero position. The zero position of

the recorder was adjustable over the whole scale.

At the start of a run, the following readings were taken on the various meters or the potentiometer:

(i) Water temperatures and flow rate. These readings were later discontinued as the temperature readings for operating purposes were available on the 12-point recorder, and they were not required for calculation purposes. A heat balance over the cooling section was not performed regularly, since the test section heat balance and the orifice meter reading checked out sufficiently well.

(ii) Inlet and outlet temperatures of mercury in the cooling section, ambient temperature and the orifice meter reading. These were required for checking the flow rate obtained by heat balance over the test section. The outlet reading was later discontinued.

(iii) The reference voltage was measured on the potentiometer and the resistance of the thermocouple plus-reference circuit determined with a universal meter. These readings were required for conversion of the probe thermocouple readings as shown in appendix B.24.

(iv) Temperatures on the inside and outside of the 1-in. glass fibre pipe insulation.

(v) Test section inlet and outlet temperatures.

(vi) Voltmeter and ammeter readings for the upper, lower and auxiliary circuits.

(vii) The two KWH meters for the upper and lower circuits were read and a stopwatch started for each meter.

A suitable zero position and scale factor on the millivolt recorder was then chosen and the thermocouple probe moved in steps from the pipe centre to the wall, or vice versa. At each radial position, the differential thermocouple reading was recorded for about $\frac{1}{2}$ minute. Further details of temperature traverses are given in the next section. In later runs, the test section outlet temperature was simultaneously recorded on the millivolt recorder as a check on the occurence of drift of the overall temperature level. This was generally small.

On completion of a temperature traverse the following readings were taken:

(i) Watches stopped and KWH meters read.

(ii) Recorder zero checked.

(iii) All temperature readings mentioned previously.

(iv) Voltmeters and ammeters.

(v) Voltage and resistance of reference system.

(vi) Wall temperatures were usually taken but were discontinued in the later runs. As noted in appendix B.25, wall temperature readings agreed reasonably well with the reading obtained from the probe thermocouple for moderate heat fluxes, but these readings were not very useful at high heat fluxes.

A complete run took approximately 30 minutes. The run was then usually repeated, traversing the probe in the opposite direction.

4.2 RESULTS

Temperature profiles were measured for Reynolds numbers in the range Re = 3,800 to 254,000, with heat fluxes varying from 340 to 6,800 BTU/hr.ft^2, as shown in Table 4.1. The mean temperature at the probe was maintained approximately constant at 120 or 180 °F, so as to maintain a constant Prandtl number. It was not the intention in these runs to investigate the effect of different Prandtl numbers .

Temperatures in the later runs were increased from 120 to 180 °F so as to allow reasonable variation of the heat flux. The value Z shown in the table is discussed later.

Experimental data together with the computed results and the calculation procedure are given in appendix B. Calculations were carried out with the aid of an ICT 1301 digital computer and calculation methods were usually chosen so as to be amenable to numerical procedures.

Heat flux was determined from the electrical input, and the Reynolds number was calculated by a heat balance over the test section. These values agreed well with those obtained from the orifice meter reading.

Temperature profiles were measured by traversing the probe along the radius from the centre of the pipe to the wall furthest away from the point of entry of the probe. Profiles were occasionally checked for symmetry by measuring temperatures at a few positions on the radius closest to the point of entry. A typical recording obtained during a traverse is shown in Fig. 20. It was confirmed that the fluctuations observed did not

TABLE 4.1

Experimental Operating Conditions

Run No.	Re x 10^{-3}	Heat Flux BTU/hrft^2	Temp. at probe, ^oF	Pr	Z x 10^4
1	3.8	430	117.9	0.021	1730
1a	4.0	470	122.4	0.021	1780
2	4.2	340	118.7	0.021	1200
3	5.7	670	123.4	0.021	1280
3a	5.8	700	124.8	0.021	1280
4	8.3	940	119.8	0.021	820
4a	8.3	960	121.7	0.021	850
5	11.4	1020	119.2	0.021	490
6	14.7	1230	124.1	0.021	350
7	24.9	940	113.1	0.021	90
8	29.6	2440	123.8	0.021	170
9	43.4	2930	108.2	0.022	90
10	95.5	3150	113.9	0.021	21
11	124	3110	112.8	0.021	12
12	172	5070	115.6	0.021	10
13	251	6670	114.1	0.021	6
13a	254	6730	114.0	0.021	6
14	10.1	1590	168.8	0.018	1030
15	12.1	940	181.6	0.017	430
16	21.8	2960	183.9	0.017	420
17	22.7	2070	182.6	0.017	270
18	27.8	1400	183.7	0.017	120
18a	28.2	1390	186.7	0.017	120

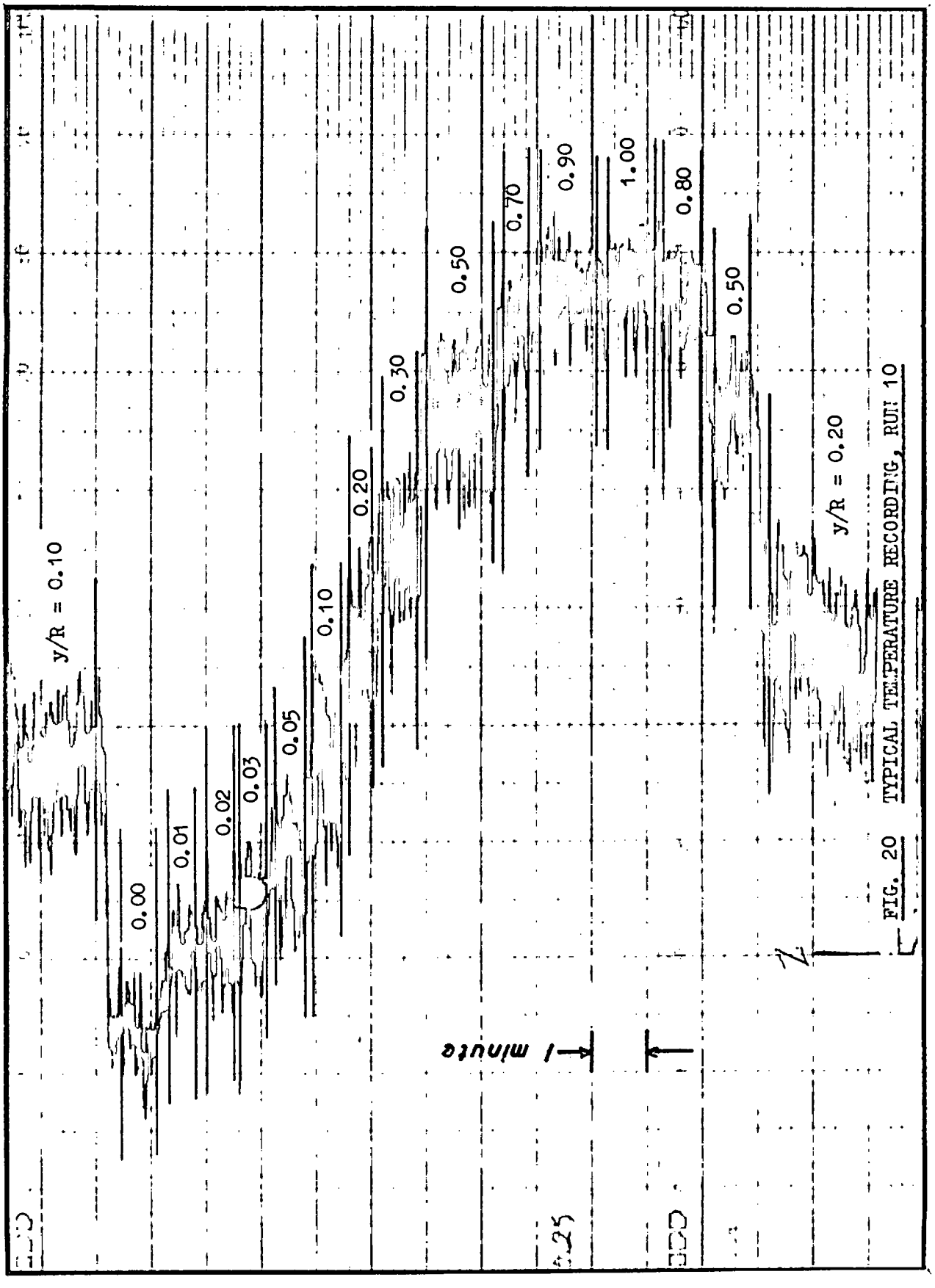

FIG. 20 TYPICAL TEMPERATURE RECORDING, RUN 10

originate in the measuring system but were a feature of the flow conditions. These fluctuations in general appeared to cover a larger temperature range over the radial positions away from the wall and the centre, and a relatively smaller temperature range in the vicinity of the wall and the tube centre. No attempt was made to interpret the significance of these fluctuations but a study of such temperature fluctuations and their relation to the eddy transport of heat promises to be an interesting field of research. While the recording shown in Fig. 20 has been damped to some extent by the thermal capacity of the thermocouple and the response of the recorder (1 second for full-scale travel), large fluctuations remain, and it is clear that a good average will be difficult to obtain as a point reading on a potentiometer. By recording the thermocouple signal a visual average is more easily taken, and by employing the differential signal technique used here, the profile may be spread over the entire recorder scale. It is thus believed that more accurate temperature profiles are obtainable by this method than by the use of a potentiometer.

Readings from the recorder are converted to temperature as shown in appendix B.24, and a typical temperature profile is plotted in Fig. 21. The plotted points represent a visual mean of the recorder fluctuations. Traverses towards the wall and away from the wall are shown, as well as temperature readings on the other side of the centre, as a check on symmetry. Good agreement is obtained. Experimental temperature profile data for all runs are given in appendix B, expressed as $(T_w - T)$. The true wall temperature, T_w, was determined by fitting the profile in the vicinity of the wall to a second-order polynamial, where the coefficient of the first-order term equals the expected slope at the wall, based on the wall heat flux.

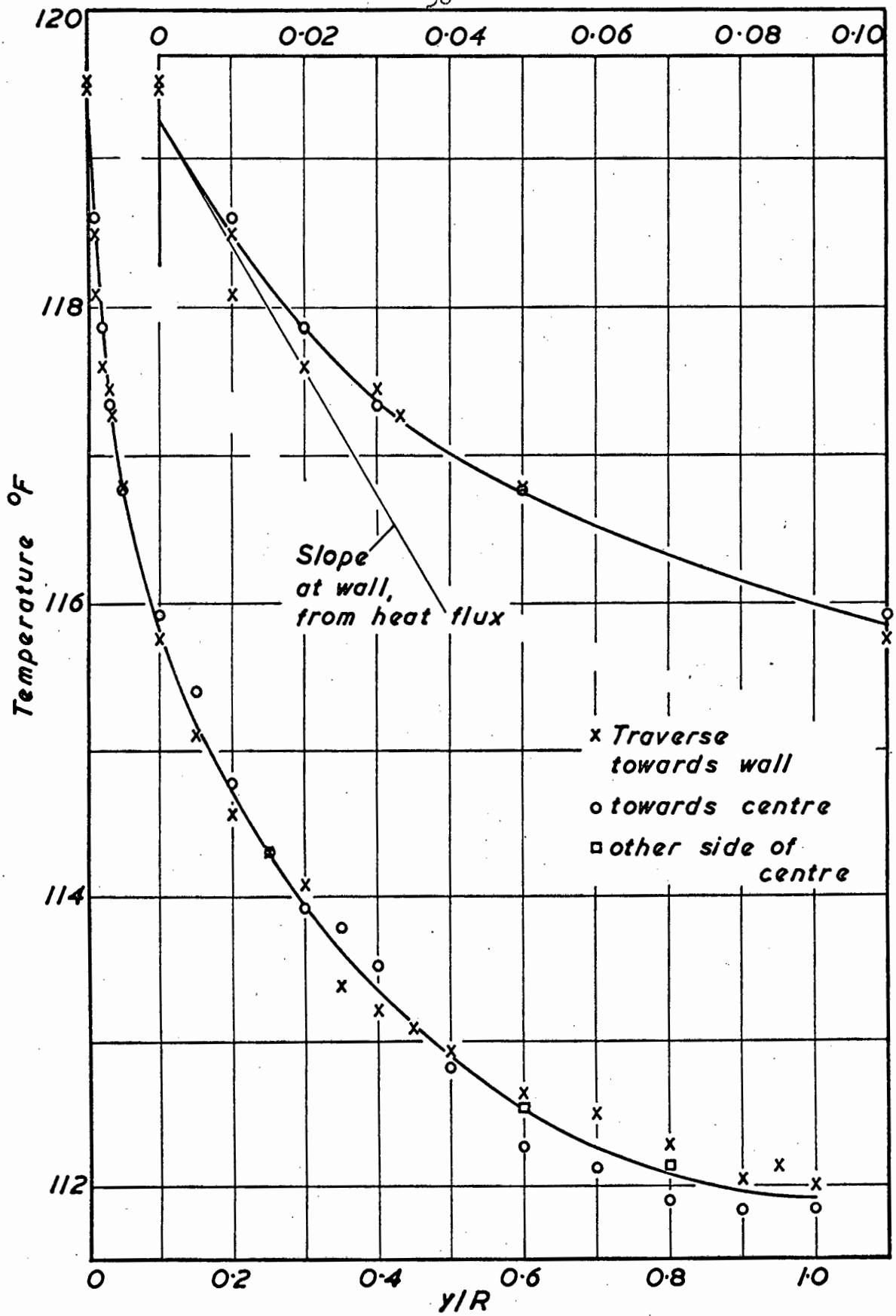

FIG. 21 TYPICAL TEMPERATURE PROFILE.

x Run 13
o □ Run 13a

Readings obtained from the 10 wall thermocouples located in the vicinity of the probe are shown in appendix B. At moderate heat fluxes these readings are in reasonable agreement with the extrapolated wall temperature, allowing for the temperature drop through the wall. Thermocouples were cemented into 1/16-in. holes drilled in the pipe, but the final depth of the thermocouple in the wall was unknown. At high heat fluxes, differences between the thermocouple readings were of the order of the temperature drop over the wall. The same difficulties were reported by Isakoff (17) and it must be concluded that thermocouples in the wall do not provide a sufficiently accurate indication of the wall temperature. The temperature obtained with the probe thermocouple in contact with the wall in general agreed well with the "extrapolated" wall temperature, T_w.

In calculating the mixed mean temperature at the probe, shown in Table 4.1, from the equation

$$T_{av} = \frac{2}{u_{av}} \int_0^1 \frac{r}{R} u T \, d\left(\frac{r}{R}\right) , \qquad (4.1)$$

the measured temperature profile and the universal isothermal velocity distribution was used. Values of $(T_w - T_{av})$ are given with the profile data in appendix B. However, as pointed out later, the velocity profile might be considerably distorted by free convection effects and in such cases the reported mean cup temperature will only be approximately correct.

4.3 DISCUSSION OF RESULTS

Temperature profile data may be used to calculate the eddy diffusivity of heat from the relationship

$$\phi(y/R) \, q_w/\rho c_p = -(\alpha + \epsilon_H) \, dT/dy \qquad (4.2)$$

where $\phi(y/R)$ represents the heat flux distribution across the radius and may be shown (app. D.23) to be

$$\phi(y/R) = \frac{2}{(r/R)\, u_{av}} \int_0^{r/R} u \left(\frac{r}{R}\right) d\left(\frac{r}{R}\right) \qquad (4.3)$$

for constant heat flux. The heat flux at the wall is given by

$$q_w/\rho c_p = - \alpha \, (dT/dy) \qquad (4.4)$$

and substituting this equation into (4.2) gives

$$\epsilon_H/\alpha = \frac{\phi(y/R)}{S_y/S_o} - 1 \qquad (4.5)$$

where S_y/S_o is the ratio of the slope of the temperature profile at y to the slope at the wall. If $\phi(y/R)$ is evaluated from equn. 4.3 by using the universal velocity profile for the term u, as shown in Appendix D. 23, then $\phi(y/R)$ depends upon the Reynolds number only. Calculation of ϵ_H/α from equn. 4.5 at a particular Reynolds number therefore requires only that the correct temperature profile be known, so that S_y/S_o may be evaluated.

In order to determine the correct temperature profile, the results of different workers are most readily compared by plotting the profiles on the usual dimensionless basis $(T_w - T)/(T_w - T_c)$ vs. y/R. Normalising the plots in this way does not affect the applicability of equn. 4.5 since the ratio of the slopes will remain the same. Typical temperature profiles, obtained in mercury and alkali metal, are shown in Fig. 22 for $Re \approx 10^4$, and in Figs. 23 and 24 for $Re \approx 4 \times 10^4$. It is apparent that large differences exist between the profiles at the lower Reynolds number and, values of the eddy diffusivity calculated from these profiles would therefore also show wide variations. At $Re \approx 4 \times 10^4$, good agreement is found for the NaK profiles (Fig. 23) but it is evident that differences still exist for the measurements made in mercury (Fig. 24).

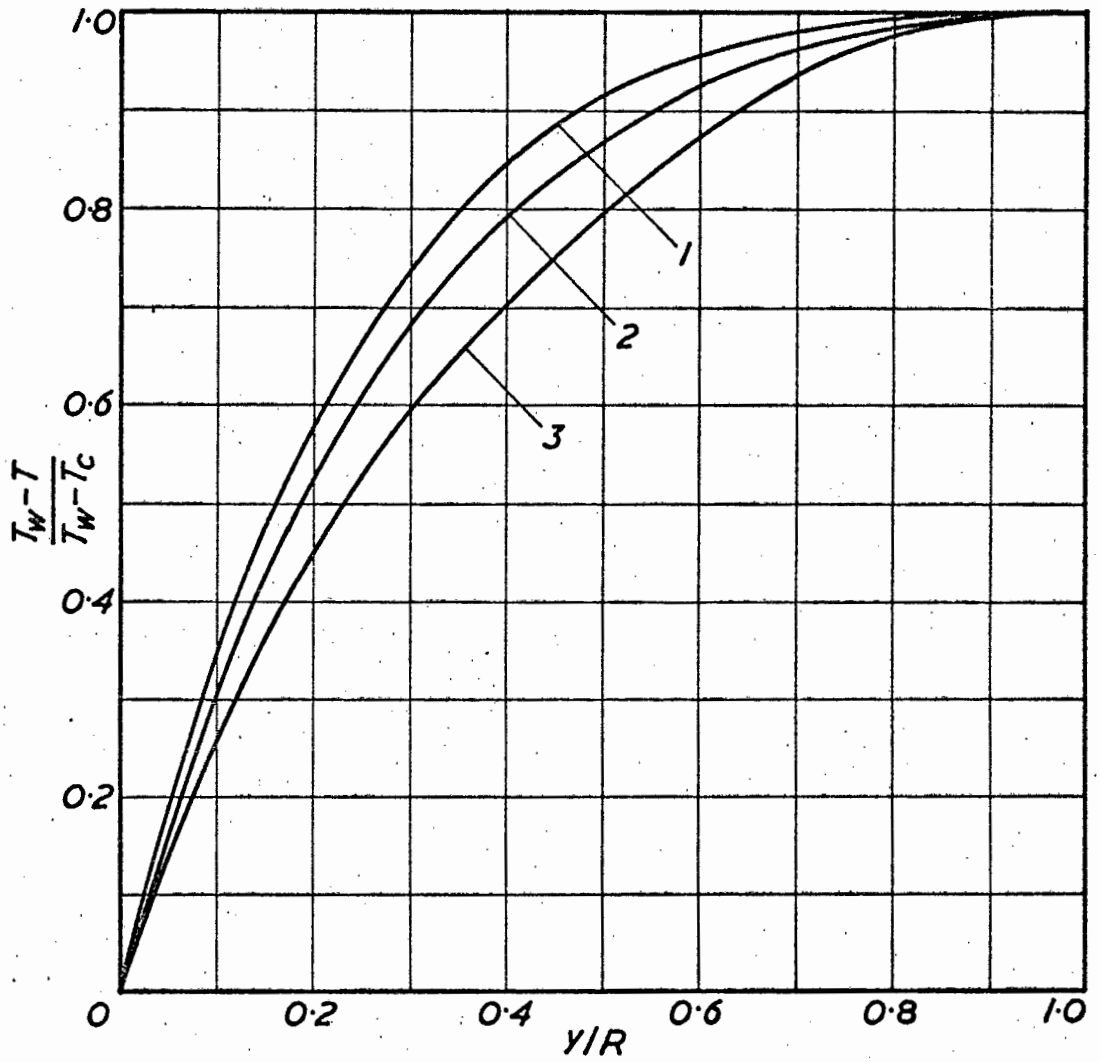

FIG. 22 TEMPERATURE PROFILES FOR Re ≈ 10^4

1. Run No. 14; Re = 10,100; Y = 94
2. Run No. 5; Re = 11,400; Y = 64
3. Kirillov et al (20); Re = 13,700; Y = 6.6

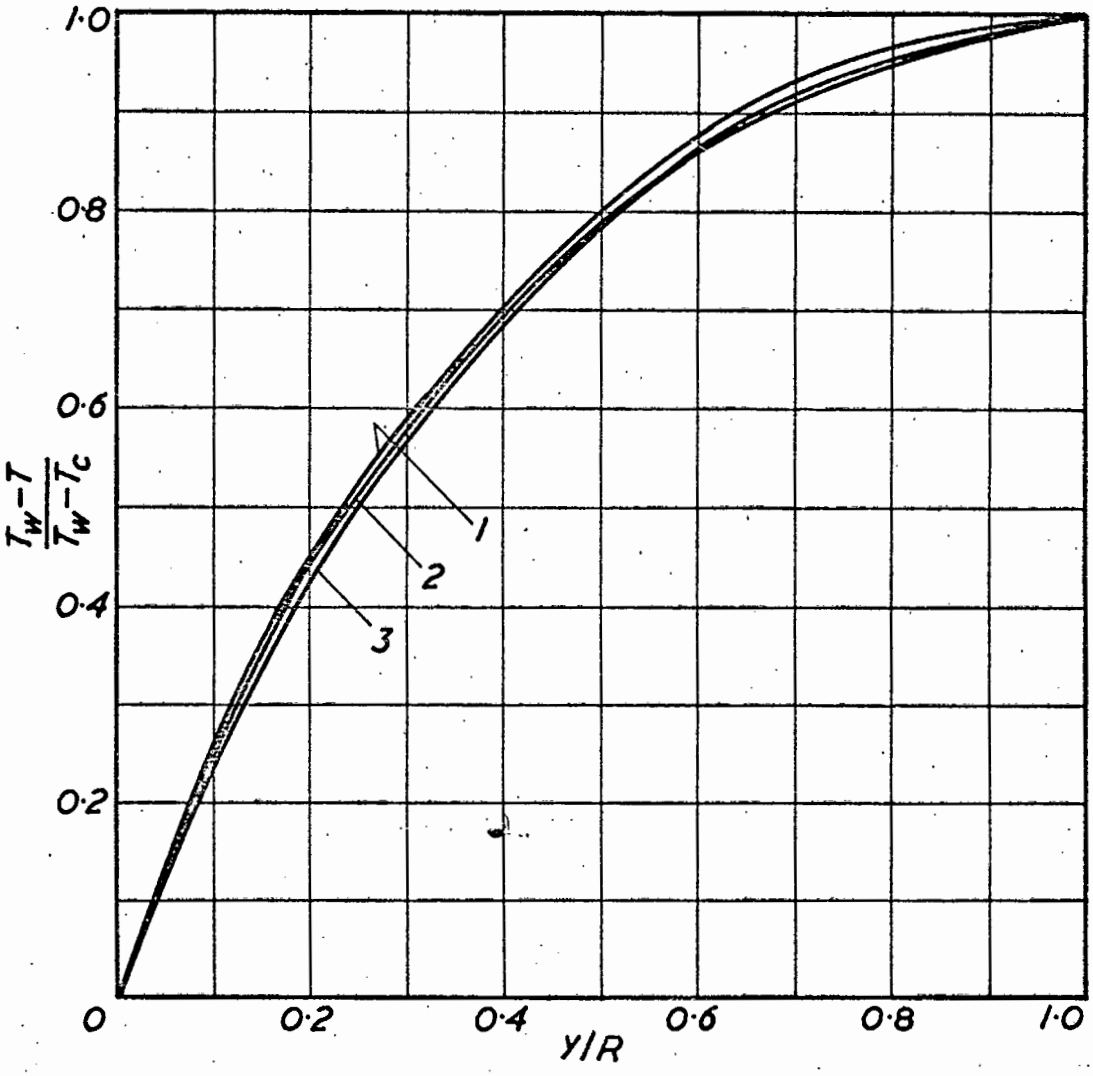

FIG. 23 TEMPERATURE PROFILES IN THE NaK EUTECTIC FOR Re ≈ 4×10^4

1. Carr (78); Re = 39,500; Y = 0.9
2. Carr (78); Re = 44,000; Y = 0.11
3. Schrock (37); Re = 41,400; Y = 0.14

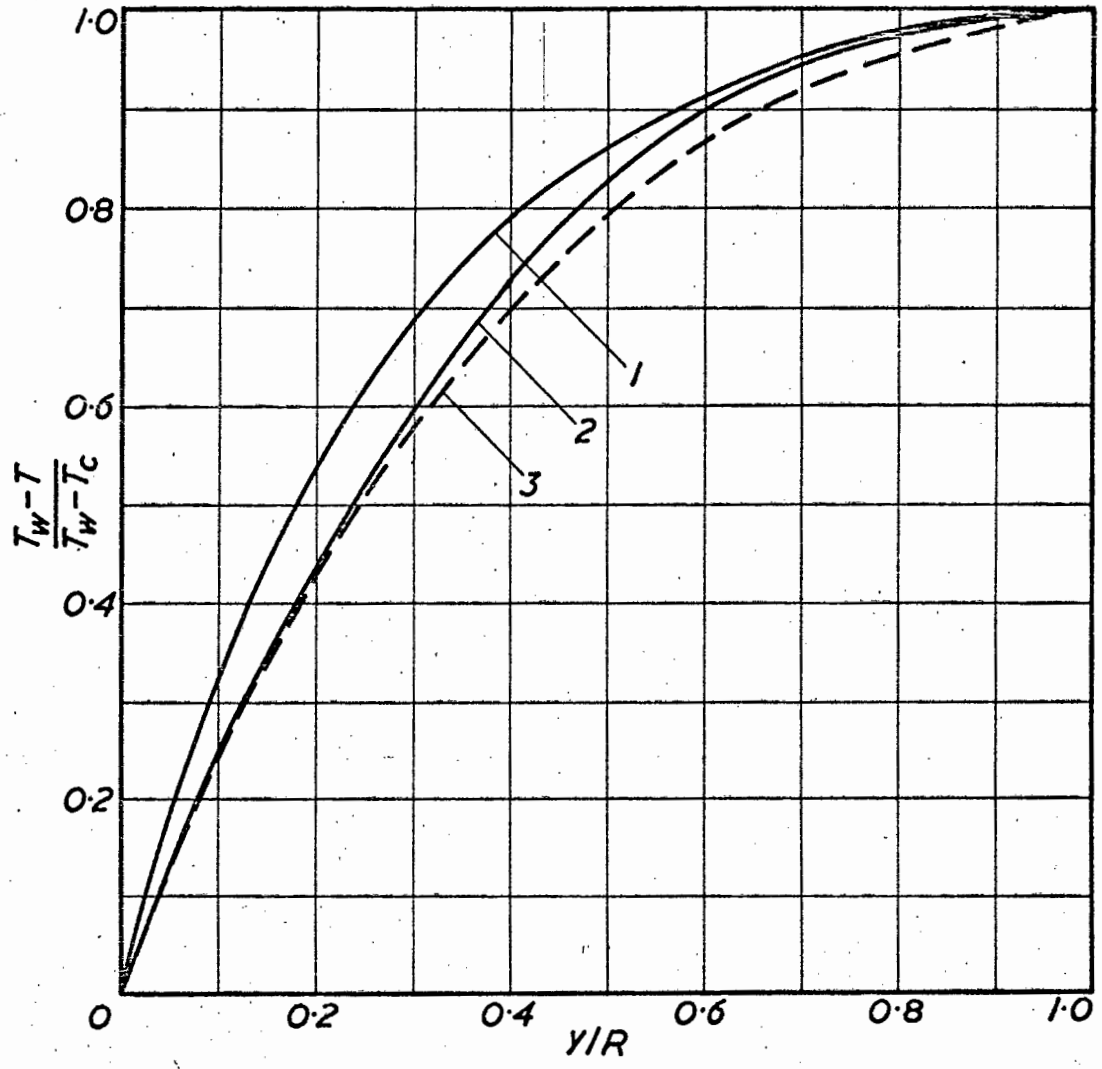

FIG. 24 TEMPERATURE PROFILES FOR Re ≈ 4×10^4

1. Subbotin et al (25); Re = 45,500; Y = 5.1 (Hg)
2. Run No. 9; Re = 43,400; Y = 17.5 (Hg)
3. Average of NaK data of Fig. 23; Y < 1.0

A possible explanation for the discrepancies observed in the reported temperature profiles arises from the work of Yantovskii (65) who analysed mixed free and forced convection and deduced that, in turbulent flow, the free convection term in the flow equation would become significant when the group

$$Y = Gr / Re^2 (f/2) \qquad (4.6)$$

was of the order of unity or greater. (This group has been transcribed from the terms used by Yantovskii into the terms used in this work). Support for the numerical magnitude of this criterion comes from the work of Schrock (37) with NaK in a horizontal tube, in which appreciable asymmetry of the temperature profile was found at $Re < 10^4$ where a typical value of Y is 2.6 (for Re = 9,800; see Appendix C.14); no distortion was found at $Re > 2 \times 10^4$ and typically Y = 0.19 (for Re = 36,000).

Values of the Yantovskii criterion have been calculated and are shown in Appendix C.1. Applying this criterion to the profiles in Fig. 22 gives a Y value of 6.6 for the NaK curve and values of 64 and 94 for the mercury curves shown, thus showing that free convection effects are significant. The presence of such effects would distort the velocity profile in comparison with the case of pure forced convection; this would in turn change the heat flux distribution and accordingly the temperature profile. According to the Yantovskii criterion, a free convection effect would therefore also exist for the mercury profiles of Fig. 24 where Y = 5.1 and 17.5. For the profiles of Fig. 23 the Y values are 0.11, 0.14 and 0.9. respectively, and the absence of a free convection effect is confirmed by the excellent agreement of the curves.

CHAPTER 5

CORRELATION OF DATA

5.1 THE EFFECT OF FREE CONVECTION

Application of the Yantovskii criterion has indicated that free convection effects can be significant in forced convection heat transfer to liquid metals, particularly mercury, for Reynolds numbers up to at least 50,000. This effect has not up to now been recognised and it should be realised that experimental work carried out in this Reynolds number region can easily be misinterpreted. Distortion of the velocity profile will cause errors in all calculations using an assumed velocity distribution. Use of the wrong velocity profile in evaluating the mean cup temperature from equn. 4.1 can lead to errors in the heat transfer coefficient; the eddy diffusivity of momentum is very sensitive to the shape of the velocity profile, and use of the wrong profile will lead to incorrect values of the ratio of eddy diffusivities. It would therefore be advantageous to be able to predict the effect of superimposed free convection on velocity and temperature profiles, or at least to be able to predict the regions where the effect ceases to be significant.

Various theoretical predictions of the velocity and temperature profiles for combined free and forced convection, in laminar flow, have been made, by Hallman (66) and others. Heat transfer rates have been measured at low Reynolds numbers by workers such as Eckert et al (67), Brown and Gauvin (68) and others (69, 70) in air and other fluids, but no velocity

profiles are reported. Ojalvo and Grosh (71) have produced a theoretical analysis for combined free and forced convection in turbulent flow, whereby velocity and temperature profiles may be predicted for $Pr > 1$, but no theoretical or experimental information is at present available whereby the effect of free convection on the velocity profile, in turbulent flow, may be predicted.

In order to consider the effect of free convection on the reported temperature profiles, it is necessary that each curve should be identified with a suitable parameter indicating the relative magnitude of the free convection effect. The Yantovskii criterion is useful in indicating the existence of such an effect, but, without modification, it does not provide an orderly progression with the amount of distortion, when the results of different workers are considered, as in Fig. 24. For the purposes of correlating all the available information, a correlating parameter of the form

$$Z = \frac{Ra}{Re} \cdot \frac{D}{L} \qquad (5.1)$$

is proposed, as discussed below.

5.2 CHOICE OF A CORRELATING PARAMETER

5.21 Rayleigh number

The Rayleigh number, Ra, is the product $Gr^* \times Pr$ and occurs naturally in free convection problems. The Grashoff number was originally concerned with the condition of free convection from a surface to a fluid at rest, and the temperature difference occurring in this dimensionless group was defined as $(T_w - T_\infty)$ where T_∞ is the temperature of the undisturbed fluid.

In applying the Grashoff number to flow in pipes, the temperature difference has been variously interpreted to be $(T_w - T_{av})$ or $(T_w - T_c)$. These definitions may be satisfactory if some form of universal temperature distribution exists, but it is easily seen that if the velocity profile, and hence the temperature profile, is distorted,

(a) the centre temperature may no longer be representative of the heat transfer situation, and

(b) the average temperature will be difficult to obtain unless both the temperature and velocity profiles are accurately known.

For these reasons it is therefore desirable to employ a temperature difference term which will not be affected by the temperature profile and it is proposed to use an "axial difference" of the form

$$\Delta T = (dT/dx)\, D \qquad (5.2)$$

which was first used, without explanation, by Hallman (61). This term, which will be constant under conditions of constant heat flux, may be readily evaluated from inlet and outlet temperatures on the test section, and is easily shown to be related to the usual radial temperature difference by a simple heat balance, i.e.

$$(dT/dx)\, D = \frac{4h}{G\, c_p} (T_w - T_{av}) \qquad (5.3)$$

An asterisk is used to distinguish the Grashoff number using the "axial difference" from the Grashoff number using a radial temperature difference.

5.22 Prandtl number

The effect of the Prandtl number is usually correlated in natural convection problems by a term of the form $Gr\ Pr^n$ where $1 < n < 2$, and for liquid metals, there is some evidence (72) that n should approach 2. Bayley et al (73), however, use the first power of the Prandtl number in their investigations on natural convection in mercury, for the reasons that much of the experimental work on more conventional fluids uses the form Gr Pr and it is not possible to draw any firm conclusions regarding an appropriate value for n from the limited Prandtl number range of their tests. The same approach is adopted here and a power of unity is used for the Prandtl number. This will hardly affect the results for liquid metals, but it is recognised that refinements will be required if the correlation is to be extended to other fluids.

5.23 D/L Ratio

The effect of the D/L ratio in correlations of combined free and forced convection is uncertain. Various powers of the D/L term, in combination with the Rayleigh number, have been suggested by different workers (73, 74). The term Gr Pr (D/L) was used in the theoretical work of Martinelli and Boelter (75) to account for the effect of superimposed free convection on laminar forced convection and the same term was found by Metais and Eckert (76) to provide the best correlation for regimes of forced, mixed and free convection in vertical flow. The same authors, however, also found that, for horizontal flow, an equally good correlation was obtained whether the D/L ratio was

employed or not. In the present work the use of the D/L ratio was found to improve the orderliness of the correlation between the results of different workers, particularly at the higher Reynolds numbers, and it has been included in the definition of Z. Much more experimental work will be required before a closer estimate of the effect of this ratio can be made.

5.24 Reynolds number

The Grashoff number is of the form of a squared Reynolds number, and a ratio of the form Gr/Re^2 may be used to provide a measure of the relative effect of free and forced convection (77). The mass flow rate, G, is inherent in the definition of the "axial" temperature difference of equn. 5.2 and therefore already occurs once in the denominator of the Rayleigh number used here. The Rayleigh number is accordingly divided by a further Re , so that Z provides a relative measure of free and forced convection.

5.3 VALUES OF Z.

Values of Z have been calculated for the mercury runs reported here, and are given in Appendix C.2. Typical values for other workers are also given. While the criteria Y and Z are not strictly comparable, it is convenient to note that the limiting condition of Y=1 corresponds approximately to $Z = 20 \times 10^{-4}$. Values of Z for the NaK runs of Carr (78) are very small in comparison with those for mercury and are all much lower than $Z = 20 \times 10^{-4}$. They may thus be considered to represent the case of no profile distortion.

5.4 FORM OF CORRELATION

The shape of the dimensionless temperature profile varies not only with the superimposed free convection effect illustrated in Figs. 22 and 24, but also with the Reynolds number. A profile in general becomes more convex as the Reynolds number increases, and, for the mercury profiles reported here, a larger free convection effect, indicated by the parameter Z, also produces a more convex shape. It therefore becomes very difficult to compare a large number of profiles on one diagram, in the form of Figs. 22 and 24.

By considering any fixed radial position (say $y/R = 0.50$) it may be seen that the dimensionless temperature increases as the profile becomes more convex, that is, as the Reynolds number or the free convection effect increases. By plotting the dimensionless temperature against the Reynolds number, with Z as a parameter, the behaviour of the profile at that radial position may be clearly observed; at the same time the plot will allow smooth curves to be drawn through the experimental points, for constant values of Z, and in this way produce a correlation for the prediction of a profile shape under given conditions.

It will not be expected that the dimensionless temperature at one radial position will completely characterise the temperature profile since the Reynolds number and free convection may be expected to have different effects in the vicinity of the wall or the tube centre. A correlation should therefore be drawn up for a number of radial positions, sufficient to allow adequate reconstruction of the temperature profile.

5.5 THE CORRELATION OF FIG. 25.

A plot of the dimensionless temperature versus Reynolds number, with parameter $Z \times 10^4$ is shown in Fig. 25 for the

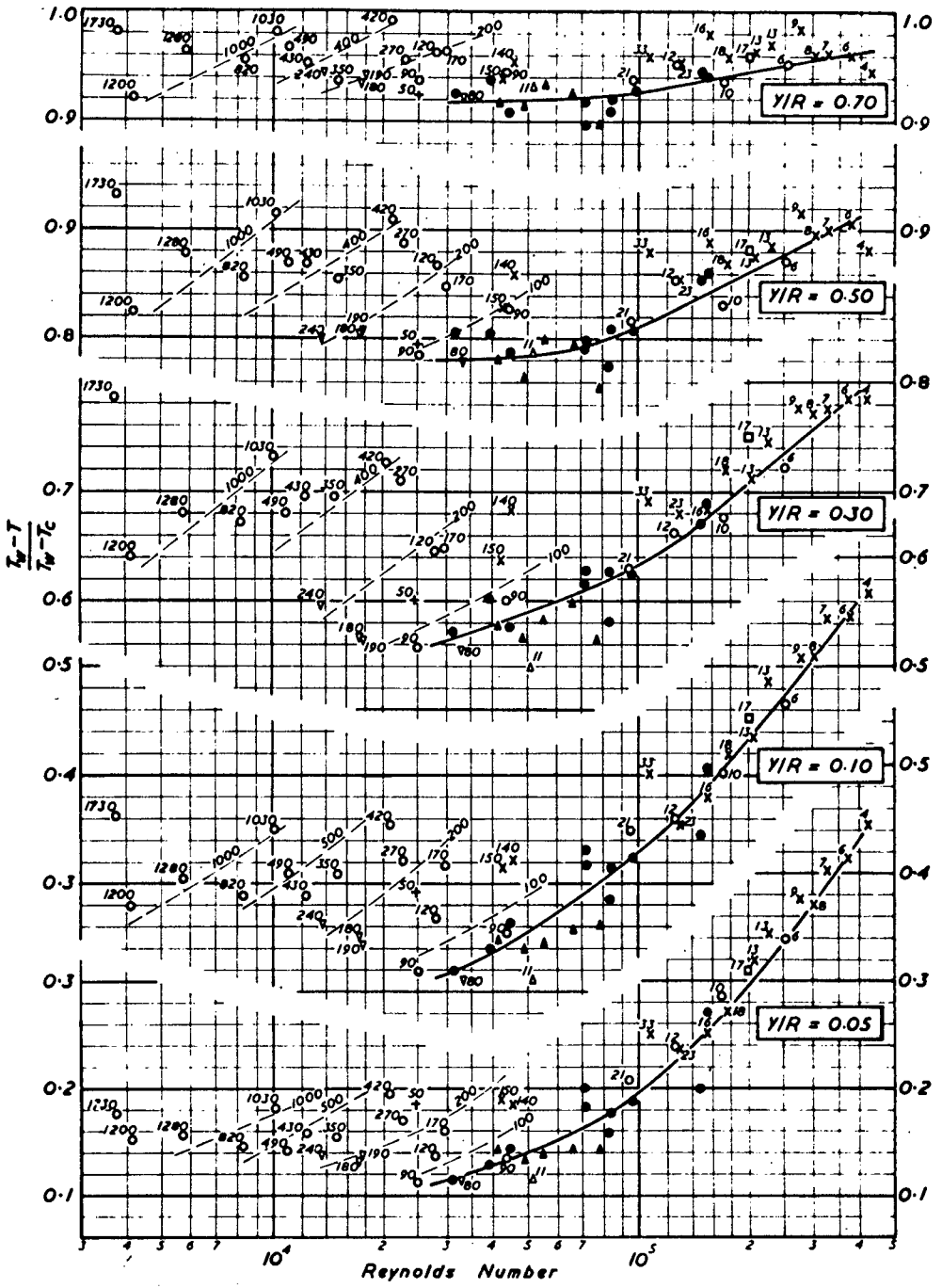

FIG. 25 CORRELATION OF DIMENSIONLESS TEMPERATURE PROFILES.

- o This work, Hg,
- x Subbotin et al.(25) Hg,
- □ Subbotin et al.(22) Hg,
- ▲ Borishanskii (26) Na,
- ● Carr (78) NaK,
- ▲ Schrock (37) NaK,
- + Subbotin et al.(22) NaK,
- ▽ Kirillov (20) NaK.

radial positions y/R = 0.05, 0.10, 0.30, 0.50 and 0.70.

Since the specific effect of free convection on the velocity and temperature profiles will depend on whether the flow is upwards, downwards, or horizontal, and since most of the profiles reported have been measured in vertical upflow, Fig. 25 is strictly applicable to this flow direction only. The data of Buyco (36) for horizontal flow of mercury are therefore not included. The NaK data of Carr (78) are for downward flow but, as mentioned above, these curves are undistorted by free convection effects so that the profile will not be affected by the flow direction; in the same way the profiles of Schrock (37) for Reynolds numbers above 2×10^4 (for NaK horizontal flow) all have $Z < 20 \times 10^{-4}$ and may also be considered unaffected by free convection. These two sets of data are therefore included in Fig. 25.

Values of Z have been calculated for the profiles of the various authors, as shown in Appendix C.2 and data points in Fig. 25 are labelled with the parameter $Z \times 10^4$. Labels on the NaK data of Carr and of Schrock have been omitted in the interests of clarity.

It is immediately evident from an inspection of Fig. 25 that a large scatter exists in the temperature profiles measured at the lower Reynolds numbers. The dotted lines indicate the trend of the data points with Z, and it appears that the dimensionless temperatures increase with Z, at a given Reynolds number, i.e. the profile becomes more convex for a larger free convection effect. At the same time it is clear that more experimental data are needed before the exact effect of free convection may be predicted; at present it is only possible to state that considerable distortion may occur for Reynolds numbers as high as 50,000. The extent of the distortion at any

Reynolds number will depend on the heat flux and other factors in the parameter Z, and may be estimated from Fig. 25.

At higher Reynolds numbers, a more orderly progression of the data is apparent, and the values of the parameter Z for most of the data are below 20×10^{-4}. It is therefore postulated that the high-Re mercury data presented here, together with the previously mentioned NaK data, represent a limiting case of no free convection effect and an average of these data is indicated by the solid line. This line is passed as well as possible through the NaK data, but is slightly biased in favour of the lower lying mercury data points. It is not possible to extend the line with any confidence to values less than $Re = 3 \times 10^4$.

Experimental data that lie considerably below these limiting curves have not been included in the correlation. These are the profiles of Isakoff (17) and Brown et al (19). The profiles of the latter are generally for Reynolds numbers considerably higher than those considered here, and cooling instead of heating was used (see Table 1.1), which should have the effect of reversing the free convection effect. Such an effect should be small, however, as evidenced by the relatively small values of Z applicable to these data (see Appendix C.24). The poor agreement of the data of these two workers with the other data reported here remains unexplained.

5.6 UNDISTORTED TEMPERATURE PROFILES

The solid lines in Fig. 25 represent data points on the average, undistorted dimensionless temperature profiles, for Reynolds numbers in the range 3×10^4 to 3×10^5. Such profiles may therefore be reconstructed from Fig. 25, as illustrated in

Fig. 26. With the data available, it is not possible to predict undistorted profiles for Reynolds numbers lower than 30,000.

Since the profiles of Fig. 26 are based on the results of a number of workers, they are less subject to experimental error and therefore preferable to individual experimental profiles for the evaluation of heat transfer characteristics of liquid metals.

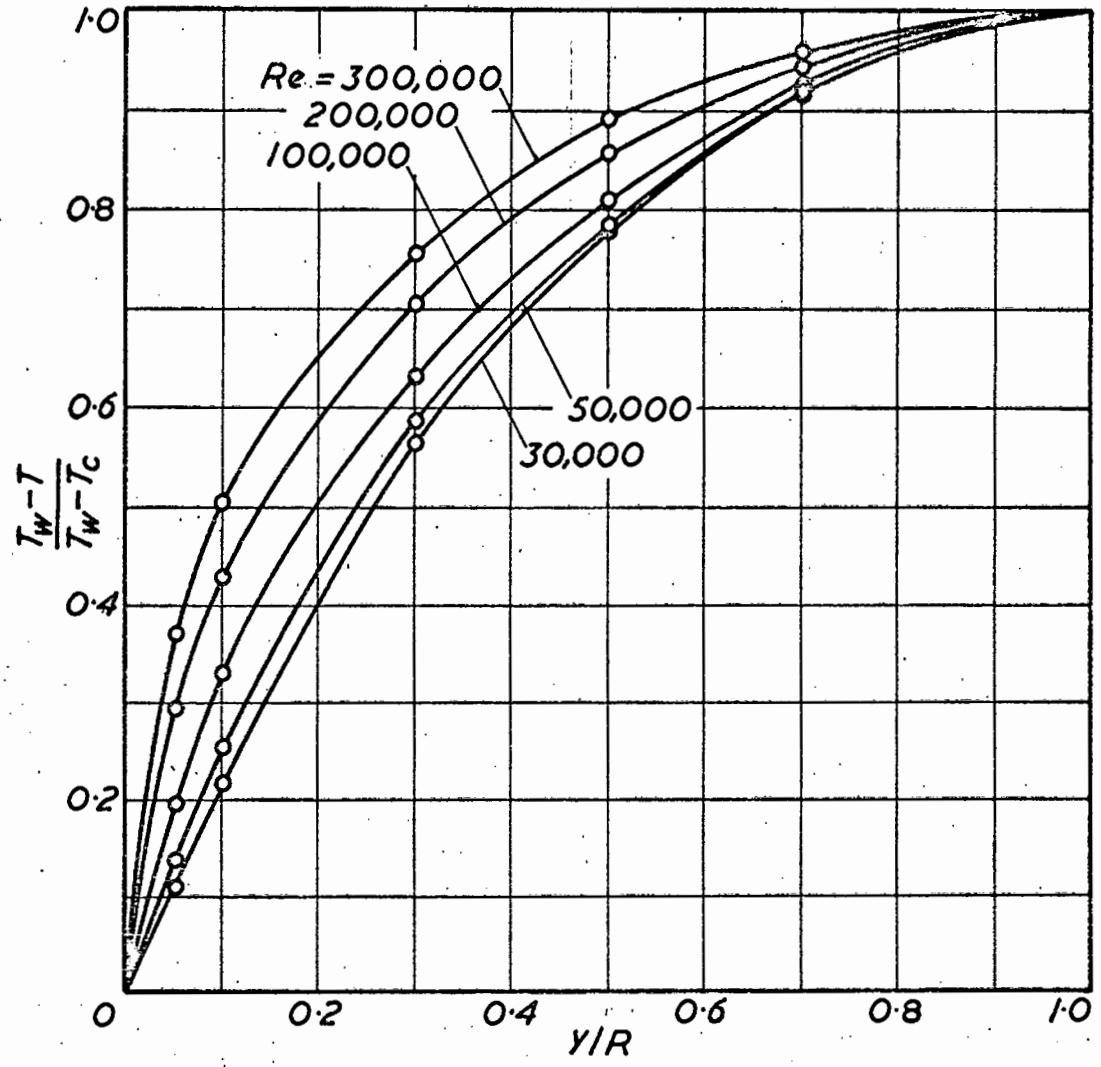

FIG 26 UNDISTORTED TEMPERATURE PROFILES FROM FIG. 25.

CHAPTER 6

CONCLUSIONS AND RECOMMENDATIONS

6.1 THE EDDY DIFFUSIVITY RATIO, ϵ_H/ϵ_M

Calculation of ϵ_H/ϵ_M requires a knowledge of the velocity and temperature profiles measured under the same conditions. Thus when a temperature profile is distorted by the effect of free convection, it is necessary to know also the form of the corresponding non-isothermal velocity profile. In the absence of such velocity data, it is not possible to use the low - Re temperature profiles reported here for the determination of ϵ_H/ϵ_M, since they have been shown to be distorted. The profiles measured at Re > 50,000, however, appear to be undistorted and they may therefore be used in conjunction with the universal isothermal velocity distribution for the calculation of the eddy diffusivity ratio. It is proposed to use the averaged profiles of Fig. 26 and thus obtain representative average values of ϵ_H/ϵ_M.

The eddy diffusivity of heat is obtained from equn. 4.5:

$$\epsilon_H/\alpha = \frac{\phi(y/R)}{S_y/S_o} - 1 \qquad (4.5)$$

Values of $\phi(y/R)$ were computed by using the universal velocity profile as adjusted by Hinze (48) and are given in Appendix D.23. Slopes were evaluated from the dimensionless temperature profiles of Fig. 26, as midpoint derivatives of a second-order regression on five points in the immediate vicinity of the point under consideration, in the same way as for the velocity profiles of Chapter 3. The slope at the wall, which is of particular importance, as a normalising factor, was obtained by fitting a

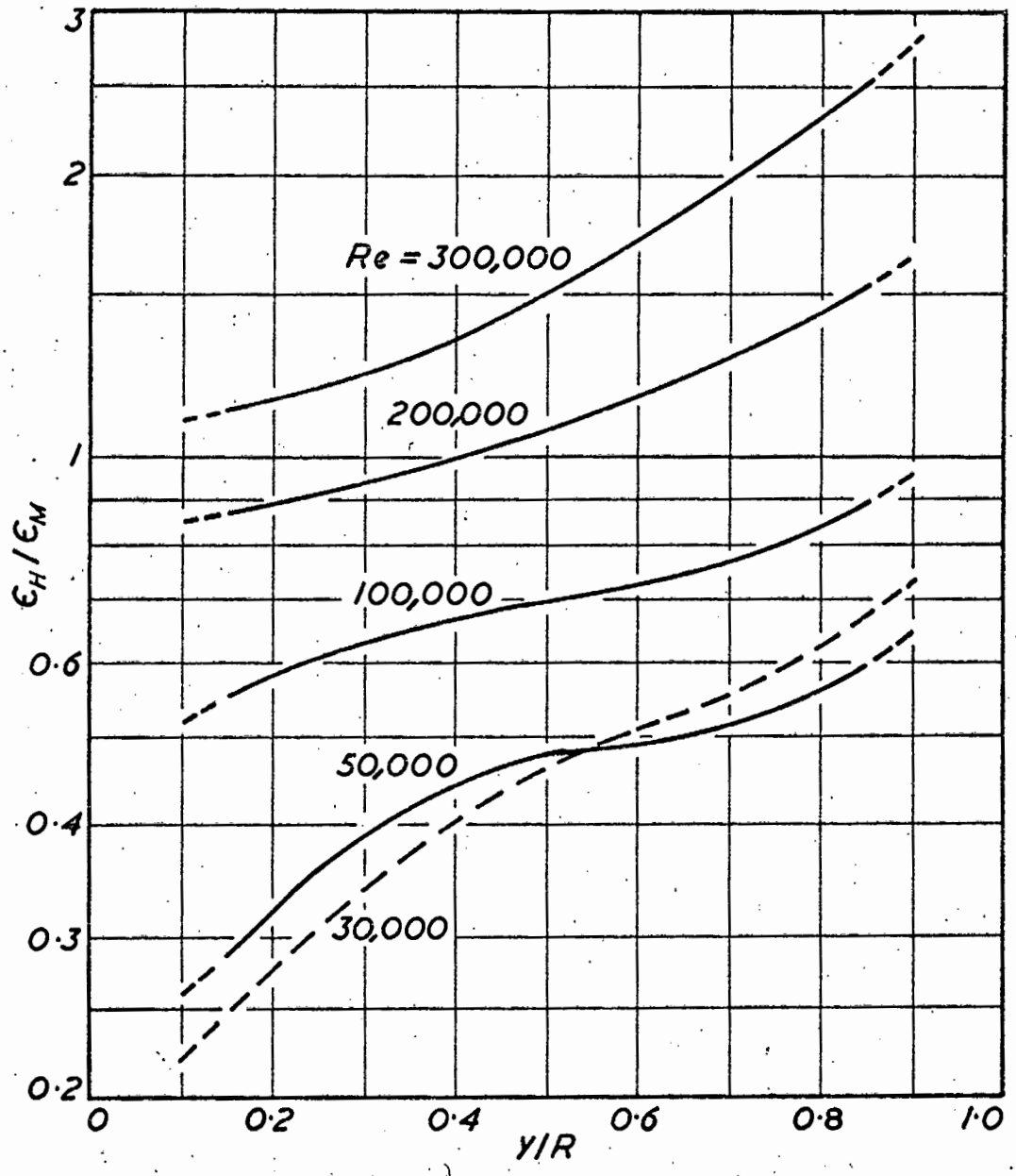

FIG. 27 : RATIO OF EDDY DIFFUSIVITIES.

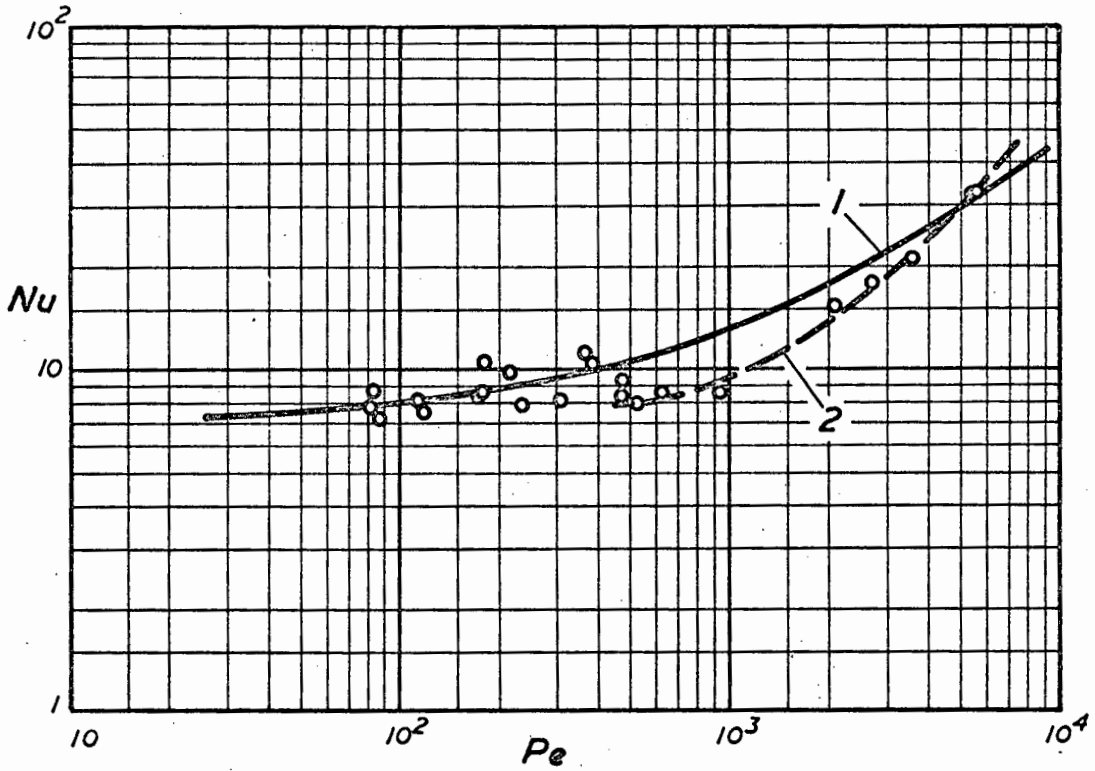

FIG. 28 PLOT OF NUSSELT NUMBERS OBTAINED IN THIS INVESTIGATION.

1. Martinelli-Lyon equation 2. Nu based on undistorted temperature profiles of Fig. 26 o Experimental results, Runs 1 - 18a.

(see appendix G.2) and values based on the recommended profiles of Fig. 26 are also shown in Fig. 28.

The data are in good agreement with the Martinelli-Lyon equation at low Peclet numbers (ca. 100), fall below the line at intermediate Peclet numbers, and then increase at a faster rate than the Martinelli-Lyon equation so that Nu values lie above that equation at high Peclet numbers. The latter is in agreement with the fact that the eddy diffusivity ratio exceeds unity at high Reynolds numbers (Fig. 27). Agreement of the data at low Peclet numbers with the Martinelli-Lyon equation is in contrast to the overall measurements of Johnson et al. (15) and may be due to higher accuracy obtainable by profile measurements. Two factors, however, should be kept in mind when interpreting data obtained at low Reynolds numbers. These are

(i) the velocity profile might be distorted by free convection effects,

(ii) the universal velocity profile might not be applicable at low Reynolds numbers.

The exact effect of superimposed free convection in turbulent flow on the velocity profile is not known, but if it is assumed that the free convection effect will increase the velocity in the vicinity of the wall, moderate increases in the calculated value of Nusselt numbers would occur, in comparison with calculations carried out using the universal (von Karman) velocity profile. This effect is illustrated by an example in appendix G.3. On the other hand, it is noted that the universal velocity profile curve used in Fig. G.1, app. G.3, crosses the line $u/u_{av} = 1.0$ at $y/R \approx 0.19$, whereas Preston and Norbury (80) indicate that the average velocity should occur at approximately $y/R = 0.25$. If this

is taken as an indication that the von Karman relations do not apply at low Reynolds numbers, and that the curve near the wall should be lowered, the average temperature and accordingly Nu would also be lower.

Heat transfer coefficients at low Peclet numbers must therefore remain tentative while uncertainty over the low-Reynolds number non-isothermal velocity profile exists.

6.3 SUMMARY OF RESULTS

Temperature profiles have been measured in mercury, over a range of Reynolds numbers from Re = 3,800 to Re = 254,000. It is shown that temperature profiles in liquid metals may be distorted by superimposed free convection effects up to Reynolds numbers of at least 50,000. Velocity profiles will also be distorted by free convection and the use of the isothermal universal velocity distribution in conjunction with distorted temperature profiles will lead to erroneous conclusions.

A criterion Z is proposed as a measure of the magnitude of the free convection effect and it appears that such effects will be negligible for $Z < 20 \times 10^{-4}$. The correlation of Fig. 25 allows prediction of the amount of distortion caused by free convection, as well as prediction of the shape of the undistorted temperature profiles. The latter have been used to calculate values of the eddy diffusivity ratio and the Nusselt number. The values of ϵ_H/ϵ_M increase from the wall to the tube centre and exceed unity for the higher Reynolds numbers. Nusselt numbers lie above the Martinelli-Lyon equation at high Peclet numbers, fall below predicted values at intermediate Peclet numbers, and agreement is indicated at low Peclet numbers. The latter statement is qualified by

a lack of definitive knowledge of the non-isothermal velocity profile at low Reynolds numbers.

For the evaluation of ϵ_M, the existence of a universal velocity profile has been assumed. The data of most investigators agree for $y/R < 0.50$ but above this value, the most accurate data available are those of Nikuradse (9) and in the absence of other evidence, ϵ_M values based on his work must be accepted.

6.4 RECOMMENDATIONS

As a result of this investigation, it is recommended that further work be undertaken in the following directions:

(a) Velocity profiles should be determined under non-isothermal conditions so as to evaluate the effect of superimposed free convection on the forced convection turbulent velocity profile. For the purpose of developing a general theory, work should be extended to the common fluids as well. On the theoretical side, the work of Ojalvo and Grosh (71) forms a convenient starting point. Experimental data will, however, be needed to check the assumptions which will necessarily be involved in such a theoretical analysis.

Availability of a method of predicting the non-isothermal velocity profile under given conditions would have allowed calculation of the ratio of eddy diffusivities directly from the distorted temperature profiles obtained in this investigation.

If any experimental investigation is to involve the use of a total-head pitot-type velocity probe, the

use of a piezometer ring for the static pressure measurement is strongly recommended. Special consideration must also be given to the pressure measuring system, since measurement of very small pressure differences will be involved, particularly at low Reynolds numbers.

(b) A review of the correlations for a universal velocity profile is long overdue. A correlation is needed which not only predicts the correct velocity profile, but also gives the correct eddy diffusivity of momentum on differentiation. Hinze (48) has introduced a correction factor to the logarithmic velocity distribution, to account for observed deviations, but the resulting curve of ϵ_M does not agree with measured values towards the tube centre. A "defect" profile is often used for the central portion of the tube, but no universal form, which also fits the data, has so far been proposed. The eddy diffusivity values of Nikuradse (9) show an unexpected shape, decreasing toward the centre, and the velocity and shear stress distribution should accordingly be checked by careful velocity and static pressure measurements in the vicinity of the tube centre.

(c) Further measurements of temperature profiles are required to supplement the information contained in Fig. 25. Readings at high heat flux for the higher Reynolds numbers, and at low heat flux for low Reynolds numbers are required, in the first place to

gauge the degree of persistence of free convection effects to high Reynolds numbers, and secondly to allow prediction of the undistorted temperature profile at low Reynolds numbers. The latter would also allow determination of the Nusselt number, from equn. 6.2.

In order to allow operation at high heat fluxes, the experimental apparatus should be designed for a basic operating temperature as high as possible.

(d) Other methods of evaluating ϵ_H and ϵ_M should be investigated. The present method of differentiating experimental profiles is open to error and a check by another method is desirable. One method that is envisaged is evaluation of the eddy diffusivity as a parameter in a theoretical model of turbulent transport, by suitable correlation of the turbulent fluctuations at two positions in the fluid.

(e) Questions of which temperature to use in evaluating physical properties, and the exact effect of Prandtl number, Reynolds number and D/L ratio, in heat transfer by mixed free and forced convection, remain to be elucidated.

NOMENCLATURE.

A	Constant
A	Heat transfer area, ft^2
a	Constant
B	Constant
b	Constant
C	Constant
C_D	Orifice discharge coefficient
c	Constant
c, c_p	Specific heat, BTU/lb.°F
D	Diameter, ft
F	Ratio of thermal resistance of total diffusion to thermal resistance of eddy diffusion only.
F'	Normalised velocity integral (equn. B.9)
f	Fanning friction factor
f	Function value
G	Mass flow rate, $lb/hr.ft^2$
Gr	Grashoff number, $D^3\rho^2\beta g(T_w - T_c)/\mu^2$
Gr*	Grashoff number, $D^3\rho^2\beta g\,\Delta T/\mu^2$ where $\Delta T = (dT/dx)D$
g	Gravitational acceleration, ft/sec^2
g_c	Gravitational constant, 32.2 $ft.lb_m/lb_f.sec^2$
h	Heat transfer coefficient, $BTU/hr.ft^2.°F$
h	Integration interval
h(y/R)	Correction factor due to Hinze(48)
K	Constant
k	Thermal conductivity, BTU/hr.ft.°F
L	Length of test section from inlet to probe, ft
l	Prandtl's(41) mixing length
Nu	Nusselt number, hD/k
n	Index
Pe	Peclet number, Re x Pr
Pr	Prandtl number, $c_p\mu/k$

Q	Heat transferred, BTU/hr
q	Heat flux, BTU/hr.ft^2
R	Radius, ft
R	Resistance, ohms
Ra	Rayleigh number, $Gr^{*} \times Pr$
Re	Reynolds number, DG/μ or $Du_{av}\rho/\mu$
r	Radial distance measured from pipe centre, ft
S	Slope of temperature profile, $^{o}F/ft$
S	Slope of dimensionless temperature profile
St	Stanton number, h/cG
T	Temperature, ^{o}F (unless ^{o}C specified)
T_{∞}	Temperature of undisturbed fluid, ^{o}F
u	Velocity, ft/sec
u^{*}	Friction velocity, $u_{av}\sqrt{f/2}$, ft/sec
u^{+}	Dimensionless velocity, u/u^{*}
V	Volume of unit mass of fluid, ft^3
x	Distance measured along tube axis, ft
Y	Yantovskii(65) criterion, $Gr/Re^2(f/2)$
y	Radial distance measured from wall, ft
y^{+}	Dimensionless distance from wall, yu^{*}/ν
Z	Natural convection criterion, $\frac{Ra}{Re} \cdot \frac{D}{L}$

α	Thermal diffusivity, $k/\rho c_p$, ft^2/hr
β	Coefficient of cubical expansion, $^{o}F^{-1}$
β	Ratio of orifice to pipe diameters
Δh	Head difference, ft
ΔT	Temperature difference, ^{o}F
ΔT	"Axial" temperature difference, $(dT/dx)D$, ^{o}F
Δx	Differential axial increment, ft
Δx	Thickness, ft

ϵ	Ratio of eddy diffusivities, ϵ_H/ϵ_M
ϵ_H	Eddy diffusivity of heat, ft^2/hr
ϵ_M	Eddy diffusivity of momentum, ft^2/hr
Θ	Dimensionless temperature, $(T_w - T)/(T_w - T_c)$
μ	Viscosity, centipoises
ν	Kinematic viscosity, ft^2/hr
ρ	Density, lb/ft^3
τ	Shear stress $\times g_c$, $(lb_f/ft^2) \times 32.2$ ft.lb_m/lb_f.sec^2
Φ	Dimensionless average temperature, $(T_w - T_{av})/(T_w - T_c)$
$\phi(y/R)$	Heat flux distribution, equn. 4.3
$\psi(y/R)$	Shear stress distribution

Subscripts

av	Average
c	At pipe centre
calc.	Calculated value
in	At inlet
out	At outlet
w	At wall
y	At radial position y or y/R
o	At radial position y = 0 (i.e. wall)
1, 2, etc.	Function value at position, or temperature, 1, 2, etc.

LIST OF REFERENCES.

1. O. Reynolds, "On the extent and action of the heating surface of steam boilers", Proc. lit. phil. Soc. Manchester, 14, 7 - 12 (1874). Reprinted in O. Reynolds, "Papers on mechanical and physical subjects", vol. I, Cambridge Univ. Press (1900) pp. 81 - 85.

2. L. Prandtl, "Eine Beziehung zwischen Wärmeaustauch und Strömungswiderstand der Flüssigkeiten", Phys. Z., 11, 1072 -1078 (1910).

3. G. I. Taylor, "Conditions at the surface of a hot body exposed to the wind", Rept.s and Memoranda of the Advisory Comm. for Aeronautics, No. 272, 423 - 429 (1916). Reprinted in G. K. Batchelor, "The scientific papers of Sir Geoffrey Ingram Taylor", vol. II, Cambridge Univ. Press (1960) pp. 27 - 32.

4. T. von Karman, "The analogy between fluid friction and heat transfer", Trans. ASME, 61, 705 - 710 (1939).

5. A. Eagle and R. M. Ferguson, "On the coefficient of heat transfer from the internal surface of tube walls", Proc. R. Soc., A127, 540 - 566 (1930).

6. L. M. K. Boelter, R. C. Martinelli and F. Jonassen, "Remarks on the analogy between heat and momentum transfer", Trans. ASME, 63, 447 - 455 (1941).

7. R. C. Martinelli, "Heat transfer to molten metals", Trans. ASME, 69, 947 - 959 (1947).

8. R. N. Lyon, "Liquid metal heat transfer coefficients", Chem. Engng Progr., 47, 75 - 79 (1951).

9. J. Nikuradse, "Gesetzmässigkeiten der turbulenten Strömung in glatten Rohren", Ver. dt. Ing. ForschHft. 356 (1932),

10. R. A. Seban and T. T. Shimazaki, "Heat transfer to a fluid flowing turbulently in a smooth pipe with walls at constant temperature", Trans. ASME, 73, 803 - 809 (1951).

11. M. A. Styrikovich and I. E. Semenovker, "Heat transfer at very low Prandtl numbers", Zh. Tekh. Fiz., 10, 1324 - 1330 (1940).

12. L. M. Trefethen, "Liquid metal heat transfer in circular tubes and annuli", Proc. of the general discussion on heat transfer, Inst. of Mech. Engng, London and ASME, 11 - 13 Sept., 1951, pp. 436 - 438.

13. D. English and T. Barrett, "Heat transfer properties of mercury", ibid. Ref. (12), pp. 458 - 460.

14. H. A. Johnson, W. J. Clabaugh and J. P. Hartnett, "Heat transfer to mercury in turbulent pipe flow", Trans. ASME, 76, 505 - 511 (1954).

15. H. A. Johnson, J. P. Hartnett and W. J. Clabaugh, "Heat transfer to lead-bismuth and mercury in laminar and transition pipe flow", Trans. ASME, 76, 513 - 517 (1954).

16. S. E. Isakoff and T. B. Drew, "Heat and momentum transfer in turbulent flow of mercury", ibid. Ref. (12), pp. 405 - 409.

17. S. E. Isakoff, "Heat and momentum transfer in turbulent flow of mercury", Ph. D. Thesis, Columbia Univ. (1952).

18. B. Lubarsky and S. J. Kaufman, "Review of experimental investigations of liquid-metal heat transfer", NACA R-1270 (1956).

19. H. E. Brown, B. H. Amstead and B. E. Short, "Temperature and velocity distribution and transfer of heat in a liquid metal", Trans. ASME, 79, 279 - 285 (1957).

20. P. L. Kirillov, V. I. Subbotin, M. Ya. Suvorov and M. F. Troyanov, "Heat transfer in a tube to sodium-potassium alloy and to mercury" Atomn. Energ., 6, No. 4, 382 (1959). Transl. as Soviet J. atom. Energy, 6, 253 - 260 (1960).

21. V. I. Subbotin, M. Kh. Ibragimov, M. N. Ivanovskii, M. N. Arnoldov and E. V. Nomofilov, "Turbulent heat transfer in a stream of molten metals", Atomn. Energ., 10, No. 4, 384 - 386 (1961). Transl. as Soviet J. atom. Energy, 10, 373 - 376 (1962).

22. V. I. Subbotin, M. Kh. Ibragimov, M. N. Ivanovskii, M. N. Arnoldov and E. V. Nomofilov, "Heat transfer from the turbulent flow of liquid metals in tubes", Atomn. Energ., 11, No. 2, 133 - 139, (1961). Transl. as Soviet J. atom. Energy, 11, 769 - 774 (1962).

23. L. S. Kokorev and V. N. Ryaposov, "Turbulent heat transfer during the flow of a heating medium of small Prandtl number along a tube", Zhurn. priklad. Mekh. tekh. Fiz., No. 2, 42, (1962). Transl. as International Chemical Engineering, 2, 514 - 519 (1962).

24. V. I. Subbotin, A. K. Papovayants, P. L. Kirillov, and M. N. Ivanovskii, "A study of heat transfer to molten sodium in tubes", Atomn. Energ., 13, No. 4, 380 - 382 (1962). Transl as Soviet J. atom. Energy, 13, 991 _ 994 (1963).

25. V. I. Subbotin, M. Kh. Ibragimov and E. V. Nomofilov, "Measurement of temperature fields for turbulent mercury flow in a tube", Teploenergetika, 10, No. 6, 70 - 74 (1963). UKAEA, Risley, Translation 658.

26. V. M. Borishanskii, T. V. Zablotskaya and N. I. Ivashchenko, "Heat transfer to molten metals during flow in pipes", Atomn. Energ., 14, No. 3, 320 - 322 (1963). Transl. as Soviet J. atom. Energy, 14, 318 - 320 (1964).

27. W. C. MacDonald and R. C. Quittenton, "A critical analysis of metal wetting and gas entrainment in heat transfer to molten metals", Chem. Engng Progr. Symp. Ser., 50, No. 9, 59 - 67 (1954).

28. M. Jakob, "Heat Transfer", vol. II, John Wiley, New York (1957) p. 521.

29. R. N. Lyon, discussion of paper by P. S. Lykoudis and Y. S. Touloukian, Ref. (32), Trans. ASME, 80, 663 (1958).

30. R. Jenkins, "Variation of eddy conductivity with Prandtl modulus and its use in prediction of turbulent heat transfer coefficients", Heat transfer and fluid mechanics institute, Stanford Univ. Press, Stanford (1951) pp. 147 - 158.

31. R. G. Deissler, "Analysis of fully developed turbulent heat transfer at low Peclet numbers in smooth tubes with application to liquid metals", NACA RM E52F05 (1952).

32. P. S. Lykoudis and Y. S. Touloukian, "Heat transfer in liquid metals", Trans ASME, 80, 653 - 666 (1958).

33 N. Z. Azer and B. T. Chao, "A mechanism of turbulent heat transfer in liquid metals", Int. J. Heat Mass Transfer, 1, 121 - 138 (1960).

34. O. E. Dwyer, "Eddy transport in liquid-metal heat transfer", A. I. Ch. E. Jl, 9, 261 - 268 (1963).

35. A. Sesonske, S. L. Schrock and E. H. Buyco, "Eddy diffusivity ratios for mercury flowing in a tube", A. I. Ch. E. Preprint No. 25, Sixth National Heat Transfer Conf., Boston (1963).

36. E. H. Buyco, "Heat and momentum transfer in liquid metals", Ph. D. Thesis, Purdue Univ. (1961).

37. S. L. Schrock, "Eddy diffusivity ratios in liquid metals", Ph. D. Thesis, Purdue Univ. (1964).

38. A. D. Carr and R. E. Balzhiser, "Temperature profiles and eddy diffusivities in liquid metals", Br. chem. Engng, 12, 53 - 57 (1967).

39. O. E. Dwyer, "Recent developments in liquid-metal heat transfer", Atomic Energy Review, 4, 3 - 92 (1966).

40. U. Grigull and H. Tratz, "Hydrodynamisches verhalten von Quecksilber bei laminarer und turbulenter Rohrströmung", Chemie-Ingr-Tech., 37, 1102 - 1106 (1965).

41. L. Prandtl, "Essentials of fluid dynamics", Blackie and Son, London (1952) pp. 124 - 129.

42. T. von Karman, "Turbulence and skin friction", J. aeronaut. Sci., 1, 1 - 20 (1934).

43. C. S. Lin, R. W. Moulton and G. L. Putnam, "Mass transfer between solid wall and fluid streams", Ind. Engng Chem., 45, 636 - 646 (1953)

44. R. G. Deissler, "Analysis of turbulent heat transfer, mass transfer and friction in smooth tubes at high Prandtl and Schmidt numbers", NACA R 1210 (1955).

45. J. Laufer, "The structure of turbulence in fully developed pipe flow", NACA R 1174 (1954).

46. D. Ross, "A new analysis of Nikuradse's experiments on turbulent flow in smooth pipes", Proc. Midwestern Conf. on Fluid Mech., 3rd Conf., Univ. Minn., 651 - 667 (1963).

47. F. H. Clauser, "The turbulent boundary layer", in H. L. Dryden and T. von Karman (editors), "Advances in applied mechanics", vol. IV, Academic Press, New York (1956) pp. 5 - 6.

48. J. O. Hinze, "Turbulence", McGraw-Hill, New York (1959) pp. 516 - 518.

49. T. E. Stanton, "The mechanical viscosity of fluids", Proc. R. Soc., A85, 366 - 376 (1911).

50. C. A. Sleicher, "Heat transfer in a pipe with turbulent flow and arbitrary wall-temperature distribution", Ph. D. Thesis, Univ. Michigan (1955).

51. P. W. Rein, Unpublished work, Univ. Cape Town (1966). Personal communication.

52. W. F. Beckwith and R. Fahien, "Determination of turbulent thermal diffusivities for flow of liquids in pipes", Research and Dev. Report IS-734, Ames Laboratory, Iowa State Univ. (1963).

53. F. Page, W. G. Schlinger, D. K. Breaux and B. H. Sage, "Point values of eddy conductivity and viscosity in uniform flow between parallel plates", Ind. Engng Chem., 44, 424 _ 430 (1952).

54. H. Reichardt, "Die Wärmeübertragung in turbulenten Reibungsschichten", Z. a. M. M., 20, 297 - 328 (1940). Transl. by L. M. K. Boelter as "Heat transfer through turbulent friction layers", NACA TM 1047 (1943).

55. R. G. Deissler, "Analytical and experimental investigation of turbulent flow in smooth tubes", NACA TN 2138 (1950).

56. B. Miller. "The laminar film hypothesis", Trans. ASME, 71, 357 - 367 (1949).

57. J. O. Hinze, op. cit. Ref. (48) p. 525.

58. D. T. Wasan, T. K. Subramaniam and S. S. Randhava, Chem. Engng, 19, 165 - 168 (1966).

59. F. H. Clauser, op. cit. Ref. (47) p. 40.

60. S. I. Pai, "On turbulent flow in circular pipe", J. Franklin Inst., 256, 337 - 352 (1953).

61. J. Nikuradse, op. cit. Ref. (9) p. 25.

62. J. Nikuradse, op. cit. Ref. (9) p. 19.

63. S. Lynn, "Center-line value of the eddy viscosity", A. I. Ch. E. Jl, 5, 566 - 567 (1959).

64. A. D. Carr and H. O. Buhr, "Liquid metal heat transfer loops", S. Afr. mech. Engr., 16, 1 - 7 (1966).

65. E. I. Yantovskii, "An estimate of the influence of free convection upon turbulent flow", Zhurn. Tekh. Fiz., 29, No. 2, 1390 - 1392 (1959). Transl. as Soviet Phys. Tech. Phys., 4, 1280 - 1282 (1960).

66. T. M. Hallman, "Combined forced and free-laminar heat transfer in vertical tubes with uniform internal heat generation", Trans. ASME, 78, 1831 - 1841 (1956).

67. E. R. G. Eckert, A. J. Diaguila and A. N. Curren, "Experiments on mixed-free- and -forced-convective heat transfer connected with turbulent flow through a short tube", NACA TN 2974 (1953).

68. C. K. Brown and W. H. Gauvin, "Combined free- and -forced convection", Can. J. chem. Engng, 43, 306 - 318 (1965).

69. T. W. Jackson, W. B. Harrison and W. C. Boteler, "Combined free and forced convection in a constant-temperature vertical tube", Trans. ASME, 80, 739 - 745 (1958).

70. G. A. Kemeny and E. V. Somers, Combined free and forced-convective flow in vertical circular tubes - Experiments with water and oil", J. Heat Transfer, 84C, 339 - 346 (1962).

71. M. S. Ojalvo and R. J. Grosh, "Combined forced and free turbulent convection in a vertical tube", AEC Res. and Dev. Report ANL-6528, Argonne National Laboratory, Argonne, Ill. (1962).

72. S. S. Kutateladze, "Fundamentals of Heat Transfer", Edward Arnold Ltd., London (1963) p. 294

73. F. J. Bayley, P. A. Milne and D. E. Stoddart, "Heat transfer by free convection in a liquid metal", Proc. R. Soc., 265A, 97 - 108 (1961).

74. D. R. Oliver, "The effect of natural convection on viscous-flow heat transfer in horizontal tubes", Chem. Engng Sci., 17, 335 - 350 (1962).

75. R. C. Martinelli and L. M. K. Boelter, "The analytical prediction of superposed free and forced viscous convection in a vertical pipe", Univ. of California Publications in Engineering, 5, No. 2, 23 - 58 (1942), as reported in Ref. (69).

76. B. Metais and E. R. G. Eckert, "Forced, mixed and free convection regimes", J. Heat Transfer, 86C, 295 - 296 (1964).

77. H. Schlichting, "Boundary Layer Theory", 4th ed., McGraw-Hill, New York (1960) p. 300.

78. A. D. Carr, Experimental work carried out at Univ. Michigan, 1965. Personal communication.

79. C. Fröberg, "Introduction to Numerical Analysis", Addison-Wesley Pub. Co., Reading, Mass. (1965).

80. J. H. Preston and J. F. Norbury, "The three-quarter radius flowmeter - a reassessment", in "Flow measurement in closed conduits", Proc. of a Symposium held at the National Engineering Laboratory (DSIR), 27th - 30th Sept. 1960, vol. I, HMSO, Edinburgh (1962) pp. 43 - 66.

81. R. B. Bird, W. E. Stewart and E. N. Lightfoot, "Transport Phenomena", John Wiley, New York (1960) p. 297.

82. S. S. Kutateladze, V. M. Borishanskii, I. I. Novikov and O. S. Fedynskii, "Liquid metal heat transfer media", Consultants Bureau Inc., New York (1959) pp. 2 - 5.

83. R. N. Lyon (editor), "Liquid-metals handbook", 2nd ed., U. S. Govt. Printing Office, Washington (1954) pp. 42 - 43.

84. S. W. Churchill and R. E. Balzhiser, "The radial heat flux", Chem. Engng Progr. Symp. Ser., 55, No. 29, 127 - 135 (1959).

85. H. S. Mickley, T. K. Sherwood and C. E. Reed, "Applied mathematics in chemical engineering", 2nd ed., McGraw-Hill, New York (1957) pp. 25 - 28.

86. "Smithsonian Physical Tables", 9th rev. ed., Washington, D. C. (1954) Table 291, reproduced in J. H. Perry, "Chemical Engineers' Handbook", 4th ed., McGraw-Hill, New York (1963) p. 3-71.

87. D. M. Considine, ed., "Process Instruments and Controls Handbook", McGraw-Hill, New York (1957) pp. 12-68 - 12-78.

88. British Standard 1042 : Part 1 : 1964, "Methods for the measurement of fluid flow in pipes. Part 1. Orifice plates, nozzles and venturi tubes", Br. Standards Inst., London (1964).

APPENDICES.

APPENDIX A VELOCITY PROFILES

APPENDIX B TEMPERATURE PROFILE MEASUREMENTS

APPENDIX C VALUES OF THE PARAMETERS Y AND Z

APPENDIX D RATIO OF EDDY DIFFUSIVITIES

APPENDIX E CALCULATION OF ϵ_M/Ru^*

APPENDIX F EQUIPMENT DETAILS

APPENDIX G HEAT TRANSFER COEFFICIENTS

APPENDIX H PHYSICAL PROPERTIES

APPENDIX A

VELOCITY PROFILES

The calculation procedure for a typical velocity run is given below.

The run chosen is Run V.7, which was carried out with the gas pressuring system shown in Fig. 10. For this run, the water manometer was vertical and the velocity profile is shown in Fig A.1. Results are summarised in Table A.1.

Radial position is taken as the centre of the pitot tube, which is 0.008 in. i.e. $y/R = 0.0099$ from the wall with the probe in the zero position. No correction for displacement of the "effective" centre was made. Preston and Norbury (80) indicate that the displacement error is very small for sharp-lipped pitot tubes.

For a typical radial position

e.g. $y/R = 0.104$, $\Delta h = 3.55$ cm water

$$u = \sqrt{2 g \Delta h}$$

$$= \left(\frac{2 \times 32.2 \times 3.55}{13.6 \times 2.54 \times 12} \right)^{1/2} = 0.743 \text{ ft/sec.}$$

The average velocity was obtained by integration from

$$u_{av} = 2 \int_0^1 u \frac{r}{R} d\left(\frac{r}{R}\right) \qquad (A.1)$$

using Simpson's rule in the same way as described for the average temperature in app. B. 26.

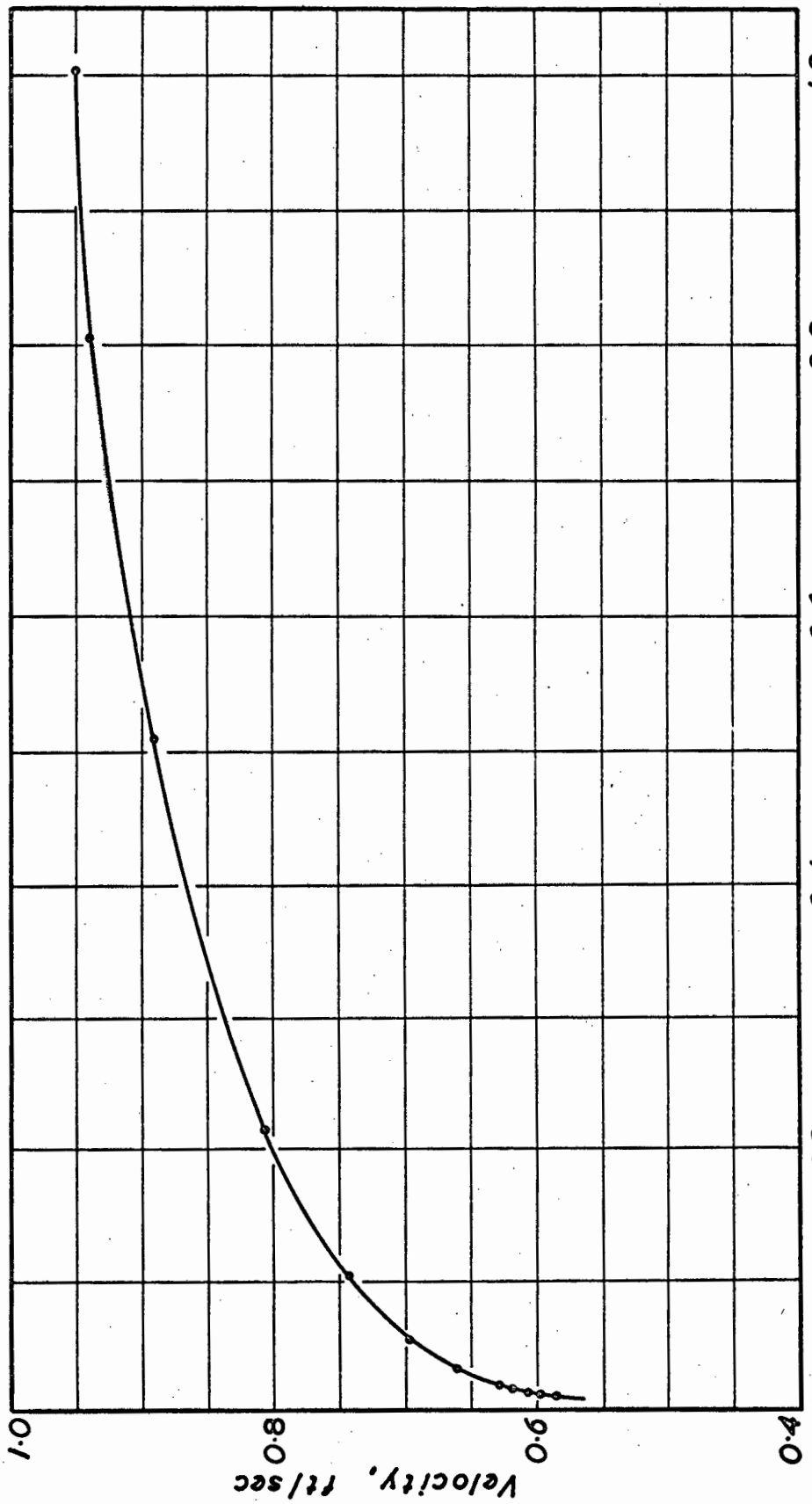

FIG. A.1 VELOCITY PROFILE IN MERCURY, RUN V.7

For this run, the value obtained is $u_{av} = 0.812$ ft/sec.

$$Re = \frac{D\,u\,\rho}{\mu} = \frac{1.624 \times 0.812 \times 848 \times 1488}{12 \times 1.55}$$

$$= 0.897 \times 10^5$$

$$\therefore \sqrt{f/2} = 0.0477 \quad \therefore u^* = 0.0387$$

Now for any radial position, u^+ and y^+ may be evaluated:

e.g. $y/R = 0.104$

$$y^+ = (y/R)\,(Re/2)\sqrt{f/2}$$

$$= 0.104 \times 0.5 \times 0.897 \times 10^5 \times 0.0477$$

$$= 222$$

$$u^+ = u/(u_{av}\sqrt{f/2}) = u/u^*$$

$$= 0.743/0.0387 = 19.2$$

TABLE A.1

VELOCITY PROFILE, RUN V.7

Radial Position y/R	Differential pressure, cm. water	Velocity, ft/Sec	y^+	u^+
0.012	2.18	0.583	25.7	15.0
0.013	2.28	0.596	27.8	15.4
0.014	2.35	0.605	29.9	15.6
0.017	2.45	0.617	36.4	15.9
0.020	2.53	0.627	42.8	16.2
0.032	2.81	0.661	68.5	17.0
0.055	3.12	0.697	118	18.0
0.104	3.55	0.743	222	19.2
0.215	4.18	0.806	450	20.8
0.510	5.10	0.891	1090	23.0
0.805	5.68	0.940	1720	24.2
1.005	5.79	0.950	2140	24.5

APPENDIX B

TEMPERATURE PROFILE MEASUREMENTS

B.1 RESULTS

Test readings and calculated results are summarised in Tables B.1 and B.2. The calculation procedure is outlined in the next section.

TABLE B.1 - TEMPERATURE PROFILE MEASUREMENTS.

Run Number	1	1a	2	3	3a	4	4a
Temperatures, °F:							
Test section inlet	59.0	58.9	74.7	60.5	59.4	60.2	60.2
outlet	123.7	127.6	122.2	129.0	129.6	125.9	127.0
Inside insulation	115.1	116.6	117.2	126.1	125.8	130.1	130.8
Outside insulation	71.3	70.2	85.6	77.7	75.8	69.5	69.7
Heat input:							
Upper circuit, KW	0.472	0.514	0.372	0.723	0.761	1.008	1.032
Lower circuit, KW	0.452	0.490	0.356	0.690	0.725	0.968	0.987
Auxiliary circuit, W	2.1	2.1	1.7	3.7	3.6	5.0	5.0
Ratio upper/lower	1.044	1.049	1.045	1.048	1.050	1.041	1.046
% Auxiliary/main	0.23	0.21	0.23	0.26	0.24	0.25	0.25
Heat loss, % of input	5.6	5.4	5.2	4.1	4.0	3.6	3.6
Net heat flux BTU/hr.ft^2	430	470	340	670	700	940	960
Mass flow rate from heat balance, lb/hrft^2 x10^{-6}	0.097	0.099	0.104	0.142	0.145	0.208	0.209
% from orifice meter	98.4	98.8	109.0	98.6	98.6	100.2	99.6
Mean cup temp., °F	117.9	122.4	118.7	123.4	124.8	119.8	121.7
Reynolds Number x 10^{-3}	3.8	4.0	4.2	5.7	5.8	8.3	8.3
Prandtl Number	0.021	0.021	0.021	0.021	0.021	0.021	0.021
Temperature Profiles:							
Wall temp., °F	119.3	123.8	120.1	125.5	127.2	122.7	124.5
T_w-T at y/R = 1.00	1.82	1.77	2.09	3.00	3.35	4.24	4.23
0.95	-	-	2.07	-	-	-	-
0.90	1.81	1.79	2.10	2.97	3.32	4.22	4.15
0.80	1.82	1.77	2.00	2.89	3.26	4.13	4.26
0.70	1.76	1.86	1.91	2.85	3.30	4.07	4.05
0.60	1.67	1.70	1.84	2.77	3.21	3.96	-
0.50	1.72	1.66	1.72	2.57	3.13	3.63	3.59
0.45	-	-	-	2.40	2.93	-	-
0.40	1.60	1.66	1.55	2.33	2.72	3.35	3.11
0.35	1.50	1.47	1.47	2.18	2.55	3.00	3.06
0.30	1.45	1.41	1.30	2.07	2.24	2.87	2.82
0.25	1.32	1.26	1.19	1.86	2.02	2.45	2.59
0.20	1.14	1.12	1.05	1.73	1.85	2.28	2.26
0.15	1.07	0.92	0.81	1.21	1.33	1.72	1.76
0.10	0.67	0.62	0.60	0.94	1.02	1.09	1.21
0.05	0.28	0.24	0.36	0.59	0.51	0.52	0.57
0.03	0.15	0.17	0.16	0.12	0.27	0.37	0.40
0.02	0.09	0.11	0.04	0.00	-	0.24	0.26
0.01	0.07	-0.01	0.03	0.05	0.02	0.00	-0.19
0.005	-	-	-	-0.01	0.18	-	-
0.00	0.09	0.04	0.00	0.17	-	0.14	0.07
T_w-$T_{av'}$, °F	1.40	1.36	1.38	2.05	2.36	2.84	2.83

TABLE B.1 ctd. - TEMPERATURE PROFILE MEASUREMENTS.

Run Number	5	6	7	8	9	10	11	12
Temperatures, °F:								
Inlet	71.3	79.0	94.9	79.8	75.3	97.5	100.4	100.1
Outlet	122.8	127.8	166.4	127.9	113.4	116.4	114.7	117.1
Inside insul.n	131.9	142.2	126.5	176.9	192.5	205.4	201.9	263.1
Outside insul.n	71.7	76.5	74.4	80.9	95.6	105.1	99.0	113.6
Heat input:								
Upper circuit, KW	1.092	1.333	1.009	2.585	3.110	3.315	3.270	5.350
Lower circuit, KW	1.051	1.242	0.954	2.470	2.945	3.180	3.154	5.100
Aux. circuit, W	5.5	6.5	4.7	13.5	16.4	17.6	17.6	29.5
Ratio upper/lower	1.039	1.073	1.058	1.047	1.056	1.042	1.037	1.049
% Aux./main	0.26	0.25	0.24	0.27	0.27	0.27	0.27	0 28
Heat loss, %	3.3	3.1	3.2	2.3	2.0	1.9	2.0	1.9
Net heat flux	1020	1230	940	2440	2930	3150	3110	5070
Mass flow rate, $lb/hr ft^2 \times 10^{-3}$	0.289	0.367	0.634	0.737	1.116	2.42	3.17	4.35
Orifice meter %	106.1	101.9	-	103.8	104.1	101.2	95.4	96.5
Mean cup temp, °F	119.2	124.1	113.1	123.8	108.2	113.9	112.8	115.6
Re $\times 10^{-3}$	11.4	14.7	24.9	29.6	43.4	95.5	124	172
Pr	0.021	0.021	0.021	0.021	0.022	0.021	0.021	0.021
Temperature Profiles:								
Wall temp, °F	122.6	127.9	116.1	131.1	116.9	119.1	117.3	121.7
$T_w - T$ at y/R=1.000	4.88	5.75	5.19	11.28	14.55	8.32	6.80	9.09
0.95	-	5.71	5.24	11.31	14.08	-	6.85	-
0.90	4.94	5.59	5.20	11.30	14.32	8.20	6.83	8.95
0.80	4.97	5.49	5.08	11.03	13.99	8.08	6.59	8.80
0.70	4.72	5.32	5.00	10.85	13.58	7.75	6.55	-
0.60	4.58	5.11	4.55	10.44	13.07	-	6.19	8.01
0.50	4.30	4.87	4.06	9.56	11.84	6.79	5.91	-
0.40	3.87	4.60	3.52	8.43	10.53	-	5.22	6.94
0.35	3.76	4.37	3.25	7.99	-	-	-	-
0.30	3.37	3.96	2.87	7.38	8.78	5.22	4.54	5.92
0.25	3.01	3.66	2.53	6.47	7.42	-	3.96	-
0.20	2.55	3.05	2.16	5.80	6.32	4.05	3.44	5.20
0.15	2.08	2.75	1.68	4.99	5.02	-	3.01	4.41
0.10	1.54	1.76	0.99	3.60	3.87	2.93	2.53	3.36
0.05	0.73	0.92	0.56	2.04	2.19	1.71	1.68	2.66
0.03	0.41	-	0.43	-	1.01	1.13	-	1.85
0.02	0.20	0.27	0.23	0.41	0.90	0.77	0.84	1.04
0.01	0.00	-	0.07	-	-	0.61	-	0.75
0.005	0.01	-	-	-	-	-	(0.11%	-
0.00	-0.02	-0.18	-0.05	-0.01	-0.38	-0.34	=0.06)	-0.24
$T_w - T_{av}$, °F	3.33	3.83	3.02	7.31	8.76	5.24	4.46	6.08

TABLE B.1 ctd. - TEMPERATURE PROFILE MEASUREMENTS.

Run Number	13	13a	14	15	16	17	18	18a
Temperatures, °F:								
Inlet	100.0	99.9	76.9	137.3	101.5	126.5	155.2	158.2
Outlet	115.2	115.0	176.1	187.3	189.5	185.5	187.9	190.3
Inside insul.n	312.3	313.5	185.1	178.9	233.7	209.7	193.7	193.1
Outside insul.n	118.8	120.0	88.7	86.8	91.1	88.4	90.6	88.4
Heat input:								
Upper circuit, KW	7.02	7.09	1.709	1.037	3.139	2.224	1.523	1.506
Lower circuit, KW	6.74	6.79	1.624	0.982	3.036	2.123	1.438	1.435
Aux. circuit, W	41.9	41.4	8.6	5.0	17.4	11.9	7.0	6.7
Ratio upper/lower	1.042	1.044	1.052	1.056	1.034	1.048	1.059	1.049
% Aux./main	0.31	0.30	0.26	0.25	0.28	0.27	0.24	0.23
Heat loss, %	1.9	1.9	3.6	5.6	2.9	3.5	4.3	4.4
Net heat flux	6670	6730	1590	940	2960	2070	1400	1390
Mass flow rate, $lb/hr ft^2 \times 10^{-6}$	6.37	6.46	0.233	0.276	0.491	0.514	0.627	0.633
Orifice meter %	98.1	96.8	102.7	99.9	99.5	103.6	99.9	99.7
Mean cup$_3$ temp, °F	114.1	114.0	168.8	181.6	183.9	182.6	183.7	186.7
Re × 10	251	254	10.1	12.1	21.8	22.7	27.8	28.2
Pr	0.021	0.021	0.018	0.017	0.017	0.017	0.017	0.017
Temperature Profiles:								
Wall temp, °F	119.3	119.3	172.4	183.8	189.8	187.2	187.6	190.1
$T_w - T$ at y/R= 1.00	7.36	7.43	4.92	3.36	8.39	6.76	6.01	5.14
0.95	7.12	-	-	-	-	-	-	5.40
0.90	7.32	7.43	4.99	3.37	8.26	6.67	5.98	5.24
0.80	7.17	7.36	4.99	3.31	8.37	6.57	5.97	5.20
0.70	6.95	7.13	4.81	3.20	8.33	6.44	5.95	5.05
0.60	6.80	6.98	4.82	3.08	7.91	6.45	5.79	4.85
0.50	6.38	6.44	4.50	3.00	7.50	5.99	5.32	4.44
0.45	6.17	-	-	2.78	-	-	-	-
0.40	5.89	5.73	4.25	2.68	6.81	5.54	4.84	4.09
0.35	5.67	5.47	3.91	2.51	6.46	-	4.35	3.90
0.30	5.26	5.34	3.72	2.31	6.06	4.85	3.93	3.55
0.25	4.96	4.96	3.32	2.26	5.70	4.33	3.35	3.05
0.20	4.59	4.48	2.90	1.67	4.75	3.93	3.04	2.61
0.15	4.00	3.85	2.44	1.27	4.04	2.97	2.44	2.09
0.10	3.41	3.34	1.60	1.04	3.15	2.16	1.72	1.59
0.05	2.47	2.47	1.01	0.61	1.60	1.27	0.89	0.64
0.03	1.87	1.92	0.51	0.26	1.01	0.76	0.56	0.39
0.02	1.38	1.38	0.27	0.27	0.65	0.44	0.44	0.32
0.01	1.71	0.71	0.19	-	0.38	0.37	0.25	0.11
0.00	-0.23	-0.26	-	-	-0.11	-	0.05	0.19
$T_w - T_{av}$, °F	5.18	5.22	3.56	2.24	5.94	4.59	3.91	3.44

TABLE B.2 - Wall temperatures

Run Number		5	6	8	9	10	11	12	13
Re x 10^{-3}		11.4	14.7	29.6	43.4	95.5	124	172	251
Heat flux, B/hrft^2		1020	1230	2440	2930	3150	3110	5070	6670
ΔT over wall*, °F		1.13	1.36	2.70	3.25	3.49	3.45	5.62	7.40
Wall temp, T_w, °F		122.6	127.9	131.1	116.8	119.1	117.3	121.7	119.3
Wall thermocouples:									
1	Downstream	123.8	128.6	134.0	122.2	124.6	122.3	129.8	132.9
2	Downstream	-	129.0	134.7	122.5	115.9	122.3	118.2	119.2
3	Downstream	123.6	128.6	133.9	122.3	117.6	122.1	121.8	120.4
4	Downstream	123.6	129.1	133.4	121.2	119.3	122.6	124.1	122.5
5	At probe	121.3	128.0	132.2	119.6	122.0	119.3	126.7	126.8
6	At probe	122.0	127.7	131.5	121.6	123.9	122.9	130.1	130.8
7	Upstream	122.8	128.2	134.7	124.2	120.7	124.9	126.6	127.5
8	Upstream	122.8	128.7	134.1	125.3	120.1	124.6	125.6	121.8
9	Upstream	Dead	-	-	-	-	-	-	-
10	Upstream	123.0	128.3	135.4	124.9	127.4	124.8	136.7	140.3

*Temperature drop over 1/8 in. wall. Exact depth of thermocouples not known.

B.2 CALCULATION PROCEDURE

Run No. 10 will be used to illustrate the method of working up the experimental data.

B.21 Heat flux

Heat input, upper coil = 1.053KWH over 19.06 minutes

= (1.053 x 60/19.06) = 3.315 KW

lower coil = 3.180 KW

auxiliary heater = 1.56A x 11.3V = 0.018 KW

6.513 KW

Total heat input = 6.513 x 3412.8 = 22,230 BTU/hr

Heat loss: Readings of thermocouples situated on either side of 1" glass fibre preformed pipe insulation:

$$T \text{ inside} = 205.4\ ^{\circ}F$$
$$T \text{ outside} = 105.1\ ^{\circ}F,\ \Delta T = 100.3\ ^{\circ}F$$

Thermal conductivity data for the insulation were obtained from the manufacturers and could be approximated as follows:

$$k = 0.01667 + 0.0000616\ T, \quad T > 92\ ^{\circ}C$$
$$k = 0.01878 + 0.0000386\ T, \quad T < 92\ ^{\circ}C$$

where T = temp., °C

Mean insulation temp. = 155.3 °F = 69.0 °C

$\therefore$ k = 0.0214 BTU/hr ft² (°F/ft)

Log mean area of insulation (3" I.D., 5" O.D.)
= 1.024 ft²/ft

Test section length = 16.3 ft.

$\therefore$ Heat loss = $kA\,\Delta T/\Delta x$ = 0.0214x1.024x16.3x100.3x12/1
= 430 BTU/hr.

$\therefore$ Net heat input = 21,800 BTU/hr.

Inside surface area of test section = πDL
= (πx0.1353x16.3) = 6.93 ft²

$\therefore$ Heat flux = 21,800/6.93 = 3150 BTU/hr ft²

B.22 Mass flow rate

The mass flow rate may be obtained by heat balance

over the test section, or from the orifice meter reading.

Heat Balance: Nett heat input = 21,800 BTU/hr

Test section outlet temp. = 116.4 °F

inlet temp. = 97.5°F, ΔT = 18.9

Mean temp. = 107.0°F; c_p = 0.0331 BTU/lb. °F

$\therefore$ Flow rate = $Q/c_p \Delta T$ = 21800/0.0331 x 18.9

= 34,800 lb/hr

Tube cross-sectional area = $\pi(0.1353)^2/4$ = 0.01437 ft²

$\therefore$ Mass flow rate = 34800/0.01437 = 2.42 X10^6 lb/hr ft²

Check: Orifice meter reading = 2.72 cm Hg (orifice no. 1) at ambient temperature, 81.1 °F

Mean of test section outlet and cooling section inlet temps. = 115.6 °F

Manometer reading is equivalent to

$$2.72 \times \frac{\rho_{81.1}}{\rho_{115.6}} = 2.72 \times \frac{844.5}{841.6} = 2.73 \text{ cm Hg}$$

From Appendix F.3, orifice coefficient = 0.616, β = 0.6927

$$\therefore \quad u_{av} = \frac{C_D \beta^2}{\sqrt{1 - \beta^4}} \sqrt{2 g \Delta h} = 0.809 \text{ ft/sec.}$$

$\therefore$ Mass flow rate = (0.809x3600x841.6) = 2.45x10^6 lb/hr ft²

This value is 101.2% of that obtained by heat balance, and is a good check. The orifice meter reading was used only for initial setting of the flow rate and was only recorded once during the run. The heat balance

value was considered the more reliable and used in further calculations.

B.23 Reynolds number

The exact Reynolds number at the probe depends on the viscosity at the mean cup temperature. Since this temperature is at present unknown, and will in turn depend on the Reynolds number (see section B.26) a temperature is initially assumed and the correct mean cup temperature established by iteration.

For this run, the mean cup temperature turned out to be 113.86 °F

$$\mu \text{ at } 113.86\ ^{\circ}F = 1.422 \text{ c.p.}$$

$$\therefore Re = DG/\mu = 0.1353 \times 2.42 \times 10^{6} / 1.422 \times 2.42$$

$$= 95{,}500$$

B.24 Temperature profile

Temperature recordings were made using the millivolt recorder and voltage reference system. The profile recording obtained for Run No. 10 is shown in Fig. 20, p. 56. Use of the voltage reference system introduced an external resistance which changed the recorder scale factor in the ratio

$$\frac{\text{Internal R + External R}}{\text{Internal R}} . \qquad \text{(B.1)}$$

Operating conditions during Run 10 were as follows:

Reference voltage = 2.481 mV.

Resistance of thermocouple + reference system = 1370 ohms.

Recorder scale factor = 0.25 mV full-scale
(Internal Resistance = 2500 ohms)
Recorder zero position = 20%

$$\therefore \text{Effective recorder scale factor} = 0.25\left(\frac{2500 + 1370}{2500}\right)$$
$$= 0.387 \text{ mV full-scale}$$

Taking as an example the temperature reading at y/R = 1.00 (100%),

Average chart reading = 78.2% (From Fig. 20)

The exact value of the average is a matter of visual judgement. It should be noted that the profile as recorded is inverted, i.e. lower temperature readings appear closer to the 100% chart position. The chart zero position of 20% represents a voltage equal to the reference voltage, while higher readings represent lower voltages and lower readings higher voltages.

Effective chart reading = - (78.2-20) = -58.2%

This represents a difference from the reference voltage of

$$(-0.582 \times 0.387) = -0.225 \text{ mV}.$$

$\therefore$ Thermocouple voltage = (2.481 - 0.225) = 2.256 mV

$\therefore$ Temperature = 110.78 °F

(Iron-constantan conversion relationships appear in appendix F)

Accuracy: It may be noted that 1% on the recorder chart under the conditions of this run represents 0.134 °F

Temperature readings for other radial positions are obtained in the same way and are shown in Fig. B.1.

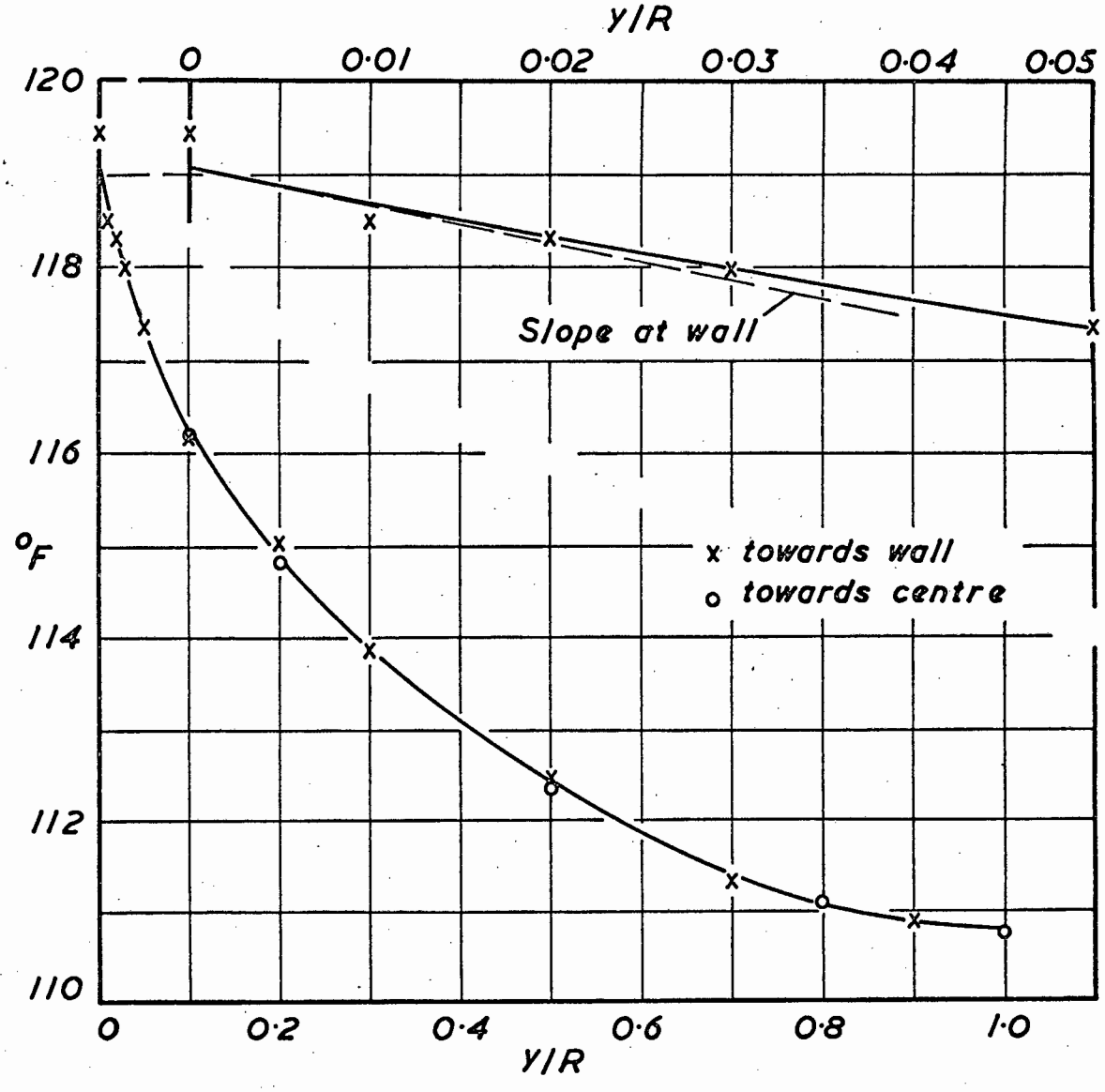

FIG. B.1 TEMPERATURE PROFILE, RUN 10.

B.25 Wall temperature

The temperature reading obtained with the probe thermocouple in contact with the wall will not necessarily be equal to the wall temperature, since the probe would also be partly in contact with the fluid. The true wall temperature was therefore determined by fitting the data in the vicinity of the wall to a second-order polynomial, where the coefficient of the first-order term equals the expected slope at the wall, as calculated from the heat flux. The procedure is illustrated as follows:

Assuming a laminar layer immediately adjacent to the wall,

$$q_w = - k \, (dT/dy)_{y=0} \qquad (B.2)$$

$$\therefore \; (dT/dy)_0 = - q_w/k \qquad (B.3)$$

Now if $T = ay^2 + by + c$ (B.4)

then $(dT/dy)_0 = (2ay + b)_0 = b = - q_w/k$ (B.5)

Thus $ay^2 + c = T + (q_w/k)\, y$ (B.6)

In this case, $q_w/k = 3150/5.33 = 591.$

This equation is set up for each experimental point in the vicinity of the wall and the resulting matrix inverted by a standard computer routine using a least-squares method. In practice this procedure was carried out for the seven points at 0.02 intervals from the wall to 0.12, based on the mean curve through the experimental points, but the use of the actual measured points would have been more correct.

The polynomial obtained by this regression technique

is shown in Fig. B.1, and the wall temperature obtained is 119.10 °F.

Readings obtained from the 10 wall thermocouples, are shown in Table B.2. It is apparent that fairly large differences exist between the readings obtained. The thermocouples were inserted into 1/16 in. holes drilled in the 1/8 in. thick tube wall and the exact depth of each couple was unknown, but the total temperature drop over the tube wall was approximately

$$\Delta T = q\Delta x/k = 3150(0.125)/12x9.4 = 3.5\ ^{\circ}F.$$

(k for stainless steel = 9.4)

The wall temperatures measured were thus of the right order, but obviously do not provide a sufficiently accurate measure of the inside wall surface temperature on their own. Slightly better agreement was obtained at lower heat fluxes.

Experimental data for all runs are reported in Table B.1 as $(T_w - T)$, where T_w is the wall temperature determined by the regression method described above. Where the experimental temperature is higher than the reference temperature, T_w, a negative value appears in the table.

The dimensionless temperature profile is obtained by plotting $(T_w - T)/(T_w - T_c)$ vs. y/R.

B.26 Mean Cup Temperature

The mean cup temperature at the probe is obtainable from the relation

$$T_{av} = \frac{2}{u_{av}} \int_0^1 \frac{r}{R}\, u\, T\, d\left(\frac{r}{R}\right) \qquad (4.1)$$

When u is expressed as u^+, this becomes

$$T_{av} = 2\sqrt{f/2} \int_0^1 \frac{r}{R}\, u^+\, T\, d\left(\frac{r}{R}\right) \qquad (B.7)$$

Calculations are shown in Table B.3 where the velocity at each radial position was evaluated from the von Karman universal velocity profile, given by equn.s 1.5a, b, c, and temperature readings were taken from the smoothed temperature profile curve. Integration was carried out by Simpson's Rule

$$\int = \frac{1}{3} h \, (f_0 + 4f_1 + 2f_2 + - - - - + 2f_{n-2} + 4f_{n-1} + f_n) \qquad (B.8)$$

for the two portions of y/R = 1.00 to 0.20 and 0.20 to 0.00. The integral for the last column in Table B.3 is 1193.8.

$$\text{Re} = 95{,}500 \qquad \therefore \sqrt{f/2} = 0.04765$$

$$\therefore T_{av} = 2 \times 0.04765 \times 1193.8 = 113.77 \ ^{\circ}F$$

The average velocity may be obtained from

$$u_{av} = 2 \int_0^1 u \frac{r}{R} \, d\left(\frac{r}{R}\right) \qquad (A.1)$$

and thus

$$F' = 2\sqrt{f/2} \int_0^1 u^+ \frac{r}{R} \, d\left(\frac{r}{R}\right) = 1.0 \qquad (B.9)$$

but it was found that, particularly at low Reynolds numbers, and using Simpson's rule for integration, the term F' was not equal to unity. This gave spurious values for T_{av}, using equn. 4.1 The reason for this discrepancy was not investigated but the calculated value of T_{av} was divided by F', the "normalised velocity integral" so as to produce the more correct value of T_{av} defined (81) by

$$T_{av} = \frac{\int_0^1 \frac{r}{R} u T \, d\left(\frac{r}{R}\right)}{\int_0^1 \frac{r}{R} u \, d\left(\frac{r}{R}\right)} \qquad (B.10)$$

For Run 10, F' = 0.9992

Thus T_{av} = (113.77/0.9992) = 113.86 °F.

TABLE B.3

CALCULATION OF MEAN CUP TEMPERATURE

y/R	y^+	u^+	T, °F	$(r/R)u^+T$
1.00	2286	24.83	110.77	0
0.95	2172	24.71	110.81	137
0.90	2058	24.57	110.88	272
0.85	1943	24.43	110.96	407
0.80	1829	24.28	111.07	539
0.75	1715	24.12	111.20	670
0.70	1600	23.94	111.36	800
0.65	1486	23.76	111.56	928
0.60	1372	23.56	111.82	1054
0.55	1257	23.34	112.06	1177
0.50	1143	23.10	112.33	1298
0.45	1029	22.84	112.64	1415
0.40	914	22.55	113.00	1529
0.35	800	22.21	113.40	1637
0.30	686	21.83	113.87	1740
0.25	572	21.37	114.38	1833
0.20	457	20.81	114.91	1913
0.18	412	20.55	115.17	1941
0.16	366	20.26	115.45	1964
0.14	320	19.92	115.69	1982
0.12	274	19.54	115.96	1994
0.10	229	19.08	116.25	1996
0.08	183	18.52	116.63	1987
0.06	137	17.80	117.06	1959
0.04	91	16.79	117.61	1896
0.02	45	15.06	118.29	1745
0.00	0	0.00	119.10	0

The use of the approximate von Karman relations (equn. 1.5) for the velocity profile, rather than a more sophisticated one (48) means the calculated mean temperature will not be particularly accurate. However, due to the uncertainty in regard to the velocity profile for mercury, and the further expectation that, for many of the reported runs, the velocity profile may be distorted, great importance can not be attached to the calculated mean cup temperature reported here. The value is accepted as a reference temperature for calculation of physical properties.

Evaluation of u^+, y^+ and the friction factor requires a knowledge of the Reynolds number, which in turn depends on the mean cup temperature. An initial temperature is therefore assumed, the physical properties and Re evaluated, and T_{av} is established by iteration.

APPENDIX C

VALUES OF THE PARAMETERS Y AND Z

C.1 THE YANTOVSKII CRITERION, Y

The Yantovskii criterion is defined as

$$Y = Gr/Re^2(f/2) \qquad (4.6)$$

where $$Gr = D^3\rho^2\beta g(T_w - T_c)/\mu^2 \qquad (4.6a)$$

and values of this criterion for the curves shown in Figs. 22–24, and referred to in the text, are calculated below.

C.11 This work, mercury

Run No. 5.: Re = 11,400 $\therefore$ f = 0.0074

From temp. profile, Tw-Tc = 4.88 °F

Mean cup temp. = 119.0 °F (Table B.1)

Physical properties of mercury, from appendix H.1

ρ = 841.3 lb/ft^3; μ = 1.407 cp; β = 0.00010

Pipe diameter = 1.624 in. = 0.1353 ft.

$$Gr = \frac{(0.1353)^3(841.3)^2\,0.00010\times32.2(3600)^2\times4.88}{(1.407\times2.42)^2}$$

$$= 3.07 \times 10^7$$

$$\therefore Y = \frac{2Gr}{Re^2 f} = \frac{2\times3.07\times10^7}{(11{,}400)^2\,0.0074} = 64$$

Similarly

Run No.	9	14
Re	43,400	10,100
Tw-Tc	14.39	4.92
Tav	108.7	168.8
Y	17.5	94

C.12 Carr (78), NaK eutectic

(a) Re = 39,500; $\therefore$ f = 0.0055; (Tw-Tc) = 19.6 °F

Physical properties are obtained from appendix H.2

Tav = 206.4°F; ν = 0.022 ft²/hr.

β = 0.00016

Pipe diameter = 1.380 in. = 0.115 ft.

$$Gr = \frac{(0.115)^3 0.00016 \times 32.2 \times (3600)^2 \times 19.6}{(0.022)^2}$$

$$= 4.06 \times 10^6$$

$$\therefore Y = \frac{2 \times 4.06 \times 10^6}{(39,500)^2 0.0055} = 0.94$$

(b) Similarly, for Re = 44,000;

(Tw-Tc) = 5.72°F; Tav = 92.5°F

$\therefore$ Y = 0.11

C.13 Kirillov et al. (20), NaK eutectic

Re = 13,700 $\therefore$ f = 0.0070; (Tw-Tc) = 8.1°C = 14.6 °F

The mean temperature is not stated but Pr is given as Pr = 0.0263. Assuming that these workers would have used the physical property data of Kutateladze (82), it is inferred that Tav = 93 °C.

Thus ν = 0.0225 ft²/hr (appendix H.2)

β = 0.00016

Pipe diameter = 40.0 mm = 0.1312 ft.

$$Gr = \frac{(0.1312)^3 0.00016 \times 32.2 (3600)^2 14.6}{(0.0225)^2}$$

$$= 4.33 \times 10^6$$

$$Y = \frac{2 \times 4.33 \times 10^6}{(13,700)^2 0.0070} = 6.6$$

C.14 Schrock (37), NaK - 56% K

Run No. 14: Re = 9760 $\therefore$ f = 0.0077

(Tw-Tc) = 9.2°F; Tav = 330.6°F

Physical properties are given by Schrock (37):

ρ = 53.0 lb/ft^3; μ = 1.03 lb/ft hr; $\beta \approx 0.00016$

D = 1.0 in. = 0.0833 ft

$$Gr = \frac{(0.0833)^3(53.0)^2 0.00016 \times 32.2 (3600)^2 \times 9.2}{(1.03)^2}$$

$$= 9.4 \times 10^5$$

$$Y = \frac{2 \times 9.4 \times 10^5}{(9760)^2 0.0077} = 2.6$$

Similarly

Run No.	19	26
Re	36,000	41,400
Tw-Tc	9.2	8.57
Tav	238.6	262.5
Y	0.19	0.14

C.15 Subbotin et al. (25), mercury

Run No. 19: Re = 45,500 $\therefore$ f = 0.0052

(Tw-Tc) = 7.86°C = 14.15°F; Tav = 21.8°C = 71.2°F.

Physical properties (appendix H.1):

ρ = 845.4 lb/ft^3; μ = 1.54 cp; β = 0.00010

Pipe diameter = 29.3 mm = 0.0962 ft

$$Gr = \frac{(0.0962)^3(845.4)^2 0.00010 \times 32.2 (3600)^2 14.15}{(1.54 \times 2.42)^2}$$

$$= 2.73 \times 10^7$$

$$Y = \frac{2 \times 2.73 \times 10^7}{(45,500)^2 0.0052} = 5.1$$

C.2 THE NATURAL CONVECTION CRITERION, Z

Z is defined as

$$Z = \frac{Gr^{*} \, Pr \, D/L}{Re} \tag{5.1}$$

where the temperature difference in the Grashoff number Gr^{*} is defined as $(dT/dx)D$.

C.21 Relation between Z and Y

Gr^{*} differs from Gr in the definition of the temperature difference, so that

$$Gr^{*} = Gr \frac{(dT/dx)D}{(T_w - T_c)} \tag{C.1}$$

Now, from equn. 5.3

$$\frac{(dT/dx)D}{T_w - T_{av}} = \frac{4h}{Gc_p} \tag{C.2}$$

and if $(Tw-Tav)/(Tw-Tc)$ is defined as Φ, then

$$Gr^{*} = Gr \left(\frac{4h}{Gc_p}\right) \Phi \, . \tag{C.3}$$

Assuming that the Martinelli-Lyon equation applies,

$$h = (k/D)(7 + 0.025 \, Pe^{0.8}) \tag{C.4}$$

Also $G = Re\mu/D$, and assuming that $\Phi \approx 0.6$ (=0.59 for Run No. 10), Gr^{*} becomes

$$Gr^{*} = Gr \left[\frac{4k(7 + 0.025 \, Pe^{0.8}) \cancel{\Phi}}{\cancel{\Phi} \; Re \; c_p} \right] 0.6$$

$$= Gr \, \frac{2.4(7 + 0.025 \, Pe^{0.8})}{Re \; Pr} \tag{C.5}$$

$$\therefore Z = \frac{2.4(7 + 0.025 \, Pe^{0.8})}{Re \; \cancel{Pr}} \, Gr \, \frac{\cancel{Pr} \, D/L}{Re}$$

$$= 2.4(7 + 0.025 \, Pe^{0.8}) \, \frac{D}{L} \, \frac{f}{2} \, \frac{Gr}{Re^2 f/2} \tag{C.6}$$

where $\frac{Gr}{Re^2 f/2} = Y$ (4.6)

Typical length/diameter ratios used by various investigators are as follows:

Borishanskii et al.(26), 25; Carr (78), 74;
Kirillov et al. (20), 20; Schrock (37), 48;
Subbotin et al. (25), 32.

In order to obtain an approximate numerical comparison between a Y value of unity, and Z, a typical L/D ratio of 50 is taken, together with a typical Prandtl Number of 0.02.

Then for Re = 40,000 and Y = 1

$$Z = \frac{2.4(12.2)0.0054}{50 \times 2} = 15.8 \times 10^{-4}$$

Similarly for Re = 10,000

$$Z = \frac{2.4(8.7)0.0076}{50 \times 2} = 15.9 \times 10^{-4}$$

and for Re = 100,000

$$Z = \frac{2.4(17.9)0.0045}{50 \times 2} = 19.3 \times 10^{-4}.$$

While the criteria Y and Z are not strictly comparable, it appears from the above that a value of Y = 1 corresponds approximately to Z = 20 x 10^{-4} and this value of Z may therefore be taken approximately as the value below which superimposed free convection will not have an appreciable effect on forced convection.

C.22 Values of Z for this work, mercury.

D = 1.624" = 0.1353 ft.
Total heated length = 16.3 ft
Length, inlet to probe = 14.2 ft; D/L = 0.00952.

Run No. 1: Re = 3,800; $(T_{out} - T_{in})$ = 64.7 °F

$\therefore$ dT/dx = 64.7/16.3 = 3.97°F/ft.

Tav = 113.4°F. Physical properties (appendix H.1):
ρ = 841.8 lb/ft^3; μ = 1.423 cp; β = 0.00010
Pr = 0.021

$$Gr^* = D^3 \rho^2 \beta g (dT/dx) D / \mu^2$$
$$= \frac{(0.1353)^4 (841.8)^2 0.00010 \times 32.2 (3600)^2 \times 3.97}{(1.423 \times 2.42)^2}$$
$$= 3.29 \times 10^6$$

$$Z = Gr^* Pr (D/L) / Re$$
$$= \frac{3.29 \times 10^6 \times 0.021 \times 0.00952}{3800}$$
$$= 1730 \times 10^{-4}$$

Values of Z for the other runs are shown in Table 4.1.

C.23 Borishanskii et al. (26), sodium

D = 40 mm = 0.1312 ft
Length, start of heating to probe = 25D
Total heated length not stated

All operating details are not given, but it is possible to calculate Z from the information available.

Re = 50,700; q = 51,000 Kcal/m^2 hr; Pe = 400

From the given Peclet number, it may be inferred that Pr = (400/50,700) = 0.0079, and, using the physical properties of Na given by Kutateladze (82), $T_{av} \approx 180°C$

ν = 54 x 10^{-8} m^2/sec = 0.0209 ft^2/hr
k = 71 kcal/m.hr.°C; β = 0.00016

It is readily shown that

$$\frac{\Delta T}{L} = \frac{4q}{k\,Pe} \quad \text{or} \quad \frac{4q}{Re\, c_p \mu} \qquad (C.7)$$

Using the first definition,

$$\frac{\Delta T}{L} = \frac{dT}{dx} = \frac{4 \times 51,000}{71 \times 400} \times \left(\frac{1.8}{3.28}\right) = 3.94 \ ^{\circ}F/ft.$$

$$Gr^{*} = \frac{(0.1312)^4 0.00016 \times 32.2 (3600)^2 3.94}{(0.0209)^2}$$

$$= 1.78 \times 10^5$$

$$Z = \frac{1.78 \times 10^5 \times 0.0079 \times 0.04}{50,700} = 11 \times 10^{-4}$$

C.24 Brown, Amstead and Short (19), mercury

D = 1.6" = 0.1333 ft

Length, inlet to probe (Station 2) = 90 diameters

A temperature profile is given for a run at Re = 660,000 and this will be used to calculate a typical value of Z for the results of these authors.

Average temp. is estimated, from the profile, to be approx. 137.4°F. Physical properties (app. H.1): ρ = 839.8 lb/ft^3; μ = 1.36 cp; Pr = 0.0196

Inlet and outlet temperatures are not available, but the required temperature difference may be estimated from equn. 5.3:

$$(dT/dx)D = \frac{4h}{Gcp}(T_w - T_{av}) = \frac{4\,Nu}{Re\ Pr}(T_w - T_{av}) . \qquad (5.3)$$

Nu may be evaluated from the given experimental results at Pe = 660,000 x 0.0196 = 12,900 as approximately Nu = 50.

Also, from the given profile, Tw = 124.5°F and therefore (Tw-Tav) ≈ 12.9°F.

$$\therefore (dT/dx)D = \frac{4 \times 50 \times 12.9}{660,000 \times 0.0196} = 0.2 \ ^{\circ}F/ft$$

$$\therefore Gr^{*} = \frac{(0.1333)^3 (839.8)^2 0.00010 \times 32.2 (3600)^2 0.2}{(1.36 \times 2.42)^2}$$

$$= 1.29 \times 10^6$$

$$\therefore Z = \frac{1.29 \times 10^6 \times 0.0196}{90 \times 660,000} = 4.3 \times 10^{-4}$$

C.25 Carr (78), NaK eutectic

D = 1.380" = 0.115 ft

Total heated length = 10.0 ft.

Length, inlet to probe = 8.5 ft.; D/L = 0.0135.

Re = 31,400; $(T_{out} - T_{in})$ = 47.8 °F

$\therefore (dT/dx) = 47.8/10.0 = 4.78$ °F/ft.

Tav = 144.7 °F. Physical properties from appendix H.2:

$\nu = 0.0266$ ft²/hr; Pr = 0.0232; $\beta = 0.00016$

$$Gr^* = \frac{(0.115)^4 0.00016 \times 32.2 (3600)^2 4.78}{(0.0266)^2}$$

$$= 7.87 \times 10^4$$

$$\therefore Z = \frac{7.87 \times 10^4 \times 0.0232 \times 0.0135}{31,400} = 7.8 \times 10^{-4}$$

Similarly,

Re	$T_{out} - T_{in}$	T_{av}, °F	Z x 10^4
39500	48.2	206.4	7.3
44000	11.0	92.5	1.1
71600	6.2	89.3	0.4
71900	25.0	194.3	2.0
83300	5.4	88.7	0.3
83600	15.5	126.5	0.9
97200	18.4	190.3	1.1
146000	3.1	88.1	0.1
153000	11.7	183.8	0.4

C.26 Kirillov et al.(20), NaK eutectic

D = 40.0 mm = 0.1312 ft

Length, inlet to probe = 800 mm ∴D/L = 0.05

Re = 13700; q = 22,200 Kcal/m²hr; Pr = 0.0263

As in Section C.13, it is assumed that Tav = 93°C.

$\therefore \nu$ = 0.0225 ft²/hr (appendix H.2)

k = 20.95 Kcal/m.hr°C (83).

From equn. C.7,

$$\frac{\Delta T}{L} = \frac{4q}{kRePr} = \frac{4x22,200}{20.95x13,700x0.0263} \times \frac{1.8}{3.28}$$

$$= 6.45 \text{ °F/ft.}$$

$$Gr^* = \frac{(0.1312)^4 0.00016x32.2(3600)^2 6.45}{(0.0225)^2}$$

$$= 2.51 \times 10^5$$

$$\therefore Z = \frac{2.51x10^5x0.0263x0.05}{13,700} = 240 \times 10^{-4}$$

Similarly

Re	q	Pr	Z x 10^4
17,330	16,000	0.0158	180
17,600	17,600	0.0154	190
33,000	20,900	0.0132	80

C.27 Schrock (37), NaK - 56% K

D = 1.0 in. = 0.0833 ft

Length, inlet to probe = 48 in., D/L = 0.0208.

Total heated length = 56 in.

Run No. 7: Re = 54,400; $(T_{out} - T_{in})$ = 13.3 °F.

$$\therefore (dT/dx)D = \frac{13.3 \times 12}{56} = 2.85 \text{ °F/ft.}$$

Tav = 220 °F. Physical properties are given by Schrock (37)

ρ = 53.9 lb/ft³; μ = 1.28 lb/ft.hr; Pr = 0.0247

$$Gr^* = \frac{(0.0833)^4(53.9)^2 0.00016x32.2(3600)^2 2.85}{(1.28)^2}$$

$$= 1.61 \times 10^4$$

$$\therefore Z = \frac{1.61 \times 10^4 \times 0.0247 \times 0.0208}{54400}$$
$$= 1.52 \times 10^{-4}$$

Similarly

Run No.	Re	$(T_{out} - T_{in})$	T_{av}, °F	$Z \times 10^4$
21	49000	14.3	223	1.88
26	41400	16.0	263	2.48
27	65600	12.3	286	1.24
28	76800	10.7	296	0.87

These Z values are all well below 20×10^{-4} and the data points in Fig. 25 are not labelled.

C.28 Subbotin et al. (25), mercury

D = 29.3 mm = 0.0962 ft

Length, inlet to probe = 945 mm; D/L = 0.0310

Run No. 19: Re = 45,500; q = 17000 Kcal/m² hr
= 6270 BTU/ft²hr.

Tav = 71.2°F ∴ Physical properties (appendix H.1):
ρ = 845.4 lb/ft³; μ = 1.54 cp; β = 0.00010
c_p = 0.0332 BTU/lb °F; Pr = 0.0246.

$$\frac{\Delta T}{L} = \frac{4q}{Re\, c_p\, \mu} = \frac{4 \times 6270}{45{,}500 \times 0.0332 \times 1.54 \times 2.42} = 4.46 \text{ °F/ft.}$$

$$\therefore Gr^{*} = 8.15 \times 10^5$$

and $Z = 140 \times 10^{-4}$

Details of other profiles reported by these authors may be obtained from Ref (25) and values of Z are shown in Fig. 25. Profiles for Reynolds numbers below 4×10^4

have approximately the same shape as those of this work, but the Z parameters are appreciably higher, possibly due to the relatively short tube length (35 diameters) used, and these profiles have not been included in Fig. 25.

For the mercury data reported by Subbotin et al. in Ref (22), the same equipment was used as in Ref (25).

$Re = 204{,}000$; $q = 41{,}000$ Kcal/m^2hr
$= 15{,}100$ BTU/ ft^2hr

No average temperature is given, but assuming that approximately the same conditions applied as in Ref (25), $T_{av} \approx 28^\circ C = 82^\circ F$ and therefore $Z = 17 \times 10^{-4}$.

C.29. Subbotin et al. (22), NaK eutectic

$D = 31.1$ mm $= 0.102$ ft

Length, inlet to probe = 976 mm; $D/L = 0.0319$

$Re = 24{,}700$; $q = 39500$ Kcal/m^2. hr.

T_{av} is not given, but if this is assumed $\approx 150^\circ C$ then $\nu = 0.0178$ ft^2/hr; $Pr = 0.0142$ (app. H.2)

$k = 21.3$ kcal/m hr $^\circ C$ (83)

$$\therefore \frac{\Delta T}{L} = \frac{4q}{kPe} = \frac{4 \times 39500}{21.3 \times 24{,}700 \times 0.0142} \times \frac{1.8}{3.28} = 11.6\ ^\circ F/ft$$

$$\therefore Gr^{*} = 2.63 \times 10^{6} \quad \text{and} \quad Z = 50 \times 10^{-4}$$

Note: Liquid metal profiles are also reported by Subbotin et al. in Ref. (21) but the equipment is not described, so that these profiles can not be used in Fig. 25.

APPENDIX D

RATIO OF EDDY DIFFUSIVITIES

D.1 CALCULATED RESULTS

Values of the ratio of eddy diffusivities, ϵ_H/ϵ_M, calculated from the dimensionless temperature profiles of Fig. 26 are shown in Table D.1 and in Fig. 27, for a Prandtl number of 0.02.

TABLE D.1

Ratio of Eddy Diffusivities

Re x 10^{-3}	30			50		
y/R	$\frac{T_w - T}{T_w - T_c}$	Slope	ϵ_H/ϵ_M	$\frac{T_w - T}{T_w - T_c}$	Slope	ϵ_H/ϵ_M
0.90	0.988	0.20	0.70	0.990	0.19	0.64
0.80	0.961	0.36	0.62	0.962	0.36	0.56
0.70	0.918	0.53	0.55	0.919	0.52	0.50
0.60	0.857	0.69	0.51	0.857	0.68	0.48
0.50	0.780	0.88	0.46	0.784	0.82	0.48
0.40	0.685	1.10	0.41	0.696	1.02	0.44
0.30	0.563	1.37	0.33	0.589	1.29	0.39
0.20	0.400	1.68	0.27	0.440	1.67	0.31
0.10	0.216	2.01	0.24	0.216	2.16	0.25
0.00	0.000	2.37	-	0.000	2.77	-
	For Re = 100,000 see Table D.2					
Re x 10^{-3}	200			300		
y/R	$\frac{T_w - T}{T_w - T_c}$	Slope	ϵ_H/ϵ_M	$\frac{T_w - T}{T_w - T_c}$	Slope	ϵ_H/ϵ_M
0.90	0.990	0.13	1.73	0.992	0.09	2.78
0.80	0.974	0.23	1.43	0.980	0.17	2.25
0.70	0.945	0.34	1.24	0.959	0.24	1.95
0.60	0.906	0.43	1.18	0.930	0.33	1.73
0.50	0.860	0.56	1.08	0.890	0.47	1.44
0.40	0.793	0.75	0.97	0.833	0.65	1.26
0.30	0.706	0.98	0.91	0.756	0.87	1.17
0.20	0.587	1.32	0.90	0.652	1.18	1.16
0.10	0.433	2.20	0.85	0.505	2.07	1.11
0.00	0.000	8.40	-	0.000	12.92	-

D.2 CALCULATION PROCEDURE

The ratio of eddy diffusivities may be calculated from equns. 4.5 and 6.1

$$\epsilon_H/\alpha = \frac{\phi(y/R)}{S_y/S_o} - 1 \qquad (4.5)$$

$$\epsilon_H/\epsilon_M = \frac{\epsilon_H/\alpha}{\epsilon_M/Ru^*} \cdot \frac{2}{Re\ Pr\ \sqrt{f/2}} \qquad (6.1)$$

Typical calculations for Re = 100,000 are shown in Table D.2 and discussed below.

TABLE D.2

Ratio of Eddy Diffusivities for Re = 100,000

y/R	$\frac{T_w - T}{T_w - T_c}$	Slope	$\phi(y/R)$	ϵ_H/α	ϵ_M/Ru^*	ϵ_H/ϵ_M
0.90	0.990	0.17	0.120	2.06	0.0435	1.01
0.80	0.966	0.32	0.238	2.32	0.0603	0.82
0.70	0.927	0.45	0.354	2.51	0.0716	0.75
0.60	0.875	0.58	0.468	2.60	0.0776	0.72
0.50	0.812	0.72	0.578	2.58	0.0796	0.69
0.40	0.732	0.90	0.682	2.38	0.0773	0.66
0.30	0.632	1.13	0.781	2.08	0.0703	0.63
0.20	0.512	1.52	0.872	1.56	0.0570	0.59
0.10	0.328	2.40	0.953	0.74	0.0350	0.45
0.00	0.000	4.46	1.000	0.00	0.0000	-

D.21 Slopes, Sy

Slopes of the dimensionless temperature profile at various radial positions were determined as the derivative of a least-squares second-order polynomial passed through five points in the vicinity of the radial position under consideration, as discussed for the case of velocity profiles in appendix E.1. These slopes, obtained from the dimensionless temperature profile are equivalent to

$$S = -\left(\frac{R}{T_w - T_c}\right)\frac{dT}{dy} \qquad (D.1)$$

but they will be divided by the slope at the wall, and since the latter will also be determined from the dimensionless profile, the term $\{-R/(T_w - T_c)\}$ will cancel.

D.22 Slope at the wall, S_o

The above method is not satisfactory for determination of the slope at the wall, since data points are not available below $y/R = 0$. The slope at the wall was therefore obtained by fitting the data in the vicinity of the wall (at 0.02 intervals from $y/R = 0$ to 0.12) to a rational function of the from $y/(ay + b)$. This function is constrained to pass through the point (0,0) and to have the same basic shape as that of the temperature profile. It is believed to be superior to an ordinary polynomial (79).

Thus for each of seven data points,

$$\Theta = \frac{(y/R)}{a(y/R) + b} \qquad (D.2)$$

$$\therefore \quad \Theta(y/R)a + \Theta b = (y/R) \qquad (D.3)$$

so that seven simultaneous equations are obtained, with two unknowns, a and b, and this matrix is then inverted by a least-squares technique using a standard sub-routine on a digital computer.

The slope is given by the differential of equn. D.2.

$$\text{i.e.} \quad S_y = \frac{b}{[a(y/R) + b]^2} \quad \text{and} \quad S_o = 1/b \qquad (D.4)$$

Thus for Re = 100,000 the relationship obtained was

$$\Theta = (y/R)/0.363(y/R) + 0.361$$

and calculated values are shown in Table D.3.

TABLE D.3

Slope from Equn. D.4

y/R	Θ	$\Theta_{calc.}$	% Error	Slope
0.00	0.000	0.0000	0.00	4.457
0.02	0.083	0.0831	-0.09	3.871
0.04	0.158	0.1556	1.54	3.394
0.06	0.219	0.2194	-0.17	2.999
0.08	0.273	0.2760	-1.09	2.670
0.10	0.328	0.3265	0.45	2.392
0.12	0.372	0.3719	0.02	2.155

By comparison, the slopes obtained by the method of the previous section, for y/R = 0.04 to 0.12 are 3.410, 3.025, 2.685, 2.435 and 2.195.

Thus $S_o = 4.457$ for Re = 100,000 .

D.23 The heat flux distribution function, $\phi(y/R)$

The heat flux at any radial position is related to the flux at the wall by $q = \phi(y/R)\ q_w$.

Consider a differential annular section of the tube cross-section of width dr at radius r from the centre.

Heat entering the section by convection

$$= 2\pi r\, dr\, u\, \rho\, c_p\, T \quad \text{(base T=0)} \qquad (D.5)$$

Heat leaving the section

$$= 2\pi r\, dr\, u\, \rho\, c_p\, (T + (\partial T/\partial x)\Delta x) \qquad (D.6)$$

where Δx is the height of the section in the direction of the flow.

Now the total heat flux entering the section at

r equals the net heat lost by convection in the fluid flowing between the centre and radius r, under steady conditions.

$$\therefore \quad q\, 2\pi r\, \Delta x \;=\; {}_0\!\int^{r} 2\pi r\, dr\, u\, \rho\, c_p\, (\partial T/\partial x)\, \Delta x \qquad (D.7)$$

and since $\partial T/\partial x$ is a constant, and independent of r for the fully developed profile under constant heat flux conditions,

$$q \;=\; \frac{\rho\, c_p\, (\partial T/\partial x)}{r}\; {}_0\!\int^{r} u\, r\, dr \qquad (D.8)$$

Also, the total heat entering the tube per unit length equals the enthalpy gained by the fluid :

$$q_w\, 2\pi R \;=\; \pi R^2\, u_{av}\, \rho\, c_p\, (\partial T/\partial x) \qquad (D.9)$$

so that

$$\frac{q}{q_w} \;=\; \phi(y/R) \;=\; \frac{2}{R\, r\, u_{av}}\; {}_0\!\int^{r} u\, r\, dr$$

$$\;=\; \frac{2}{(r/R)\, u_{av}}\; {}_0\!\int^{r/R} u\, \left(\frac{r}{R}\right)\, d\left(\frac{r}{R}\right) \qquad (4.3)$$

Similar derivations may be found elsewhere (17,84).

The velocity was evaluated using a three-layer universal velocity profile :

(i) Laminar layer, $y^+ < 5$: $\qquad u^+ \;=\; y^+ \qquad (1.5a)$

(ii) Buffer layer, $5 < y^+ < 30$:

$$u^+ \;=\; 5 \ln y^+ - 3.05 \qquad (1.5b)$$

(iii) Turbulent layer, $y^+ > 30$:

The relationship given by Hinze (48) was used i.e.

$$u_c^+ - u^+ \;=\; -2.44 \ln(y/R) + 0.8 - h(y/R) \qquad (3.10)$$

where h(y/R) is a correction factor deduced from the work of Laufer (45), and is a function of y/R.

In order to predict u from this equation it is necessary to evaluate u_c^+. This is done by assuming

that the turbulent and buffer layer equations predict the same value of u^+ at $y^+ = 30$.

Thus $$u_c^+ = (u_c^+ - u^+)_{y^+=30} + u^+_{y^+=30} \qquad (D.10)$$

and $u^+_{y^+=30}$ is given by $(5 \ln 30 - 3.05) = 13.959$

$$\therefore u_c^+ = (u_c^+ - u^+)_{y^+=30} + 13.959. \qquad (D.11)$$

Since $$y^+ = 0.5\,(y/R)\,Re\,(f/2)^{1/2}, \qquad (A.2)$$

the first term on the right-hand side of equn. D.11 may be evaluated from equn. 3.10 above for $y/R = 60/(Re\,(f/2)^{\frac{1}{2}})$.

Thus equn. 3.10 becomes

$$u^+ = u_c^+ + 2.44 \ln (y/R) - 0.8 + h(y/R) \qquad (D.12)$$

where u_c^+ is evaluated as above.

Calculations were carried out on a digital computer for the radial positions $y/R = 1.00(0.05)0.20(0.02)0.00$. Values of the correction factor $h\,(y/R)$ were obtained from Hinze (48) and fed into the program as data. Values for $y^+ = 30$ were obtained by interpolation. Integration was carried out by Simpson's rule.

Values of $\phi(y/R)$ for a number of Reynolds numbers are shown in Table D.4.

Similar calculations using the relationship proposed by Lin et al. (43) for the laminar and buffer layers did not differ by more than 0.001 from the values given here for Re = 30,000 and by not more than 0.006 for Re = 5,000, so that it may be said that $\phi(y/R)$ is not particularly sensitive to small changes in the velocity profile used.

D.24 ϵ_M and ϵ_H/ϵ_M.

Values of the eddy diffusivity of momentum are taken

TABLE D.4

Heat flux distribution function, $\phi(y/R)$.

$Re \times 10^{-3}$	5	10	20	30	50	100	200	300
y/R								
1.00	0.000	0.000	0.000	0.000	0.000	0.000	0.000	0.000
0.95	0.067	0.064	0.062	0.061	0.061	0.060	0.059	0.059
0.90	0.133	0.128	0.124	0.123	0.121	0.120	0.118	0.118
0.85	0.199	0.191	0.186	0.183	0.181	0.179	0.177	0.176
0.80	0.265	0.254	0.247	0.244	0.241	0.238	0.235	L.234
0.75	0.330	0.316	0.307	0.304	0.300	0.296	0.293	0.292
0.70	0.394	0.377	0.367	0.363	0.358	0.354	0.351	0.349
0.65	0.456	0.438	0.426	0.421	0.416	0.411	0.408	0.406
0.60	0.518	0.497	0.484	0.479	0.473	0.468	0.464	0.462
0.55	0.578	0.555	0.541	0.535	0.529	0.523	0.519	0.516
0.50	0.637	0.612	0.596	0.590	0.584	0.578	0.573	0.570
0.45	0.693	0.666	0.650	0.644	0.637	0.631	0.626	0.623
0.40	0.748	0.720	0.702	0.696	0.689	0.682	0.677	0.675
0.35	0.800	0.770	0.753	0.746	0.739	0.732	0.727	0.725
0.30	0.850	0.819	0.801	0.794	0.787	0.781	0.776	0.774
0.25	0.897	0.866	0.848	0.841	0.833	0.827	0.823	0.821
0.20	0.941	0.910	0.891	0.885	0.878	0.872	0.868	0.866
0.18	0.958	0.926	0.908	0.901	0.895	0.889	0.885	0.883
0.16	0.973	0.942	0.924	0.918	0.911	0.906	0.902	0.901
0.14	0.988	0.958	0.940	0.933	0.927	0.922	0.919	0.917
0.12	1.000	0.972	0.955	0.949	0.943	0.938	0.935	0.933
0.10	1.010	0.986	0.969	0.963	0.957	0.953	0.950	0.949
0.08	1.018	0.998	0.982	0.976	0.971	0.967	0.965	0.964
0.06	1.022	1.007	0.994	0.989	0.984	0.981	0.979	0.978
0.04	1.022	1.013	1.004	0.999	0.995	0.992	0.991	0.990
0.02	1.015	1.012	1.008	1.006	1.003	1.002	1.001	1.001
0.00	1.000	1.000	1.000	1.000	1.000	1.000	1.000	1.000

from Fig. 19, due to Nikuradse (9), and are considered to be the best available for the reasons given in Chapter 3.

Taking a typical liquid metal Prandtl number of 0.02, for Re = 100,000

$$2 / (\mathrm{Re\ Pr}\ (f/2)^{1/2}) = 0.0213$$

and ϵ_H/ϵ_M is obtained from equn. 6.1 as

$$\epsilon_H/\epsilon_M = \frac{(\epsilon_H/\alpha)}{(\epsilon_M/Ru^*)} \times 0.0213$$

APPENDIX E

CALCULATION OF ϵ_M/Ru^*.

E.1 VALUES OF ϵ_M/Ru^*.

Values of the eddy diffusivity of momentum in the dimensionless form ϵ_M/Ru^* may be obtained from measured velocity profiles.

Using a linear shear stress distribution and assuming $\epsilon_M >> \nu$, the shear : velocity relation 1.2 becomes

$$(\tau_w/\rho)(1 - y/R) = \epsilon_M \, du/dy \qquad (E.1)$$

$$\therefore u^{*2} (1 - y/R) = \epsilon_M \frac{u^*}{R} \frac{d(u/u^*)}{d(y/R)} \qquad (E.2)$$

$$\therefore \epsilon_M/Ru^* = \frac{(1 - y/R)}{du^+/d(y/R)} \qquad (3.11)$$

Velocity readings were taken from the given profile at intervals of $y/R = 0.05$ from the centre to $y/R = 0.20$ and then at intervals of $y/R = 0.02$ to the wall. The slope of the velocity profile at a given radial position was determined by fitting a second-order polynomial to the five points in the immediate vicinity of the point under consideration, by a least-squares matrix inversion technique. Differentiation of the polynomial

$$u = a (y/R)^2 + b (y/R) + c \qquad (E.3)$$

gives $$du/d(y/R) = 2a (y/R) + b, \qquad (E.4)$$

from which the slope at that point may be evaluated. A plot of this straight line also gives a good indication of the trend of the slope curve at the radial position under consideration. This procedure was found to compare well with the Douglass-Avakian method (85), where a fifth-order polynomial is fitted to seven data points at a time.

Calculated results are given in Tables E.1 and E.2.

TABLE E.1

ϵ_M/Ru^* for data of Laufer (45)

Re = 500,000 based on u_c.

y/R	u/u_c	Slope, $d(u/u_c)/d(y/R)$			ϵ_M/Ru^*
		y/R-1	y/R	y/R+1	
0.00	0.000				
0.02	0.655				
0.04	0.709	17.23	8.025	-1.182	0.0042
0.06	0.738	2.061	1.490	0.919	0.0222
0.08	0.761	1.283	1.040	0.797	0.0311
0.10	0.778	0.993	0.850	0.707	0.0373
0.12	0.793	0.795	0.745	0.695	0.0416
0.14	0.807	0.737	0.680	0.623	0.0445
0.16	0.821	0.694	0.615	0.536	0.0481
0.18	0.832	0.611	0.560	0.509	0.0516
0.20	0.842	0.527	0.496	0.419	0.0568
0.25	0.865	0.490	0.421	0.351	0.0628
0.30	0.884	0.418	0.358	0.298	0.0688
0.35	0.900	0.348	0.308	0.268	0.0743
0.40	0.914	0.296	0.282	0.268	0.0749
0.45	0.927	0.280	0.254	0.228	0.0762
0.50	0.941	0.261	0.230	0.199	0.0765
0.55	0.950	0.233	0.202	0.171	0.0784
0.60	0.960	0.189	0.172	0.155	0.0819
0.65	0.968	0.178	0.158	0.138	0.0780
0.70	0.975	0.155	0.132	0.109	0.0800
0.75	0.982	0.136	0.110	0.084	0.0800
0.80	0.986	0.111	0.088	0.065	0.0800
0.85	0.990	0.077	0.074	0.071	0.0714
0.90	0.993	0.073	0.070	0.067	0.0503
0.95	0.997				
1.00	1.000				

TABLE E.2
VALUES OF ϵ_M/Ru^*

	Laufer (45), Air Re = 50,000			Rein (51), Air Re = 36,700		
y/R	u/u_c	$\frac{d(u/u_c)}{d(y/R)}$	ϵ_M/Ru^*	u, ft/sec	$\frac{du}{d(y/R)}$	ϵ_M/Ru^*
0.08	0.687	1.335	0.0288	30.05	54.5	0.0310
0.14	0.745	0.820	0.0438	32.40	33.8	0.0466
0.20	0.786	0.591	0.0562	34.30	26.6	0.0550
0.30	0.836	0.450	0.0651	36.30	17.7	0.0725
0.40	0.876	0.362	0.0693	37.80	14.4	0.0765
0.50	0.909	0.322	0.0649	39 20	12.6	0.0728
0.60	0.940	0.278	0.0601	40.35	11.0	0.0667
0.70	0.965	0.200	0.0626	41.40	9.8	0.0561
0.80	0.980	0.128	0.0653	42.30	7.3	0.0502
0.90	0.990	0.102	0.0041	42.85	4.1	0.0447
1.00	1.000	0.000		43.10	0.0	
	Sleicher(50), Air Re = 40,000			Stanton(49), Air Re = 40,900		
y/R	u, ft/sec	$\frac{du}{d(y/R)}$	ϵ_M/Ru^*	u, cm/sec	$\frac{du}{d(y/R)}$	ϵ_M/Ru^*
0.08	44.05	95.8	0.0264	1061	1765	0.0335
0.14	48.30	59.5	0.0397	1140	1140	0.0484
0.20	51.20	37.6	0.0584	1200	921	0.0557
0.30	54.35	29.2	0.0659	1280	712	0.0631
0.40	57.05	24.6	0.0670	1343	582	0.0662
0.50	59.25	20.5	0.0670	1397	460	0.0698
0.60	61.15	16.8	0.0653	1435	382	0.0672
0.70	62.60	14.3	0.0575	1473	324	0.0594
0.80	64.00	10.6	0.0518	1500	230	0.0558
0.90	64.75	4.5	0.0610	1518	122	0.0526
1.00	64.90	0.0		1525	0	

TABLE E.2 continued

Beckwith and Fahien (52) Water, Re = 18,770				Page et al. (53) Air in channels, Re=53,200	
y/R	u^+	$\frac{du^+}{d(y/R)}$	ϵ_M/Ru^*	$\epsilon_M \times 10^3$	ϵ_M/Ru^*
0.08	15.17	25.00	0.0368	3.33	0.0256
0.14	16.28	14.93	0.0576	-	-
0.20	17.03	11.42	0.0701	7.37	0.0567
0.30	18.00	8.21	0.0852	9.66	0.0744
0.40	18.70	6.16	0.0974	10.61	0.0816
0.50	19.22	4.85	0.1030	10.76	0.0828
0.60	19.67	4.12	0.0971	10.45	0.0804
0.70	20.05	3.14	0.0956	10.00	0.0770
0.80	20.32	2.32	0.0862	9.69	0.0746
0.90	20.50	1.39	0.0720	9.52	0.0733
1.00	20.60	0.00			

Sesonske et al. (35) Mercury, Re=99,000			Sesonske et al. (35) Mercury, Re=62,000	
y/R	ϵ_M/ν	ϵ_M/Ru^*	ϵ_M/ν	ϵ_M/Ru^*
0.10	102	0.0443	68	0.0440
0.20	150	0.0652	92	0.0595
0.30	186	0.0808	107	0.0692
0.40	208	0.0904	116	0.0751
0.50	213	0.0925	119	0.0770
0.60	203	0.0882	116	0.0751
0.70	183	0.0795	110	0.0712
0.80	154	0.0669	97	0.0627

This work, mercury Run V.7, Re = 89,700				This work, mercury Run V.33, Re = 89,200		
y/R	u, ft/sec	$\frac{du}{d(y/R)}$	ϵ_M/Ru^*	u, ft/sec	$\frac{du}{d(y/R)}$	ϵ_M/Ru^*
0.08	0.724	0.970	0.0367	0.715	0.995	0.0359
0.14	0.768	0.630	0.0518	0.759	0.680	0.0490
0.20	0.801	0.460	0.0673	0.795	0.457	0.0679
0.30	0.837	0.324	0.0836	0.832	0.340	0.0799
0.40	0.866	0.264	0.0880	0.863	0.284	0.0819
0.50	0.890	0.216	0.0896	0.889	0.250	0.0776
0.60	0.909	0.180	0.0860	0.913	0.230	0.0675
0.70	0.926	0.156	0.0745	0.935	0.194	0.0600
0.80	0.940	0.106	0.0730	0.952	0.140	0.0554
0.90	0.947	0.050	0.0774	0.963	0.074	0.0524
1.00	0.950			0.966		

E.2 CALCULATION METHOD

The calculation method is illustrated for the results Laufer (45), and relevant details are given for other workers.

E.21 Laufer (45), air

Data at two Reynolds numbers, 50,000 and 500,000 (based on centre velocity), for air in a 10-in D. pipe are reported by Laufer. The latter run appears to be accepted as the more accurate.

For Re = 500,000 (based on u_c):

Following the procedure outlined above, Table E.1 shows the velocity data, as u/u_c, read from Laufer's curve, together with the slope obtained, and two further points, evaluated from the straight line of equn. E.4, on either side of the point under consideration. These latter points enable the slope of the best-fit second-order polynomial to be plotted as a straight line, as shown in Fig. E.1.

The straight lines in this plot give a good indication of the trend of the slope curve, as mentioned above. The way in which the slope plot curves away from the direct approach to zero near the centre may be observed here. This is discussed in Section 3.31.

The method used here does not permit the slope to be calculated for the last two data points on either end of the range.

Integration of the velocity data to determine the mean velocity gives

$$u_{av} / u_c = 0.855$$

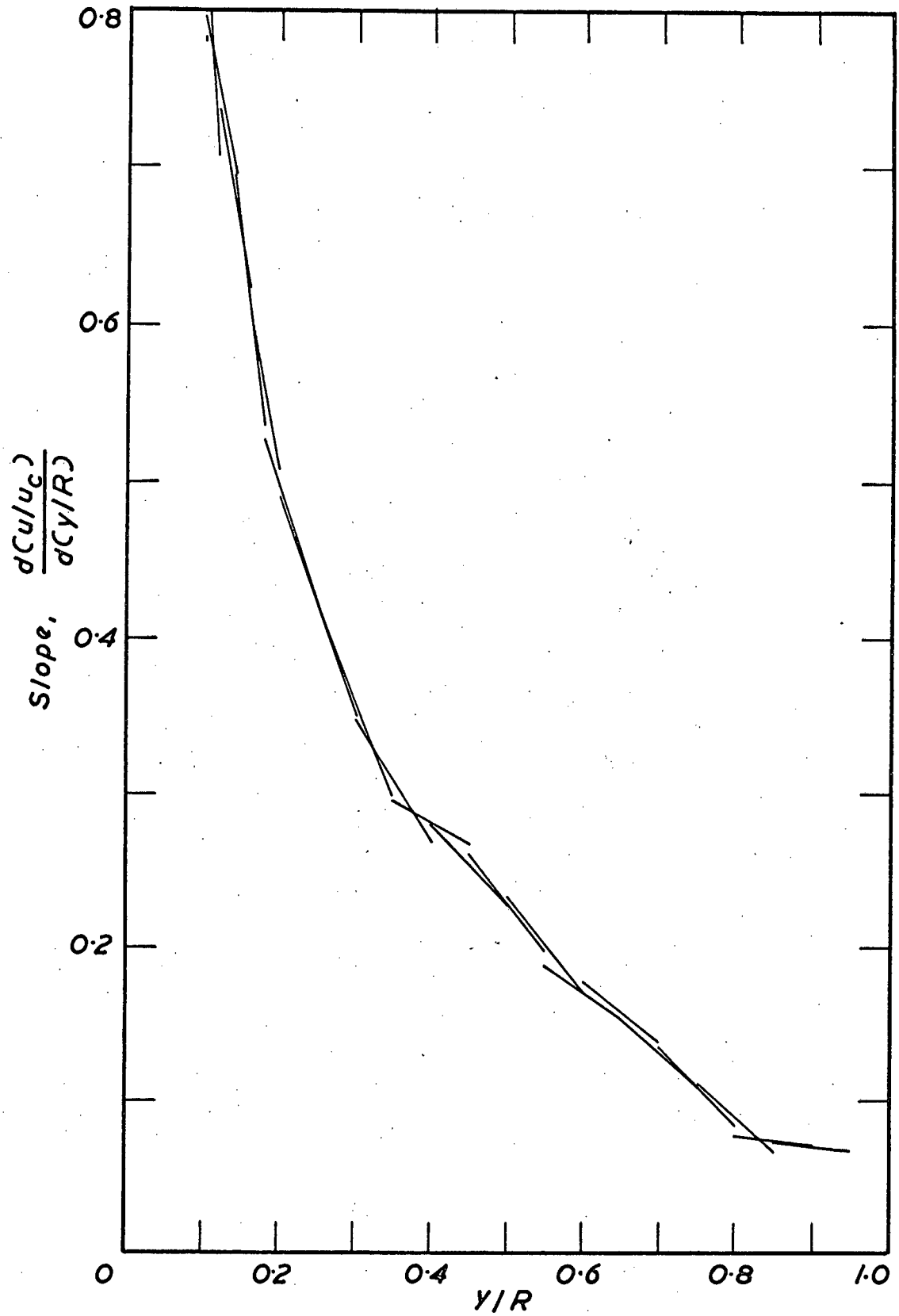

FIG. E.1 SLOPE OF LAUFER'S (45) VELOCITY PROFILE AT Re = 428,000.

and thus Re based on the average velocity is

$$\text{Re} = 500{,}000 \times 0.855 = 428{,}000$$

$$\therefore f = 0.0034; \quad \sqrt{f/2} = 0.0412$$

$$\text{Thus } \frac{u^+}{u_c} = \frac{u_{av}}{u_c}\sqrt{f/2} = 0.0352$$

At any radial position, e.g. y/R = 0.40

$$\epsilon_M/Ru^* = \frac{(1 - y/R)u^+/u_c}{d(u/u_c)/d(y/R)} \qquad \text{(E.5)}$$

$$= \frac{0.6 \times 0.0352}{0.282} = 0.0749$$

Values of ϵ_M/Ru^* are given in Table E.1.

For Pe = 50,000 (based on u_c), data are also given as u/u_c. Integration gives $u_{av}/u_c = 0.8068$.

Thus Re = 40,300 and $u^+/u_c = 0.0418$

Calculation proceeds as above and results are given in Table E.2.

E.22 Rein (51), air.

A number of profiles were measured in a 2-in I.D. pipe.

Re = 36,700, $\sqrt{f/2} = 0.0524$

u_{av} by integration from profile = 34.99 ft/sec.

$$\therefore u^* = 1.83$$

Now $$\epsilon_M/Ru^* = \frac{(1 - y/R)\, u^*}{du/d(y/R)} \qquad \text{(E.6)}$$

E.23 Sleicher (50), air.

Eleven runs are reported

Taking Run P6, Re = 40,000:

$\sqrt{f/2} = 0.052$, $u_{av} = 52.8$ ft/sec, $u^* = 2.74$

Thus ϵ_M/Ru^* may be evaluated from equn. E.6.

E.24 Stanton (49), air.

Velocity profiles are reported in smooth and rough pipes.

For the smooth pipe, D = 4.93 cm. and centre velocity = 1525 cm/sec.

Average velocity, by integration is 1241 cm/sec

$$\therefore \text{Re} = \frac{4.93 \times 1241 \times 0.075 \times 1488}{(2.54 \times 12)^2 \quad 0.018} = 40{,}900 .$$

Assuming an air temp. of ca. 70°F

$\therefore \sqrt{f/2} = 0.0518, \quad u^* = 64.2$ cm/sec.

ϵ_M/Ru^* is evaluated from equn. E.6.

E.25 Beckwith and Fahien (52), water.

Four velocity profiles are given. Data are given in the form u/u_{av} and u^+ vs. $(1 - y/R)^2$.
Values of ϵ_M/Ru^* for the highest Reynolds number, Re = 18770, are shown in Table E.2. These values of ϵ_M obtained by the curve-fitting method, are slightly higher than those calculated by the authors themselves.

E.26 Page, Schlinger, Breaux and Sage (53), air in channels.

These authors report a number of velocity profiles measured in a channel about 0.7 in. wide.

For Run 43 (isothermal), Re = 53,200; $u_{av} = 88.7$ ft/sec.

Calculated values of ϵ_M are reported.

Taking R as half the channel width, R = 0.0285 ft.

$\sqrt{f/2} = 0.0515 \therefore Ru^* = 0.0285 \times 88.7 \times 0.0515 = 0.130$

For y/R = 0.80, for example, $\epsilon_M = 9.69 \times 10^{-3}$

$$\therefore \epsilon_M/Ru^* = 9.69 \times 10^{-3}/0.130 = 0.0746$$

Values at other radial positions are shown in Table E.2.

E.27 Sesonske, Schrock and Buyco (35), mercury.

Values of ϵ_M/ν are given for four experimental runs. Two typical Reynolds numbers are

Re = 99,000; $\sqrt{f/2}$ = 0.0464; $2/Re\sqrt{f/2}$ = 4.35×10^{-4}

At y/R = 0.40, ϵ_M/ν = 208

$\therefore$ ϵ_M/Ru^* = $208 \times 4.35 \times 10^{-4}$ = 0.0905

For Re = 62,000; $\sqrt{f/2}$ = 0.0498, $2/Re\sqrt{f/2}$ = 6.48×10^{-4}

ϵ_M/Ru^* is calculated in Table E.2.

E.28 This work, mercury.

Two velocity runs will be considered. These are Runs No. V.7 and V.33. The former has been discussed in Appendix A and is shown in Fig. A.1. V.7 was measured with the gas pressuring system, while V.33 was measured with the "Prandtl-type" gauge, discussed in Chapter 2.

Run V.7 : Re = 89,700, $\sqrt{f/2}$ = 0.0477

u_{av} = 0.812 ft/sec, u^* = 0.0387

Run V.33 : Re = 89,200, $\sqrt{f/2}$ = 0.048

u_{av} = 0.809 ft/sec, u^* = 0.0388

Values of ϵ_M/Ru^* for both runs were evaluated from equn. E.6 and are given in Table E.2.

APPENDIX F.

EQUIPMENT DETAILS

F.1 HEATING COILS

F.11 Main heating coil

Tape width = 0.499 in.
Tape thickness = 0.0305 in.
Resistance = 0.0375 ohms/ft.

Angle of wire to pipe ca. $84\frac{1}{2}$ deg.
Average gap between windings = 0.067 in.

Tube outside diameter = 1.900 in.
O.D. of windings = 2.02 in.

Areas covered by main windings:

Upper, above probes	=	0.922 ft^2
Upper, below probes	=	3.140
Total upper	=	4.062 ft^2
Total Lower	=	3.948 ft^2
		8.010 ft^2

Resistances: Upper winding = 3.360 ohms
Lower winding = 3.246 ohms

Electrical connections are shown in Fig. F.1. The wattmeter in the lower circuit was connected over the coil only, so as to record only energy entering the system, and not that dissipated in the control resistance.

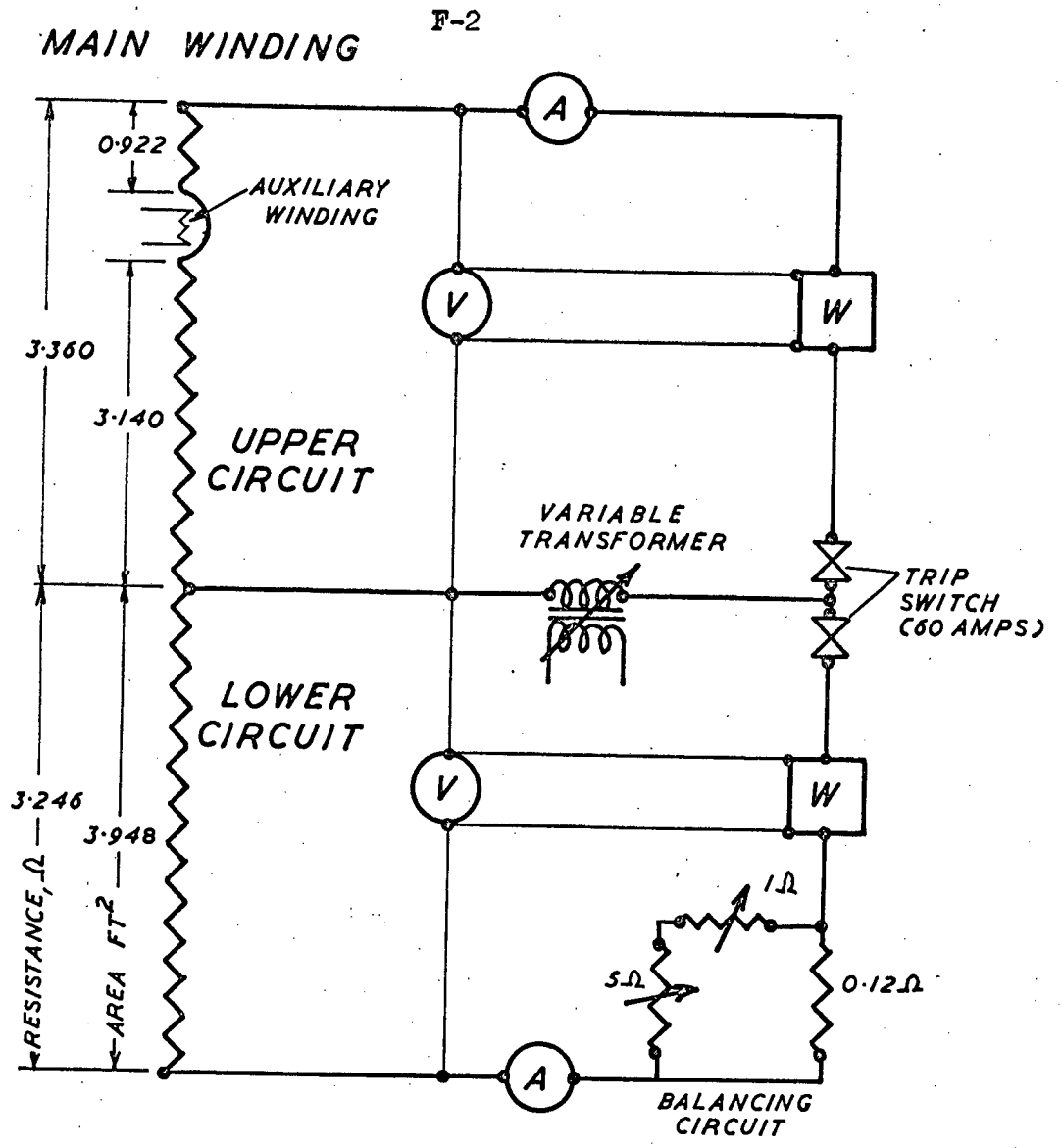

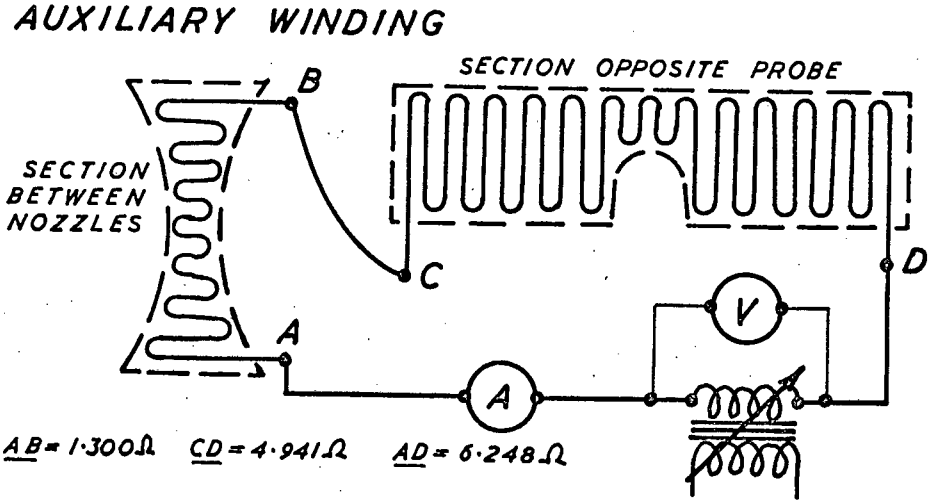

FIG. F.1 HEATING CIRCUITS.

A Ammeter V Voltmeter W KWH meter

F.12 Auxiliary heater

The area left uncovered by the main winding was

(i) the section opposite the probes, and containing the static tap, 3.44 in. along the circumference and 0.77 in. wide (= 2.65 sq. in.)

(ii) the section containing the probe nozzles, and occupying the rest of the circumference, 2.53 in, 1.40 in. wide (= 3.55 sq. in.).

The auxiliary heater was constructed of 24 SWG nichrome wire, 1.634 ohms/ft., and consisted of two sections:

(a) the first section covering the 2.65 sq. in. in part (i) above and with a resistance of 4.941 ohms

(b) the second section, fitted into the small area between the nozzles. Resistance of total winding, (a) and (b) = 6.248 ohms .

It was decided to maintain a constant heat flux over the area opposite the probe entry (see section 4.1). Thus the heat input over Section (a) should be in the ratio of areas covered by this part and the main winding.

i.e. $2.65/(8.010 \times 144) = 0.23\%$

of the main winding heat input. Accordingly the ratio of heat input over the total auxiliary winding to that over the main coil should be

$$\% \text{ Aux./main} = 0.23 \times \frac{6.248}{4.941} = 0.29\% .$$

Electrical connections are shown in Fig. F.1.

F.2 THERMOCOUPLES

Iron-constantan as well as copper-constantan thermocouples were used. Tube wall couples and the couples in the cooling water were copper-constantan, and the others iron-constantan. Since it was thought desirable to be able to use the test section inlet temperature as a reference point, both iron and copper couples were installed at the inlets to the test sections. The copper couples were covered by epoxy resin so as to avoid amalgamation with the mercury.

F.21 Switching Panel

The thermocouple switching panel may be seen (partly obscured) in the main view of the apparatus, Fig. 5, and the wiring diagram is given in Fig. F.2. Thermocouple leads from the apparatus were brought to multi-pole selector switches on the panel, where the iron and copper couples were kept separate. The setting of switch A determined whether the iron or the copper circuit was being used. The reference selector allowed the heated section inlet, the cooled section inlet, or ice, to be selected as reference point. Switch B allowed "calibration" of the above two "references" versus ice. Switch D determined whether the iron or copper couple was being used. As the inlet temperatures were found to be unsatisfactory as reference points, in normal operation the "reference" selector was on either the copper or the iron "ice" position and switch B on "reference". Only when it was desired to measure inlet temperatures was B switched to "calibrate".

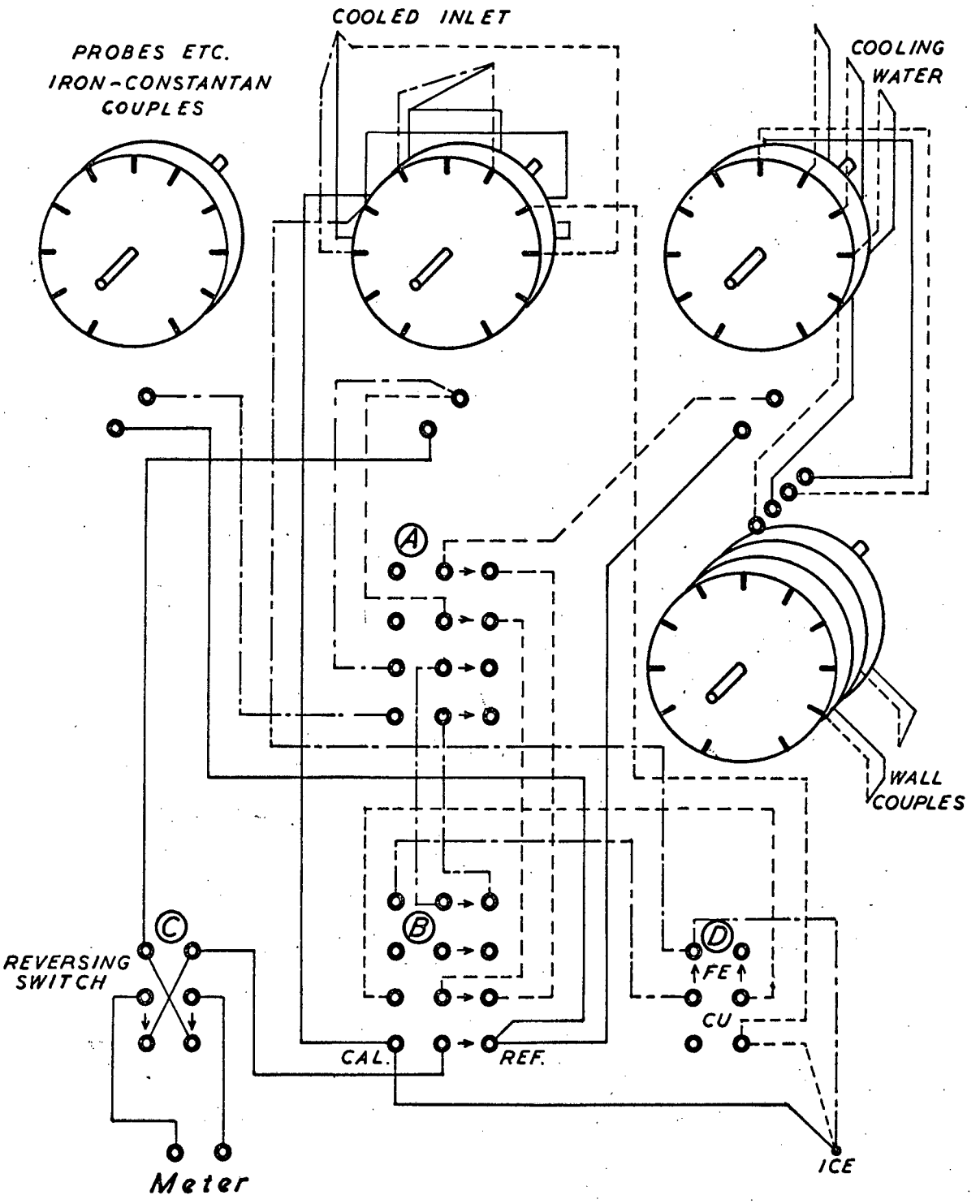

FIG. F.2 THERMOCOUPLE SWITCHING PANEL.

--- Copper —·— Iron —— Constantan

As mentioned in Section 2.52, an external millivolt reference source was eventually used. For this purpose the "meter" position in Fig. F.2 was connected to the "thermocouple emf" position in Fig. 9.

F.22 Calibration

Inlet, outlet, and probe thermocouples were calibrated against a standard thermometer in an oil bath. Fig. F.3 is a portion of the resulting calibration chart and shows that the thermocouples are in excellent agreement with standard tables. The latter were therefore used in calculations. For numerical purposes, the temperature range was broken up into a number of straight lines, and Table F.1 prepared as an aid to temperature conversion.

F.3 ORIFICE METER

The upper crosslink was utilised as a flow meter. The same 1.624 in. I.D. pipe, as in the test sections, was used, with a straight meter run of 3.8 ft., providing 20 diameters upstream and 7 diameters downstream of the orifice plate. Pressure taps were situated on the underside of the pipe, 1 in. on either side of the orifice plate.

Three orifice plates were manufactured, to BSS standards (88). The meter assembly was removed from the apparatus and each orifice plate calibrated separately, with water, over a range of Reynolds numbers.

e.g. Orifice No. 1. Orifice D. = 1.125 in.

$$\beta = 0.6927, \quad \beta^4 = 0.2303, \quad \sqrt{1 - \beta^4} = 0.877$$

$$u_{av} = \frac{\beta^2 C_D}{\sqrt{1 - \beta^4}} \sqrt{2g\,\Delta h} \qquad (F.1)$$

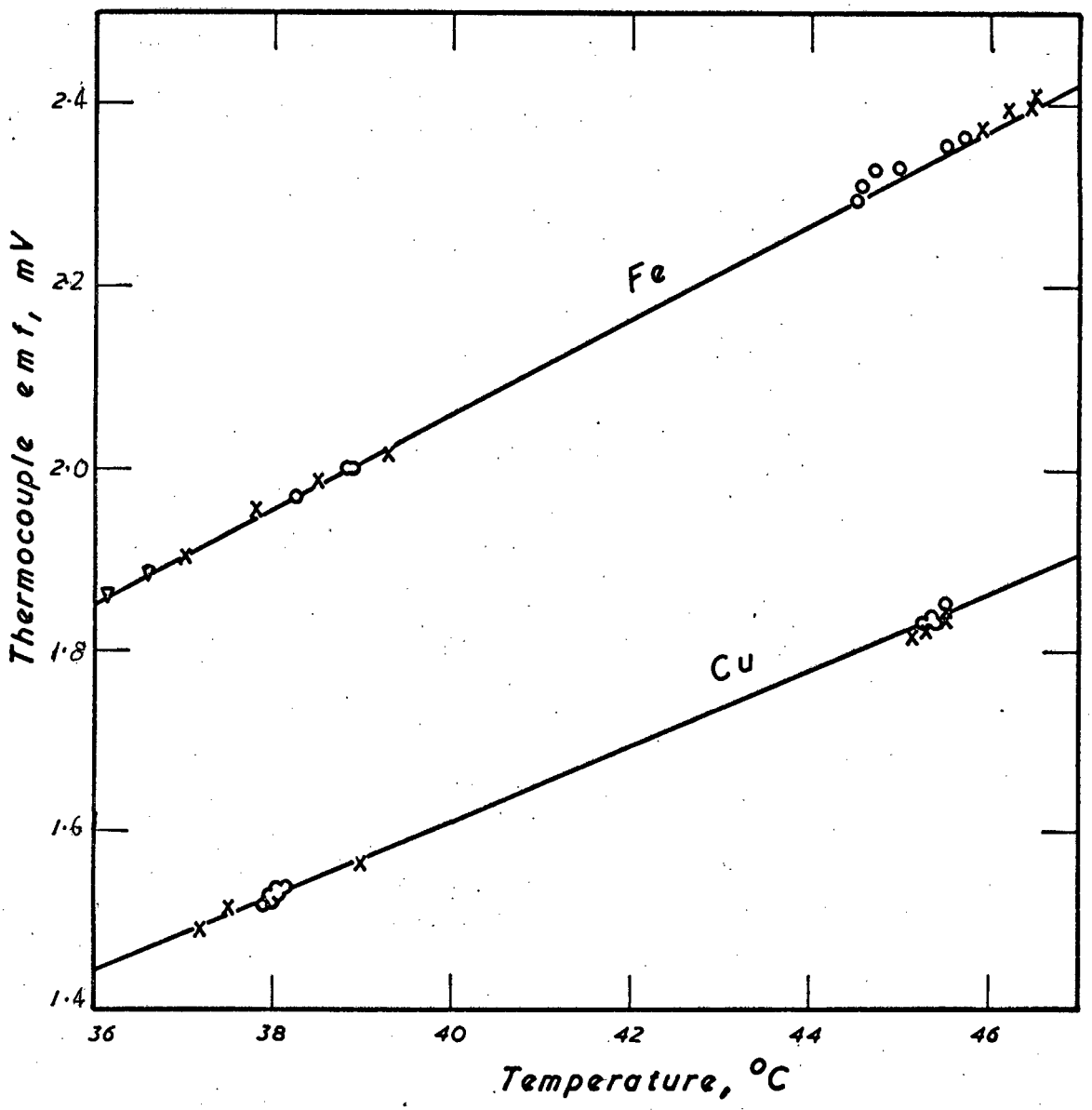

FIG. F.3 PORTION OF THERMOCOUPLE CALIBRATION CHART.

o Heated section outlet x Cooled section inlet

▽ Cooled section outlet

—— Temperature-emf relationship from standard tables(87).

TABLE F.1 - TEMPERATURE CONVERSION FOR COPPER-CONSTANTAN AND IRON-CONSTANTAN THERMOCOUPLES

(Straight-line approximations to data from standard tables (87).)

COPPER - CONSTANTAN

°C	mV	°C/mV
0	0.000	
		→ 25.71
10	0.389	
		→ 25.13
20	0.787	
		→ 24.57
30	1.194	
		→ 24.04
40	1.610	
		→ 23.53
50	2.035	
		→ 23.15
60	2.467	
		→ 22.68
70	2.908	
		→ 22.27
80	3 357	
		→ 21 93
90	3.813	
		→ 21.55
100	4.277	

IRON - CONSTANTAN

°C	mV	°C/mV
0	0.00	
		→ 20.00
10	0.50	
		→ 19.23
20	1.02	
		→ 19.23
30	1.54	
		→ 19.23
40	2.06	
		→ 19.23
50	2.58	
		→ 18.87
60	3.11	
		→ 18.52
100	5.27	
		→ 18.35
140	7.45	
		→ 18.02
190	10.22	

Example: 1.900 mV (Copper-constantan)

$T = 40 + (1.900 - 1.610) \times 23.53$

$= 40 + 6.82$

$= 46.82\ ^{\circ}C$

Typical runs:

Water collected = 141.8lb in 35.2 sec.

Manometer reading = 6.7 cm mercury
(mercury-water manometer)

From equn. F.1, $C_D = 0.615$;

Orifice Reynolds number = 8.3×10^4

For a number of further runs, C_D (average) = 0.616

Orifice no.	1	2	3
D, in.	1.125	0.9375	0.3125
β	0.6927	0.5775	0.1925
$\frac{\beta}{\sqrt{1-\beta^4}}$	0.877	0.943	0.999
C_D, average	0.616	0.617	0.622

APPENDIX G.

HEAT TRANSFER COEFFICIENTS

G.1 NUSSELT NUMBERS

Values of Pe and Nu for the runs reported here are given in Table G.1.

The calculation method may be illustrated with reference to Run 10:

$$Pe = Re \times Pr = 95,500 \times 0.0214 = 2040$$

$$Nu = \frac{h\,D}{k} = \frac{q}{T_w - T_{av}} \times \frac{D}{k}$$

$$= \frac{3150}{5.24} \times \frac{0.1353}{5.32} = 15.3$$

TABLE G.1 - NUSSELT NUMBERS

Run No.	1	1a	2	3	3a	4	4a	5
Pe	80.9	82.3	87.2	118	121	173	174	241
Nu	7.8	8.7	6.2	8.2	7.5	8.4	8.5	7.8

Run No.	6	7	8	9	10	11	12	13
Pe	304	534	611	947	2040	2670	3650	5360
Nu	8.1	7.9	8.4	8.6	15.3	17.8	21.1	32.7

Run No.	13a	14	15	16	17	18	18a
Pe	5430	181	210	374	391	477	480
Nu	32.8	10.5	9.8	11.5	10.5	8.3	9.3

G.2 NUSSELT NUMBER FROM DIMENSIONLESS TEMPERATURE PROFILE

The Nusselt number is expressed as

$$Nu = \frac{h\,D}{k} = \frac{2R}{k} \cdot \frac{q_w}{T_w - T_{av}} \quad . \qquad (G.1)$$

Now the slope of the dimensionless temperature profile at y/R=0 is

$$S_o = \left[\frac{d\left(\frac{T_w - T}{T_w - T_c}\right)}{d(y/R)} \right]_0 = - \frac{R}{(T_w - T_c)} (dT/dy)_o \qquad (G.2)$$

Also,

$$q_w = - k\,(dT/dy)_o \qquad (G.3)$$

Substituting G.2 and G.3 into G.1,

$$Nu = \frac{2\,S_o}{\left(\frac{T_w - T_{av}}{T_w - T_c}\right)} \qquad (6.2)$$

The term $(T_w - T_{av})/(T_w - T_c)$ was evaluated for each of the undistorted average profiles given in Fig. 26 from the relation

$$\left(\frac{T_w - T_{av}}{T_w - T_c}\right) = - 2 \int_o^1 \frac{u}{u_{av}} \left(\frac{T_w - T}{T_w - T_c}\right) \frac{r}{R}\, d\left(\frac{r}{R}\right) \qquad (G.4)$$

in the same way as illustrated in app. B.26, and values of S_o were taken from Table D.3.

Values of Nu and Pe, assuming a Prandtl number of 0.02, are shown in Table G.2.

TABLE G2 - NUSSELT NUMBERS FOR DIMENSIONLESS TEMPERATURE PROFILES

Re	Pe	S_o	Φ	Nu
30,000	600	2.37	0.575	8.22
50,000	1000	2.77	0.589	9.41
100,000	2000	4.46	0.627	14.2
200,000	4000	8.40	0.688	24.4
300,000	6000	12.92	0.733	35.3

G.3 EFFECT OF VELOCITY PROFILE ON NUSSELT NUMBER

The Nusselt number is dependent on the difference $T_w - T_{av}$. T_{av} is determined by

$$T_{av} = 2\int_0^1 \frac{u}{u_{av}} T \left(\frac{r}{R}\right) d\left(\frac{r}{R}\right) \qquad (4.1)$$

and is thus dependent on the velocity distribution, particularly near the wall where the factor r/R is large.

In order to obtain some impression of the effect of the velocity profile on T_{av}, and hence on Nu, the above integration was carried out using

(a) the temperature profile of Run 1

(b) the velocity profiles shown in Fig. G.1.

The profile labelled 1 is based on the von Karman relations, equn. 1.5. The other profiles incorporate increasingly higher velocities near the tube wall, but all have

$$2\int_0^1 \frac{u}{u_{av}} \frac{r}{R} d\left(\frac{r}{R}\right) = 1 .$$

Resulting values of Nu are shown in Table G.3. The Nusselt number is seen to increase with increasing distortion. It may also be inferred that, if the velocity profile was lowered rather than raised near the wall, lower values of Nu would be obtained.

TABLE G.3 EFFECT OF PROFILE DISTORTION ON NUSSELT NUMBER.

Curve	$(T_w - T_{av})°F$	Nu
1	1.400	7.80
2	1.384	7.89
3	1.370	7.97
4	1.346	8.11

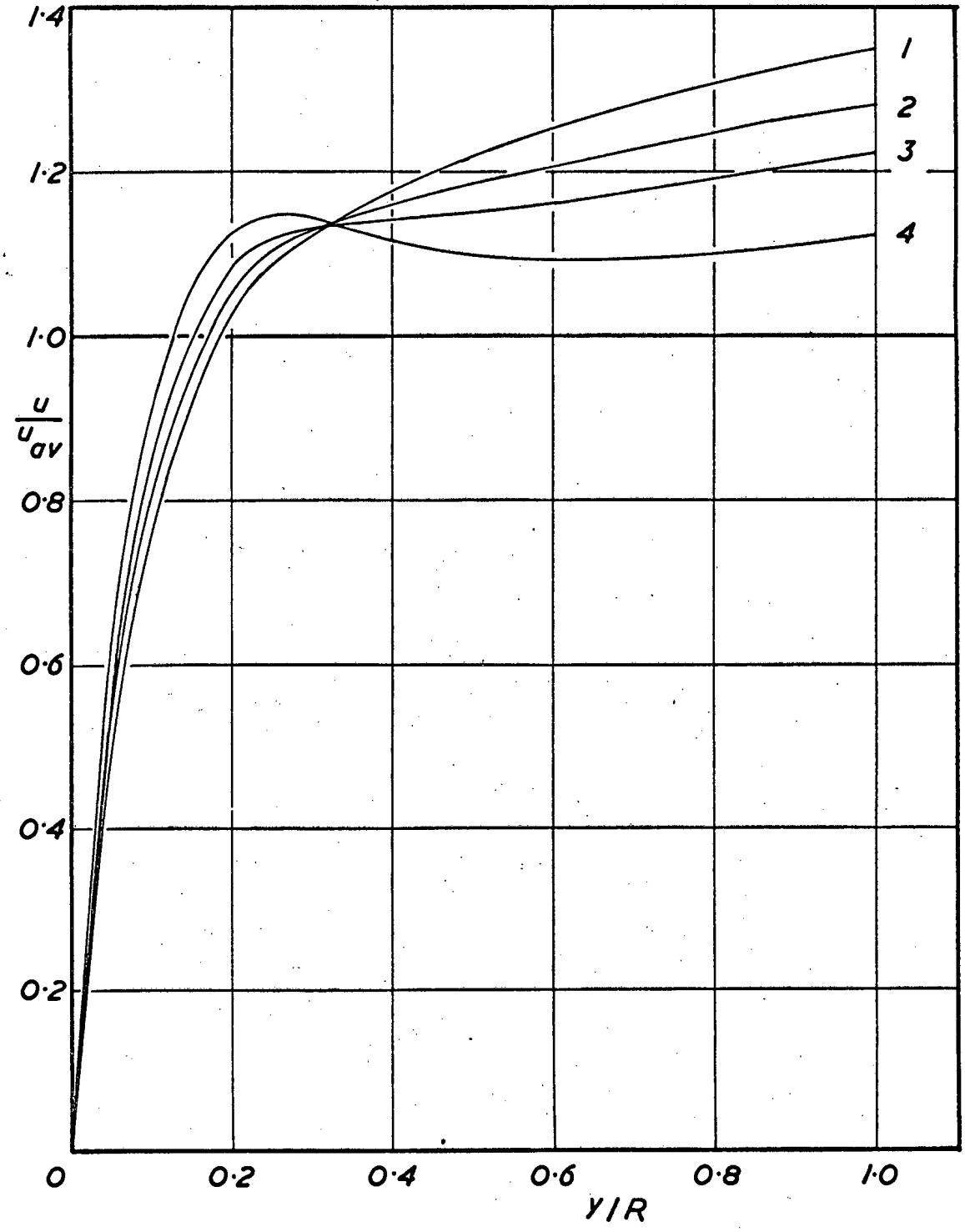

FIG. G.1 DISTORTED VELOCITY PROFILES.

1 Undistorted profile, from equn. 1.5 for Re = 3800

2, 3, 4 Increasing amounts of distortion

APPENDIX H

PHYSICAL PROPERTIES

H.1 PHYSICAL PROPERTIES OF MERCURY

The physical properties employed in the calculations presented here are shown in Figs. H.1(a) and (b).

For data on the density of mercury, values from the Smithsonian tables (86) were used. These data are comprehensive and in good agreement with other references (82, 83).

For thermal conductivity, specific heat and viscosity the data of the Liquid-metals Handbook (83) were used, and Fig. H.1(a) also shows the data given by Kutateladze et al. (82).

The coefficient of thermal expansion may be approximated as

$$\beta = \frac{2(V_2 - V_1)}{V_2 + V_1} \cdot \frac{1}{\Delta T} \qquad (H.1)$$

over a small temperature range, where

V = volume of 1 unit of mass,

ΔT = the temperature difference over which the volume change is determined.

From equn. H.1,

$$\beta = \frac{2(1/\rho_2 - 1/\rho_1)}{1/\rho_2 + 1/\rho_1} \cdot \frac{1}{\Delta T} \qquad (H.2)$$

$$= \frac{2(\rho_1 - \rho_2)}{\rho_1 + \rho_2} \frac{1}{\Delta T} \qquad (H.3)$$

From the Smithsonian tables (86)

S.G. @ 40°C = 13.4969

S.G. @ 60°C = 13.4482

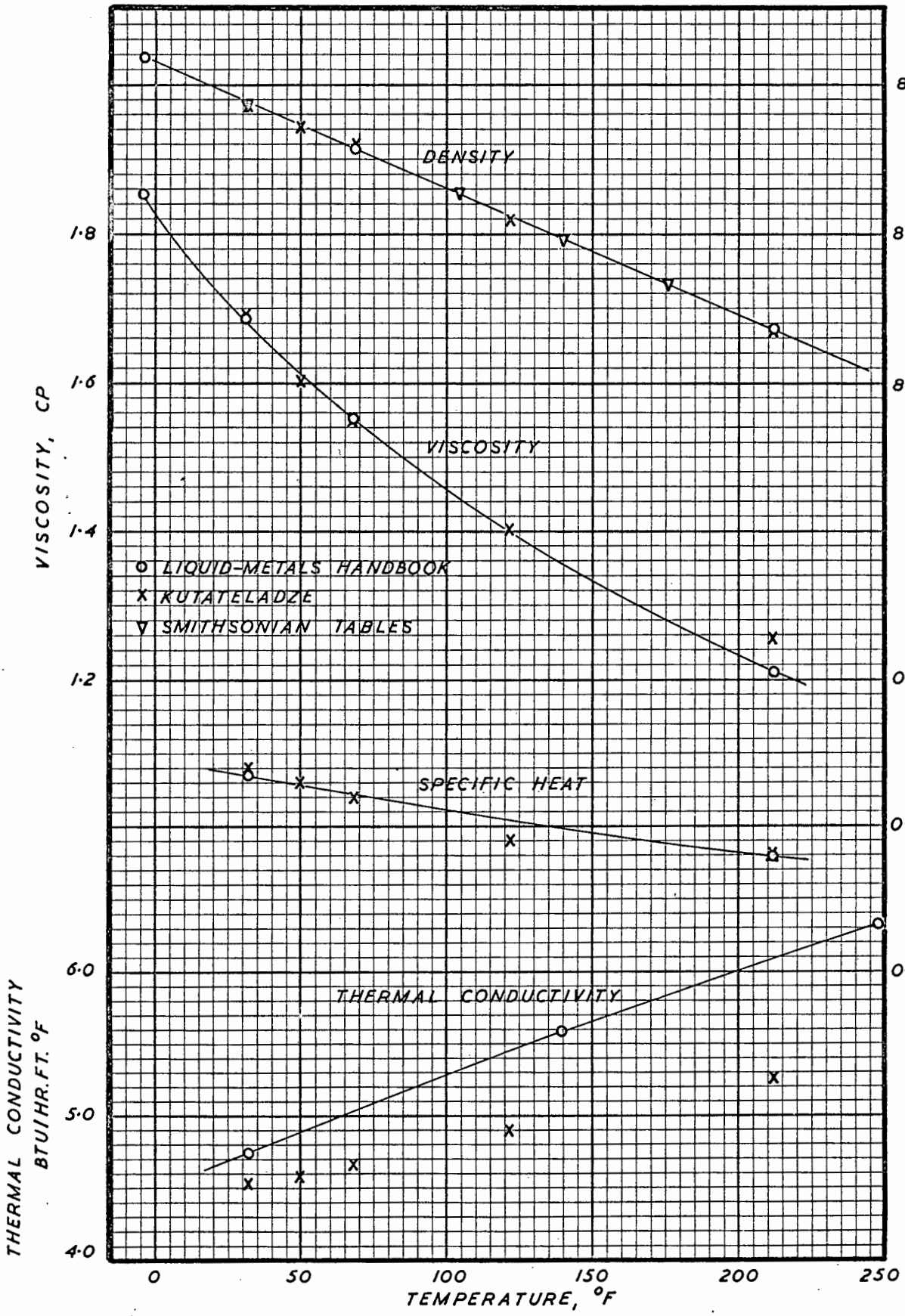

FIG. H.1(a) PHYSICAL PROPERTIES OF MERCURY.

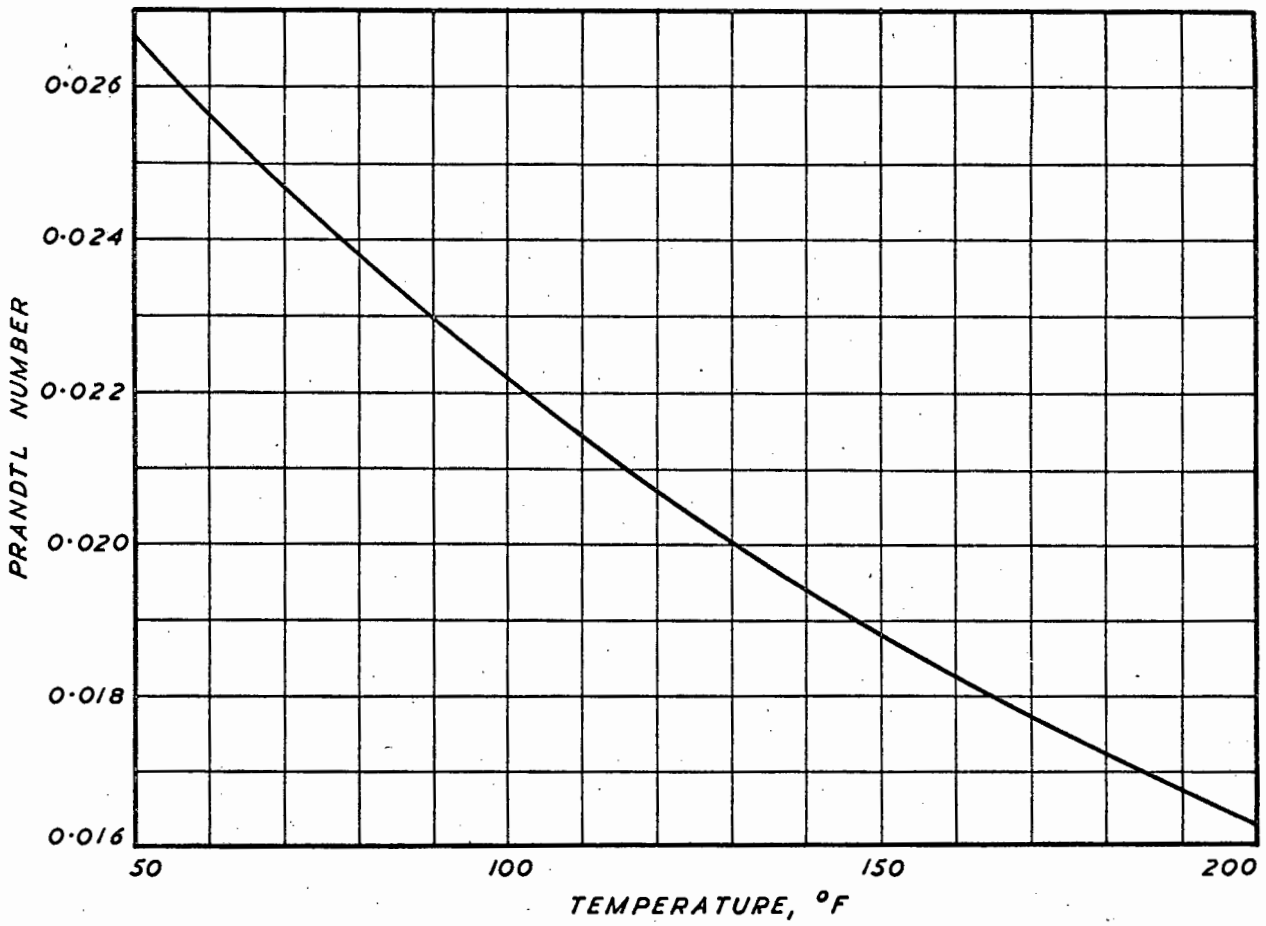

FIG. H.1(b) PRANDTL NUMBER FOR MERCURY.

$$\rho_1 - \rho_2 = 0.0487, \qquad \rho_1 + \rho_2 = 26.95$$

$$\therefore \beta = \frac{2 \times 0.0487}{26.95 \times 20 \times 1.8} = 0.00010\ ^\circ F^{-1}.$$

This figure varies very little with temperature.

For use on a digital computer, the physical properties of Fig. H.1 may be approximated by straight lines over the range 60-200°F, as follows:

Density: $\rho = 851.412 - 0.0846\ T$ lb/ft^3

Thermal conductivity:

$$k = 4.47 + 0.0075\ T \text{ BTU/hr ft } ^\circ F$$

Specific heat:

$$c_p = 0.03348 - 0.0000036\ T \text{ BTU/lb } ^\circ F$$

Viscosity:

$60 < T < 80$,	$\mu = 1.768 - 0.0031\ T$
$80 < T < 120$,	$\mu = 1.752 - 0.0029\ T$
$120 < T < 140$,	$\mu = 1.686 - 0.00235\ T$
$140 < T$,	$\mu = 1.6552 - 0.00213\ T$

Purity of mercury used:

A spectrochemical analysis was carried out on the mercury used. Trace contaminants were present in approximately the following quantities:

Ag ≈ 100 ppm; Au, Ca, Mg ≈ 10 ppm; Cu ≈ 0.5 ppm.

H.2 PHYSICAL PROPERTIES FOR THE NaK EUTECTIC MIXTURE

The physical properties used in processing the results of other workers who used the NaK eutectic are given below.

In general the data given in the Liquid-metals Handbook (83) for the NaK eutectic were used, and comparisons with the

data given by Kutateladze (82) for 75%K NaK are made.

Density data from the LMH are very slightly lower than Kutateladze

Vicosity data from LMH are slightly below Kutateladze

Specific heat data from the LMH are considerably below that from Kutateladze

Thermal conductivity data from LMH have a flatter temperature slope than the Kutateladze data and are therefore considerably higher at the lower temperatures.

Kinematic viscosity given by the two references are comparable and are shown in Fig. H.2. The curve is drawn through the LMH data, and in the low-temperature region, where only the data of Kutateladze are available, the curve is drawn to follow the same slope.

The Prandtl number for the two references differs considerably due to the differences in specific heat and thermal conductivity, and values calculated from the LMH data are given in Fig. H.2.

The coefficient of thermal expansion may be calculated from the density data given by the LMH:

$$\rho \text{ at } 100\ ^{\circ}C = 0.847 \text{ gm/cm}^3$$

$$\rho \text{ at } 250\ ^{\circ}C = 0.811 \text{ gm/cm}^3$$

$$\beta = \frac{2(0.847 - 0.811)}{0.847 + 0.811} \times \frac{1}{150 \times 1.8} = 0.00016\ ^{\circ}F^{-1}.$$

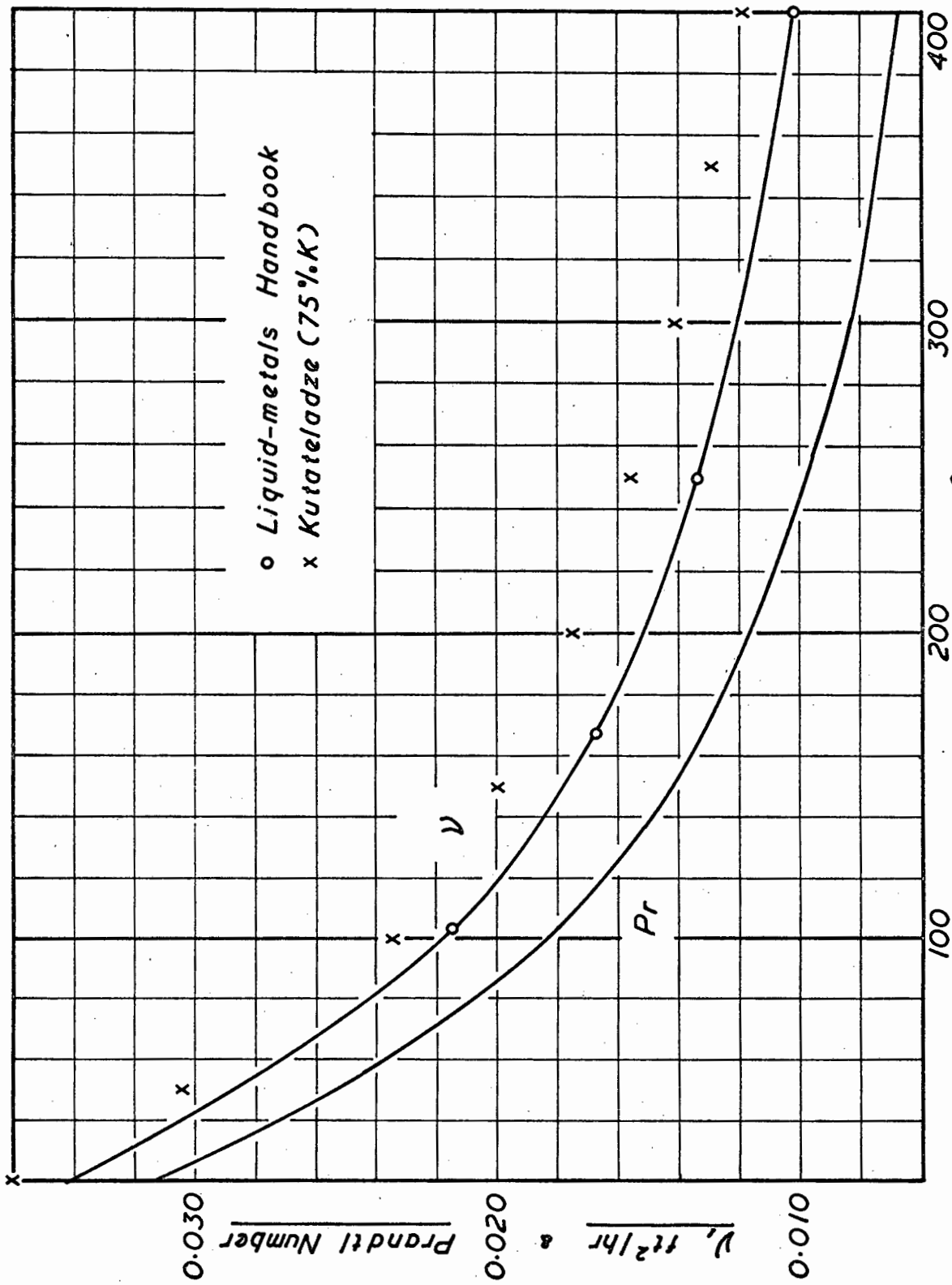

FIG. H.2 KINEMATIC VISCOSITY AND PRANDTL NUMBER FOR THE NaK EUTECTIC.